Fracture Behaviour Analysis of AA7075 Aluminium Alloy by Finite Element and Boundary Element Methods

Submitted in fulfilment of the academic requirements for the degree of **Master of Engineering** in the **Department of Industrial Engineering,** Faculty of Engineering, and the Built Environment at the Durban University of Technology.

Obuya, Tryphone Oloo

Supervisors: Prof. Samson Oluropo Adeosun

Prof Oludolapo Akanni Olanrewaju

DECLARATION

I, Obuya Tryphone Oloo, declare that:

The research presented in this thesis is my original work, except where indicated otherwise. This thesis has not been submitted for any degree or examination at any other institution. It does not include data, images, graphs, or other information from other individuals unless explicitly acknowledged. Similarly, it does not feature writing from others unless specifically cited. When quoting other written sources, I have paraphrased their words while referencing the general information attributed to them. If I have used their exact wording, it is enclosed in quotation marks and properly referenced. This thesis does not include text, graphics, or tables copied from the internet unless specifically acknowledged, with sources detailed in the dissertation and reference sections.

Signature Date: _____

Name: Obuya Tryphone Oloo.

BY SUPERVISOR

This thesis has been presented to be examined with my approval as the university supervisor.

Name: Prof. Oludolapo Olanrewaju

Signature: _

Date: 23/10/2025

Name: Prof. Samson Oluropo Adeosun

Signature:

Date: _____

ABSTRACT

Fracture mechanics is a field of study that focuses on the behaviour of materials containing cracks under stress, particularly for high-strength aluminium alloys like AA7075 series that are used in aerospace as well as automobile industries because of their high strength-to-weight ratio. This study focuses on fracture test experiments and the analysis of the behaviour of AA7075 under various loading conditions through finite element analysis (FEA) and boundary element techniques (BET) to determine life estimation, stress distribution, stress intensity factors (SIF), and energy release rates (ERR) during fracture. The FEA model is developed for a standard edge-cracked specimen of dimensions w= 50 mm, thickness 5 mm, and initial crack length, a= 10 mm. Under tensile loading of 10 kN, the stress intensity factor is computed as approximately 18.2 MPa√m, which agrees well with experimental observations. The corresponding energy release rate obtained from the simulation is 82.5 J/m², indicating a predominantly brittle fracture mode due to the alloy's T6 temper. Using BET analysis, crack propagation trajectories are simulated, showing a stable crack growth phase until the critical crack length a_c= 18.4 mm, beyond which unstable fracture occurs. The predicted fracture toughness for the alloy is found to be 25.6 MPa√m, consistent with literature values for AA7075-T6, ranging between 24 - 28 MPa√m. The simulated fatigue crack growth rate follows the Paris law with constants, C = 1.2 x 10^{-10} and m = 3.5, producing a fatigue crack growth rate between 1×10^{-6} and 5×10^{-4} mm/cycle for ΔK values from 10 to 20 MPa√m. The meshing and loading properties of Ansys 2024R2 are utilized for the boundary conditions, while the FEA inbuilt functions in MATLAB incorporate experimental data to predict behaviour under Mode I fracture. From the analysis, it is determined that stress intensity factors depend on both crack length and specimen geometry. The energy release rates and stress distribution at the crack tip

are largely influenced by the applied stress, with peak von Mises stresses reaching 460 MPa near the crack tip region. These analysed data aid engineers in determining life estimation and crack propagation limits in AA7075 components. The study concludes that components made from AA7075 should maintain service stresses below 70% of the yield strength (≈350 MPa) to prevent premature crack propagation, improving fatigue life and reducing economic and safety risks.

ACKNOWLEDGEMENT

I would like to extend my heartfelt gratitude to my supervisors, Prof. Samson Adeosun and Prof. Oludolapo Akanni, for their guidance throughout this project, their invaluable revision support, and their insightful advice. Their assistance has been crucial to my progress. I also appreciate Mr. Elisha Aura for his help in interpreting the experimental data.

I would like to thank my fellow graduates, particularly Grace Kiarie, for being a sounding board for my ideas and providing an extra set of eyes on my derivations and code.

I acknowledge my own hard work, as well as the staff at the faculty and the international office of DUT for their financial support. My thanks also go to the workshop technicians at Jomo Kenyatta University of Technology for their assistance during the experimental sessions, without which this project would not have been possible.

Finally, I am grateful to my friends and family for their unwavering support throughout my graduate school journey. Their encouragement has been invaluable during both the challenging and rewarding times.

CONTENTS

Declaration ii

Abstract iii

Acknowledgement v

Contents vi

List of Figures x

List of Tables xii

List of Abbreviations xiii

List of Symbols xv

Research output xvi

Chapter One 1

1.1 Introduction. 1

1.1.1 Types of fractures 3

1.2 Problem Statement 4

1.3 Aim of the Study 6

1.4 Research Objectives 6

1.5 Research Questions 7

1.6 Research Hypothesis: 7

1.7 Justification for This Research 8

1.8 Methodology 10

1.9 Significance of the Study 11

1.10 Limitations of the Study 12

1.11 Structure of Thesis 14

1.12 Conclusion 14

1.13 Contributions of the Study to Knowledge 15

Chapter Two 16

2.1 Literature review 16

2.1.1 Introduction 16

2.2 Scholarly studies on Fracture parameters under loading 17

2.3 Linear Elastic Fracture Mechanics and its Applications 26

2.4 Finite Element Analysis as a technique of solving Fracture Mechanics 27

2.5 Boundary Element Techniques 30

2.6 Fatigue and Fracture Toughness Testing 33

2.7 Summary 36

Chapter Three 37

3.1 Methodology 37

3.1.1 Introduction 37

3.2 Methodology of achieving the Objectives 39

3.2.1 Tensile and Fatigue Test 39

3.2.2 Linear Finite Element Method 42

3.3 Finite Element and Boundary Element Methodology 45

3.3.1 Finite Element Methodology 45

3.3.2 Boundary Element Technique Methodology. 47

3.4 Analytical Evaluation of Fracture Mechanics Parameters. 49

3.4.1 Stress intensity factor Evaluation. 49

3.4.2 Fatigue crack growth and Crack life estimation of A7075 50

3.4.3 Stress distribution around the crack tip. 51

3.4.4 Energy Release rate during fracture 52

3.5 Simulation of Fracture Mechanics. 52

Chapter Four 56

4.1 Introduction 56

4.2 Results of the Fatigue test experiment. 57

4.2.1 Evaluation of Stress Intensity Factor (SIF) 60

4.2.2 Evaluation of Fatigue Crack growth and Life Estimation..... 62

4.2.3 Evaluation of Energy Release Rate 64

4.2.4 Evaluation of Stress Distribution at the Crack tip 66

4.3 Results from the simulation..... 69

4.4 Comparison of Experimental and Simulated Data 71

4.5 Scanning Electron Microscope observation of the specimen..... 73

4.6 Correlations of the results to the Objectives. 77

Chapter Five 80

5.1 Conclusion and Recommendations from the Study 80

5.1.1 Conclusion from the Study..... 80

5.1.2 Recommendations 81

References 83

Appendix 88

LIST OF FIGURES

Figure 3.1: Summary Flowchart of the Research Methodology 38

Figure 4.1: Specimens with a 3mm pre-notch..... 57

Figure 4.2: Samples used for the tensile test and the loaded sample. 58

Figure 4.3: Force applied against the corresponding stroke..... 60

Figure 4.4: Stress intensity against time graph. 61

Figure 4.5: Change in crack length with increase in loading cycles. 62

Figure 4.6: Crack growth rate against change in stress intensity factor(r-Curve)..... 64

Figure 4.7: Energy release rate against time graph. 66

Figure 4.8: Linear Stress distribution simulation around crack tip and propagation areas. 69

Figure 4.9: Polar Stress Distribution simulation around the crack tip and propagation areas. 69

Figure 4.10: Simulated deformation under loading. 70

Figure 4.11: Equivalent simulated elastic strain. 70

Figure 4.12: Simulated stress distribution around crack tip and propagation area. 71

Figure 4.13: Simulated Strain Energy distribution..... 71

Figure 4.14: Cracked surface of AA7075 sample as observed at x2300 magnification on SEM.

..... 74

Figure 4.15: Surface appearance of crack and area around crack after fracture tests. 74

Figure 4.16: Surface appearance of crack and area around crack before fracture tests 75

Figure 4.17: ImageJ analysis of the control sample specimen for existing deformities before fracture tests. 76

LIST OF TABLES

Table 4.1: Chemical composition of AA7075 by wt% of each element 56

Table 4.2: Experimental data collected during the Fracture test. 59

Table 4.3: Experimental data calculated during fracture test. 59

Table 4.4: Comparison of Experimental and Simulation results 72

Table 4.5: ImageJ results of dimensions of pre-existing deformation and pre-crack sizes on the control sample specimen 77

LIST OF ABBREVIATIONS

Abbreviation	Full Meaning
AA7075	Aluminium Alloy 7075
FEA	Finite Element Analysis
BET	Boundary Element Techniques
SIF	Stress Intensity Factor
ERR	Energy Release Rate
SEM	Scanning Electron Microscope
LEFM	Linear Elastic Fracture Mechanics
CT	Compact Tension
XFEM	Extended Finite Element Method
VCCT	Virtual Crack Closure Technique
SCC	Stress Corrosion Cracking
CAD	Computer-Aided Design
CFD	Computational Fluid Dynamics
DCE%	Degree of Cold Expansion (percentage)

Abbreviation	Full Meaning
FCI	Fatigue Crack Initiation
J-integral	Contour Integral for Energy Release Rate
GLEFM	Energy Release Rate from LEFM
GH	Energy Release Rate of Hyperelastic Solids
MPa	Megapascal
GPa	Gigapascal

LIST OF SYMBOLS

Symbol	Description
K_I	Mode I Stress Intensity Factor
K_II	Mode II Stress Intensity Factor
K_III	Mode III Stress Intensity Factor
G	Strain Energy Release Rate
J	J-integral (Energy Release Rate)
σ	Stress
ϵ	Strain
a	Crack length
P	Applied load
r	Radius of crack hole
τ	Shear stress
ν	Poisson’s ratio
E	Young’s Modulus
da/dN	Crack growth rate per cycle

RESEARCH OUTPUT

The following papers have been generated from this study awaiting publication.

1. T.O Oloo, S.O Adeosun, and O.A Olanrewaju (2024) - Fracture mechanics of Aluminium 7XXX, Simulation Techniques, and Engineering Applications. A comprehensive review. (Under review at Advances in Materials Science and Engineering – Wiley Publishers)
2. T.O Oloo, S.O Adeosun, and O.A Olanrewaju (2025) - Experimental Analysis of Fracture mechanics of Aluminium 7075 alloy plate with edge crack using MatLab software. (Under review at Advances in Materials Science and Engineering – Wiley Publishers)

CHAPTER ONE

1.1 Introduction.

Aluminium 7075 is a lightweight, ductile, and corrosion-resistant metal widely used in various industries, including aerospace, automotive, and construction. Its good ductility allows it to absorb significant energy before failure, which is advantageous in applications requiring energy absorption, such as vehicle crash structures [1]. Aluminium alloys such as 7075 are often designed to have good fatigue resistance, but they can still be prone to fatigue cracks under cyclic loading conditions. While aluminium naturally resists corrosion due to a protective oxide layer, certain alloys can be prone to stress corrosion cracking, particularly in marine environments. Additionally, aluminium can exhibit brittle behaviour at low temperatures and may be susceptible to creep at high temperatures [2].

Aluminium alloy 7075 has primarily aluminium with zinc, magnesium, and copper. These elements make it possible for it to form precipitates during heat treatment, which is responsible for its high strength. The series is preferred in aeronautics since it has high mechanical strength when compared to other groups of alloys defined by Aluminium Association Inc in early 1950s by the United State of America. This is the reason AA7075 are used in commercial flights. Al 7075 has high commercial strength, they can be heat treated for strength, they are non-wieldable, they have high weight/strength ratio and have high formability and ductility. The most common Al 7075 alloys are 7178, 7075, and 7030. In this group, Al 7075 family has the highest Zn content. The 7075 series are applicable in aerospace, welding, hydraulics and in the mobile industry. Since Al 7075 is used majorly in high stress environment, it is important to study its fracture mechanics.

Fracture mechanics is the study of the energy release and behaviour during the fracture of materials. Aluminium 7075 series alloys are no exception since their energy release depends on the material properties, stress states, and environmental influences. Understanding this property of aluminium interplay is important for accurately predicting the performance and maintaining the reliability of components built from these strong alloys. Aluminium 7075 series alloys, known for their high strength and lightweight properties, are extensively used in critical aerospace and automotive applications where structural integrity is paramount. However, these alloys are also susceptible to specific fracture mechanisms that can compromise safety and performance [3]. Understanding the fracture behaviour of these alloys under various conditions is crucial for improving their reliability and extending their application range. The energy release characteristic during fracture of Al 7075 is the material's capacity to prevent crack growth. The strain energy release rate (G) identifies the amount of energy that is dissipated for a given area of fracture growth.

Fracture mechanics is a fundamental factor in assessing the structural integrity of components made from 7075 alloys since it quantifies material's ability to resist fracture propagation. Although widely documented in many standards, established testing methods such as the three-point bending test and the compact tension (CT) test, typically necessitate complex pre-cracking procedures and specialized equipment [4]. This has prompted the development of alternative methods for evaluating fracture toughness. Spherical identification tests, as well as uniaxial tensile tests, are examples of procedures used to determine fracture toughness.[5] Krafft *et al*. proposed using unnotched tensile tests to determine fracture toughness. His main thesis revolved around a critical threshold value within the surface of the aluminium that triggers crack propagation [6]. However, it properly determines both the size of the plastic zone and the distribution of internal strain. As a result, many scholars have proposed enhancements to the Krafft model. Furthermore, correlations employing strain energy density [7] and artificial

neural network models have been developed. However, the effectiveness of these models is sometimes limited to specific materials, which might lead to errors when applied to 7075 materials or structures with degraded mechanical properties. Stress Intensity Factors (SIFs) are fundamental parameters in fracture mechanics, quantifying crack severity and enabling the prediction of fatigue crack growth and structural life. Various analytical, numerical (including FEM, XFEM, VCCT), and experimental methods are employed to determine or estimate them, often involving complex calculations that depend on geometry, loading, and crack characteristics. SIFs for different loading modes (Mode I, II, III) characterize the near-tip stress singularity. The distribution of stresses, including von-Mises stresses and the non-singular T-stress, provides further insight into the stress state around crack tips and notches. SIFs and energy release rates are directly related, with specific formulas for isotropic materials and more complex relationships for anisotropic and interface materials. These concepts and methods are applied across various engineering problems, from analyzing cracked aircraft lugs and welded joints to simulating brittle fractures in computer graphics.

1.1.1 Types of fractures

Fractures occur when a material splits into two or more pieces due to stress. This phenomenon is common in various materials, including metals like aluminium, ceramics, and polymers. Understanding the types of fractures is crucial in materials science for predicting how materials behave under different conditions and for designing materials that can withstand stress without failing. Ductile fracture involves significant plastic deformation before the material breaks. The crack does not propagate rapidly, and the fracture surface is typically rough and fibrous with noticeable necking, where the material narrows at the point of failure.

Aluminium often exhibits ductile fracture under tensile stress, making it capable of absorbing a lot of energy before breaking [8].

In contrast, brittle fracture occurs with little to no plastic deformation, and the crack propagates rapidly. The fracture surface is usually flat and smooth with a granular texture. While high-strength steels and ceramics are prone to brittle fracture, aluminium can also exhibit this type of fracture at low temperatures or under high strain rates [9]. The fracture surface is characterized by striations or beach marks, indicating the progressive nature of crack growth. Aluminium components in aircraft structures often experience fatigue fractures due to the repetitive stress cycles they undergo [10].

Stress corrosion cracking (SCC) is a form of fracture that results from the interaction of tensile stress and a corrosive environment. The fracture surfaces typically show intergranular or trans granular cracking patterns. Aluminium alloys used in marine environments can be particularly susceptible to SCC [11]. Creep fracture occurs due to prolonged exposure to high temperatures and stress, leading to time-dependent deformation and eventual failure. The fracture surface may show dimples or voids, indicating slow, continuous deformation. Aluminium components in high-temperature applications, such as engine parts, are vulnerable to creep fracture [12]. Understanding the fracture behaviour of aluminium is essential for ensuring the reliability and safety of aluminium components. By studying the different types of fractures and the specific behaviours of aluminium under various conditions, engineers can design safer and more durable structures.

1.2 Problem Statement

High strength in Aluminium 7075 series alloys makes them susceptible to various fracture mechanisms, including fatigue fracture, stress corrosion cracking (SCC), and brittle

fracture at low temperatures [13]. These fracture behaviours pose significant risks to the reliability and safety of aerospace and automotive structures. The primary problem is the lack of comprehensive understanding of the fracture mechanics of these alloys under diverse operational conditions, which hinders the development of more resilient alloys and the implementation of effective maintenance strategies and to enhance the safety and performance of structures that utilize these materials.

Aluminium 7075 series alloys are commonly used in high-stress environments, such as aircraft fuselage and wing structures, where the failure of a single component could lead to catastrophic consequences. Understanding how these alloys behave under different stress conditions helps in designing more structures that are resilient [14].

It is quite expensive to carryout probe on an already occurred accident in addition to the loss resulting from the accidents due to fracture. It is cheaper to carryout research on ways of curbing fracture on structural components. Various engineering and mathematical models can be used to depict fracture as exemplified on previous scientific research.

The alloys often undergo cyclic loading during their service life, making them susceptible to fatigue fractures. By studying their fatigue behaviour, engineers can predict the lifespan of components and develop maintenance schedules to prevent unexpected failures. Aluminium 7075 series alloys can exhibit different fracture behaviours at varying loading conditions. Understanding how loading orientation and conditions influences fracture mechanisms such as brittle fracture or ductile is vital for ensuring the material's stability while in operation. Insights from fracture mechanics studies can inform the development of new alloys or the enhancement of existing ones, leading to improved mechanical properties and better performance in practical applications [15]. Meeting stringent aerospace and automotive

safety standards requires a thorough understanding of material behaviour. This study contributes to ensuring that aluminium 7075 series alloys meet these standards by providing detailed fracture mechanics data.

The investigation of fracture mechanics in Aluminium 7075 series alloys is essential for advancing their application in critical engineering fields. By understanding and addressing the factors that influence fracture behaviour, this study aims to improve the safety, performance, and longevity of structures that rely on these high-strength materials. Through rigorous analysis and testing, analysing and simulate fracture related problems while suggesting solutions to the problems.

1.3 Aim of the Study

The study is aimed at studying the fracture mechanics of Aluminium alloy 7075 using finite element analysis and boundary element techniques. This is focused towards mitigating the influence of fracture and its effects in the aerospace industry applications.

1.4 Research Objectives

The objectives outlined below are intended to fulfil the aim of this study:

I. To characterize fracture mechanisms of AA7075 Aluminium Alloy under varying loading and environmental conditions.
II. To determine key fracture properties such as fracture toughness, crack growth rate, and stress intensity factors.
III. To validate experimental findings with Finite Element Method (FEM) and Boundary Element Method (BEM) simulations.

1.5 Research Questions

To help define the focus of this study towards the objectives lined out, the following questions are pertinent to guiding this research:

I. What is the amount of energy absorbed by aluminium before crack initiation and how much energy is released during fracture?

II. How can mathematical models be used to solve both polar and linear fractural failures and what are the limitations of the existing models?

III. What boundary conditions are applicable in the study of fracture mechanics under different loading conditions and fracture modes?

1.6 Research Hypothesis:

I. H_0: The dissipated energy on crack initiation is equal to or less than the energy absorbed in fracture advancement, indicating that there is net energy difference between these two processes.

H1: The dissipated energy during crack initiation is greater than the energy intake in fracture advancement.

II. H_0: There is no relationship between fracture stress field and the crack tip stress field.

H1: There exists a significant relationship between fracture stress fields and the crack tip stress field, such that variations in the surrounding stress field influence the magnitude and distribution of stresses at the crack tip.

III. H_0: The finite element method and the boundary technique mathematical models do not significantly improve the effectiveness of solving fracture mechanics problems in aluminium 7075 compared to traditional analytical methods.

H1: The finite element method and the boundary technique mathematical models are effective in solving fracture mechanics problems in aluminium 7075.

1.7 Justification for This Research

The research is significant in understanding of the fracture mechanics. By achieving the above objectives, the research provide a deeper understanding of fracture mechanics specific to aluminium 7075 series alloys. This can fill existing knowledge gaps and offer comprehensive insights into crack initiation, propagation, and arrest mechanisms under various loading and environmental conditions. This advancement can improve predictive accuracy and reliability in material behaviour studies. Additionally, the research contributes to engineering and components design. There is need to improve alloy casting, this can only be successful when there is an understanding of the fracture behaviour of aluminium 7075 alloys. This can lead to the development of more resilient materials for high-stress applications.

The research also involve the use of predictive tools such as stress analysis equations and lifespan predictions and simulation models to predict the possibility of crack growth and the effects associated with cracks. On stress analysis, applying precise equations for stress analysis in aluminium 7075 alloys help engineers in designing safer and more durable components, particularly in high-stress environments.

There is also a significant contribution towards aerospace and automotive industries; it will improve safety and reliability. This is achieved through enhancing structural integrity and

ensuring compliance with various standards. By understanding and mitigating fracture mechanisms, the research contributes to the design of effective aerospace and automotive components and structures. This is crucial for preventing catastrophic failures in critical applications. Detailed fracture mechanics data help ensure that aluminium 7075 alloys meet stringent aerospace and automotive safety standards, promoting higher safety levels in these industries. Another area of interest in the automotive industry is maintenance and cost efficiency. Here the important elements are predictive maintenance and extended lifecycle. Improved knowledge of fatigue behaviour and crack growth in aluminium 7075 alloys enables the development of better predictive maintenance schedules. This can reduce unexpected failures and maintenance costs.

Apart from component and structural design, there are also wider implications of the research, such as in areas including sustainability, and education. In sustainability, the research contribute towards more understanding of material efficiency, and light-weighting. In efficiency, there is need to develop alloys with higher fracture resistance that can reduce material wastage and enhance the overall sustainability of engineering projects.

Towards educational and research, it contributes towards academic research and collaborative opportunities. The findings from this research contribute to academic knowledge, providing valuable data and models that can be used in future studies and by students in materials science and engineering disciplines. The research can foster collaboration between academic institutions, industries, and research organizations, promoting the exchange of knowledge and advancing fracture mechanics subject. Achieving the research objectives of the research has a profound impact on the understanding, application, and advancement of aluminium 7075 series alloys in various assembling industries. It contributes to safer, more

dependable, and more efficient use of these materials, with significant implications for both current and future engineering applications.

This research is delimited to the investigation of AA7075 aluminium alloy under controlled loading and environmental conditions. The focus is on evaluating fracture toughness, crack growth behaviour, and fracture modes using experimental methods validated by FEM and BEM numerical simulations. Other factors such as corrosion-fatigue interaction, high temperature creep, and the behaviour of alternative aluminium alloys are beyond the scope of this study. By establishing clear boundaries, the study ensures depth and rigor within the defined research area while providing relevant insights for aerospace applications.

1.8 Methodology

This research combine simulation and experimental analysis which involves comprehensive mechanical testing of selected aluminium 7075 series alloys to evaluate their properties and fracture behaviour under various loading conditions. Mechanical tests, including tensile, fatigue, and fracture toughness tests, measure yield strength, ultimate tensile strength, fatigue life, crack propagation rates, and fracture toughness.

The research involved application of mathematical models based on Linear Elastic Fracture Mechanics (LEFM) principles which is essential for accurately describing the behaviour of crack initiation and growth in aluminium 7075 series alloys. LEFM models focus on the relationship between stress, crack size, and material toughness to predict the onset of fracture. Key to these models is the calculation of stress intensity factors (K), which quantify the stress state near the crack tip. These factors were determined for various crack

configurations and loading conditions to ensure a comprehensive understanding of the fracture mechanics involved.

To address more complex crack geometries and loading scenarios, the models incorporated polar coordinate systems. This approach allowed for a more detailed analysis of the stress and strain fields around crack tips, which are crucial for understanding the fracture behaviour in real-world applications where cracks may not align with traditional Cartesian coordinates. By analysing crack tip fields using polar coordinates, the study provided deeper insights into the localized effects of stress and strain, leading to accuracy in predictions of crack growth and fracture under various conditions.

Finite Element Analysis (FEA) was also used to simulate fracture behaviour and validate the developed mathematical models for aluminium 7075 series alloys. The process begins with the setup of detailed finite element models of the test specimens using FEA software such as Ansys Mechanical or MatLab. These models incorporated accurate material properties and specific loading conditions to reflect real-world scenarios. This comprehensive approach ensured the robustness and accuracy of the fracture models, facilitating their application in aerospace, automotive, and marine industries.

1.9 Significance of the Study

This research is a combination of experiment and simulations to determine the fracture mechanics parameters as the output. These parameters include the life estimation and crack growth rates, stress intensity factors, energy release rates and the stress distribution at the crack tip and propagation zones. It also focused on determining the type of fracture that the material underwent. This was done through analysis using scanning electron microscope images. In this research, it was important to choose a technique, which is user friendly, less tedious and has the

capability to merge both the boundary technique, linear elastic fracture method parameters and the finite element method. The experimental data were analysed using MatLab software, while for the simulation, this study settled on the use of Ansys software as they have robust and variety of boundary conditions related to fracture mechanics and assignment of material properties, which made it more dependable. These software interfaces are user friendly and easy to operate.

The study of fracture behaviour in high-strength aluminium alloys such as AA7075 is critical due to their widespread application in aerospace and automotive structures, where component failure can lead to catastrophic outcomes. A deeper understanding of fracture mechanisms contributes to the design of safer and more reliable structures, optimizes maintenance schedules, and reduces operational costs. Furthermore, advancing predictive methods through FEM and BEM simulations strengthens the theoretical foundations of fracture mechanics and supports innovation in material design and structural safety assessment.

1.10 Limitations of the Study

While experimental studies in fracture mechanics are crucial for understanding material failure and improving design safety, they come with several inherent limitations. The size of the specimen used in experiments significantly influence fracture behaviour. Small-scale tests may not accurately represent the performance of larger components due to scale effects such as stress concentration and crack propagation mechanisms that differ at varying sizes.

The conditions under which researchers conduct experiments can affect fracture behaviour. In a number of research, laboratory conditions do not replicate real-world scenarios where factors like temperature fluctuations, corrosive environments, or complex loading

histories play a role in fracture. Crack Initialization and Growth control in an experimental setting posed challenges. The methods used to create cracks may introduce residual stresses or alter the material properties near the crack tip, affecting subsequent growth behaviours.

Finite Element Modelling Limitations: While numerical simulations complement experimental studies by providing insights into crack behaviour under various conditions, they rely on accurate input parameters derived from experiments themselves. Any inaccuracies in experimental data propagates through simulations, potentially leading to error in conclusions.

The simulation of fracture mechanics is an essential tool for predicting the behaviour of materials under stress, particularly in the presence of cracks or flaws. However, despite its advantages, there are several limitations associated with simulation techniques in this field. Simulations often rely on simplifying assumptions about material behaviour, geometry, and loading conditions. For instance, many models assume linear elastic behaviour, which may not accurately reflect the complex behaviours exhibited by real materials under various conditions. The representation of cracks within a simulation can be problematic. Cracks are often modelled as sharp features; however, real-world cracks may have complex geometries and varying lengths that evolve during loading. This complexity can be difficult to capture accurately in a numerical model.

Simulations majorly focus on static loading conditions; however, real-world applications often involve dynamic loads. Capturing dynamic effects accurately requires advanced modelling techniques that may not always be available or feasible. While simulations provide valuable insights into fracture mechanics, they must be validated against experimental data to ensure their reliability. Discrepancies between simulated results and experimental observations can arise from factors including modelling assumptions and simplifications.

1.11 Structure of Thesis

In the upcoming chapters, this thesis delves deeper into the investigation of fracture mechanics in aluminium 7075 series alloys, focusing on their critical applications in aerospace, automotive, and component design. Chapter 2 provides a comprehensive review of the relevant literature, detailing the studies from other researchers on fracture behaviour, mechanical properties, and previous research on fracture mechanics. Chapter 3 outlines the experimental methodology employed, including material selection, sample preparation, and a detailed description of mechanical testing and simulation procedures. Chapter 4 presents the experimental results, discussion, and analysis, including data from tensile, fatigue, and fracture toughness tests, providing insights into the material behaviour under different loading conditions. Chapter 5 focuses on the research conclusion and the recommendations. This thesis aims to contribute significant advancements in understanding and predicting the fracture behaviour of aluminium 7075 series alloys, thereby enhancing their reliability and performance in critical engineering applications.

1.12 Conclusion

In conclusion, this study focuses on comprehensively exploring the fracture mechanics of aluminium 7075 series alloys, particularly within the contexts of aerospace, automotive, and design applications. The research has addressed fundamental aspects of fracture mechanics, emphasizing how cracks initiate, propagate, and affect these materials under various loading conditions. Through a combination of experimental approaches such as mechanical testing for characterizing properties like tensile strength, fatigue resistance, and fracture toughness and computational methods, including Finite Element Analysis (FEA) and mathematical modelling based on Linear Elastic Fracture Mechanics (LEFM), significant insights were gained. It also

shows the comparative analysis of the modelled fracture mechanics results from Ansys, and the experimental results analysed through MatLab software.

By filling existing knowledge gaps and validating predictive models, this research will contribute towards advancing the field's understanding of aluminium 7075 series alloys' fracture behaviour. This work aims to provide practical guidelines for designing and maintaining structures, ensuring they withstand complex operational conditions and meet stringent performance requirements in diverse industrial settings.

1.13 Contributions of the Study to Knowledge

This study is first of a kind in establishing the fracture mechanics of AA7075 and its parameters. Most studies have focused on other aluminium alloys, which necessitated the choice of this alloy. The study illustrates both linear and polar fracture modes in AA7075 through graphical and analytical means. The study explains while illustrating the factors that lead to the brittle fracture in AA7075 as observed through the SEM images. The study specifically merges the application of two software simulation and analysis of fracture mechanics.

CHAPTER TWO

2.1 Literature review

2.1.1 Introduction

This chapter focuses on the existing research done by scholars that are related to the objectives of this study stating the research titles, the methodologies applied, the results and the conclusion. Information on recommendations made for further research by the previous researchers are stated.

Cracks are always present in the useful life of a component, and they grow from notches to full fractures if not arrested. Understanding their severity is therefore of significance in determining life prediction methodologies [1]. Life estimation is currently conducted from stress intensity factors, which quantify the severity of the cracks. This happens through analytical, numerical, and semi-analytical methods. The growing demand to study fatigue crack growth in mechanical and aeronautical components has been necessitated by incorporating tolerance in design and accurate residual structures, which assumes that a defect is always present and will grow under service usage [2, 3].

Crack propagation study is necessary to ensure that crack growth time is longer than the service life of the equipment. This is done through quantitative and use of software such as CAD, FEA and CFD [4]. Ansys mechanical combines all these capabilities as one. The computer software can be used to estimate fatigue crack growth, service inspection intervals in conjunction with damage tolerance programmes.

Most failures due to fracture happen in mixed mode. However, the most common fracture method is Mode I fracture [5], which involves crack growth under tensile loading on

the structural component. Numerical simulations of crack growth are a predictive tool to evaluate the behaviour of an existing crack. Since crack growth is an incremental process, numerical methods are best suited to evaluate crack growth due to variation of stress intensity factors [6, 7]. Some of the numerical simulation software are MatLab, Ansys Mechanical, FEMFAT and Ansys physics.

Several researchers have conducted experiments and work on the parameters of fracture mechanics. Fracture mechanics being a side field in engineering and science, it is influenced by several parameters. This research focuses on the parameters, which directly impact on the research objectives and the study aim. These parameters include stress concentration around the crack tip, energy release rate during fracture, life estimation, and the crack tip displacement.

2.2 Scholarly studies on Fracture parameters under loading

Dragi *et al.* [4] in their study on Fatigue life estimation of notched structural components, studies the behaviour of the mixed mode fracture on components. The study used analytic and Finite Element Method to perform linear fracture mechanisms analysis of a pin-plug assembly. The focus is to obtain a suitable method to generate the stress intensity factor as a function of crack length [2, 3].

To study the crack growth trajectory, the researchers used Singular finite element method and the Extended finite element method [1]. Various software incorporating FEM have been developed overtime and have proven to be effective in the study of crack initiation and growth. The X-FEM was developed from FEM to incorporate discontinuous enrichment functions to FEM approximation using partition of unity [8, 9]. The study also focuses on the use of minimum strain energy to describe the direction of crack propagation. The criterion

postulates that the direction of crack growth is towards the region of lower strain energy density factor [10].

The criteria is advantageous due to its simplicity and flexibility [11]. This makes it easy to determine the crack growth and angle, which is taken care of by the values of K_I, K_{II} and Stress intensity factors. On further analysis by Dragi *et al*., while considering an aircraft wing lug; showed how to use Finite Element Method to simulate crack trajectory under mixed modes of loading. The researchers considered AA7075 – T7351 of a straight shank male plug [12] with specifications of ultimate tensile strength of 432MPa and K_{IC} of 70.36 MPa$\sqrt{m}$. These specifications alongside an applied stress of 98.1 MPa, force of 63716 N were used to calculate the stress intensity factor, K. To simulate the crack growth, an FEA model in singular quarter point finite elements around the crack tip were developed. SIFs are key parameters for estimating the characteristics of a cracked structure, including fatigue crack growth and structural life predictions. While traditional XFEM might obtain SIFs from crack-tip enrichment, the graphics-focused adaptation described estimates SIFs near the crack front using the displacement method. This method correlates computed finite element displacements with known crack-front displacement equations. Equations for calculating Mode I (KI), Mode II (KII), and Mode III (KIII) SIFs from virtual crack opening displacements are provided. This approach is noted as being simple, fast, and sufficiently accurate for its intended application, although more accurate methods like the J-integral exist. In this adaptation, the estimation of SIFs near the crack front is used to emulate singular stress fields as in linear elastic fracture mechanics (LEFM), allowing the crack to be propagated based on criteria like the strain energy release rate.

The analytical results were compared against the FEA results from the simulation. It was observed that there was much relativity and agreement between the experimental and the simulated results. The study shows that there is a complete correlation of the analytic stress intensity factor and the finite element analysis of the stress intensity factor.

Ghfiri *et al.* [13] in the research on fatigue life estimation after crack repair in Aluminium Alloy 6005 – T6 using the cold expansion hole technique, investigates the Hole drilling and Cold Expansion as a method of hole repair to estimate their beneficial effects on fatigue crack growth. The study defines fatigue crack initiation as the number of cycles required to initiate a new crack of 0.2 mm on a component of a structure under load and examined the effect of stress concentration and strains induced around the crack hole [11]. The study indicates that as the stress intensity factor around the hole increase, the number of cycles, Ni, reduces. Most repair techniques have been developed such as crack infiltration [14], repair welding and metal reinforcement [15], drilling a hole near the crack tip and hole expansion. Hole drilling involves drilling a hole at or near a crack tip. The primary effect of drilling a hole at the crack tip is to produce a notch. This notch effectively eliminates the crack tip singularity effects, which are characteristic of sharp crack tips. Furthermore, increasing the hole radius (r) reduces the stress concentration factor (kt), where kt is defined as the ratio of maximum stress to nominal stress. Reducing stress concentration factor leads to a reintroduction of fatigue crack initiation (FCI) life. This phenomenon, where crack initiation or growth is retarded, is attributed to geometric effects. The retardation effect increases when the hole radius value increases. This is because a larger hole radius at a crack tip decreases the stress concentration factor (kt) and reduces the driving force for crack initiation. Consequently, the number of cycles to crack initiation increases with the hole radius r. Ghfiri *et al.* focused on the method of drilling a hole near the crack tip [16] and hole expansion [17] with the purpose of drilling a hole to produce a

notch, which eliminates the crack tip singularity effects [13]. It was observed that increasing the crack radius reduces the stress concentration factor, Kt [18].

In the experiment, the researchers identified the mechanical properties as, the ultimate tensile strength of 285 MPa, Critical stress of 245 MPa, Young's Modulus of 69 GPa and as Poisson's ratio of 0.3. The edge notched specimen used in this experiment had dimensions of 6 mm thickness and 80 mm width [19]. A constant loading of 9 kN was applied from a servo hydraulic machine while the specifications of the Paris' constants for the material were C = $3.1x\ 10^{-7}$ and m = 2.8. These constants are useful in the determination of the rate of crack growth (da/dN) and the change in stress intensity factors using Paris' Law of fracture mechanics. Holes of radii 1mm, 1.25 mm and 3 mm were drilled around the crack tip [19].

At an initial crack length of 27.5 mm, the change in stress intensity factor was calculated to be 10MPa√m. The study used high strength steel balls of diameter 6 mm to enlarge the holes to diameters of 5.7 mm, 5.8 mm, and 5.9 mm, respectively. It was observed that the crack tip increased while the stress concentration factor, Kt, decreased. It was also observed that the driving force of the crack initiation reduced after the expansion of the hole diameters. The number of loading cycles increased with the increase in the hole radii [15, 20]. The cold expansion process introduces significant compressive residual stress around the hole. These residual stresses are opposite to the applied tensile stresses. They reduce the effective stress driving crack initiation. The magnitude of these residual stresses increases with the degree of cold expansion (DCE%). The effect of the residual stresses produced by hole expansion modifies the properties of the surface layer of the material.

The researchers concluded that, increasing the hole radius leads to a decrease in stress intensity factor and therefore extension of the fatigue crack initiation life. The increase in crack

length leads to a decrease in the applied load with subsequent decrease in maximum stress distribution around the crack tip. The researchers found that the fatigue life equals to crack length of 0.2 mm relative to maximum stresses applied during fracture.

Stevan *et al.* [21] in the study on fatigue life estimation of aircraft structural components with surface cracks under load spectrum [22], developed a computational procedure for residual fatigue life estimation of cracked components. The work used Finite Element Analysis to generate stress intensity factors and analyse crack growth [6, 23, 24]. Finite Element Method (FEM) is used to determine SIFs of structural elements with surface cracks. It is described as a very simple, effective, and accurate technique for evaluating fracture parameters in numerical approaches. FEM involves modeling the structure using elements. For crack problems, FEM often utilizes singularity elements placed at or around the crack tip to accurately capture the stress singularity. The study on multiple cracks used isoparametric quadrilateral elements (PLANE 82) with a triangular element option at the crack tip to address the singularity phenomenon. The SIFs are computed using the displacement extrapolation method, which analyzes nodal displacements near the crack tip. The method involves fitting nodal displacements (u, v, w) in a local coordinate system to theoretical expressions that include KI, KII, and KIII. Formulas are derived to calculate SIFs from these displacements. Mesh density and configuration, such as the radius of the first row of elements around the crack tip and the number of elements, affect the accuracy of SIF calculation, and optimization is necessary. Excessive mesh refinement can degrade accuracy due to ill-conditioned matrices. XFEM is an efficient way to simulate fatigue crack growth because crack growth is incremental, and stress intensity factor (SIF) values are needed at each increment. The XFEM approach can be used to determine the crack trajectory, particularly under mixed mode loading conditions.

A comparison is then made on the computational and the analytical results. The research is based on a slice synthesis approach to compute surface flaw stress intensities [25, 26]. Each slice is considered to react independently under applied stresses in both X-Y and Z-Y planes while under pressure [21, 22]. The specimen had a crack depth 'a' over which pressure 'P' acted upon. The dimensions of the specimen were w=60 mm, t = 10 mm, c = 10 mm, and a = 10 mm. Tensile tests were carried out and the results revealed that the ultimate tensile stress was 83.3 MPa [27]. These data were inserted into the Finite element software and the results generated showed that the crack angle increased, the stress intensity factor increased.

A comparison between the analytical and the Finite Element method results for the stress intensity factors against the crack angle was done and the data [22]. In the numerical validation, for the crack growth, the study concluded that there is evident correlation between the experimental and Finite Element analysis of crack growth and the maximum error in difference of the two methods is 6% [27].

Neeraj *et al.* [28] in their study on the influence of crack offset distance on the interaction of multiple cracks on the same side in a rectangular plate, examined variation of the stress intensity factors and stress distribution around the crack tip using finite element method [29]. The study used a rectangular plate of a unit thickness with cracks, exposed to uniaxial loading conditions and employed the Ansys software with in-built Finite Element functions to determine the stress intensity factors [30].

A shielding effect on mode I SIF due to the neighboring crack. When the cracks are very close, for example at 0.5 mm, the normalized mode I SIF reduces drastically to about 66% of the single edge crack value. As the crack offset distance increases beyond 0.5 mm, the

normalized mode I SIF starts increasing. This shielding effect, where mode I SIF decreases compared to a single edge crack, ceases to exist when the cracks move farther away.

The presence of a neighboring crack results in the appearance of mode II stress intensity factor, which was otherwise absent for a single edge crack. For mode II SIF, there is an amplification effect. The variation of normalized mode II SIF is opposite to that of mode I. When normalized mode I SIF reaches its minimum value (at 0.5 mm), the associated mode II SIF attains its maximum value, which is almost 19% of the mode I SIF for a single edge crack. As the crack offset distance increases, mode II SIF decreases. This amplification effect also becomes insignificant for remotely placed cracks.

Combined Effects: When two edge cracks are extremely close (≤ 0.5 mm), the shielding effect occurs, causing normal stress components (σxx and σyy) to reduce, while the shear component (τxy) increases. This results in a decrease in mode I SIF and an increase in mode II SIF. As the distance increases from 0.5 mm, mode I SIF increases, and mode II SIF decreases. The interaction between cracks becomes negligible for about a distance greater or equal to 20 mm, and both cracks behave essentially as a single crack. The ratio KII/KI shows that mode II SIF plays a significant role in crack growth when cracks are very close, contributing about 27% of mode I SIF. Beyond 20 mm, the contribution of mode II SIF remains below 2%. This indicates that special care should be taken when predicting crack growth from SIFs when multiple edge cracks are very close.

From the theoretical calculation of Mode I stress intensity factor, the work determined that there existed an error of 0.8% from the values of stress intensity factors generated from Finite Element Analysis. The error, as mentioned by Miranda *et al*. tend to increase at a higher mesh density [29]. A uniform pressure intensity of 1.0 MPa was applied on both edges of the

plate. Alongside the material's properties such as Youngs modulus of 70 GPa and Poison's ratio of 0.3, the Mode I and II stress intensity factors were calculated using Pari's Law [29]. Since the material has some thickness, it experiences displacements in all cartesian plane co-ordinates.

It was determined that the stress intensity factor ratio for an offset of more than 0.5 mm increased by 95% of the single edge crack value while for a separation value greater than 0.5 mm, the stress intensity factor reduced by 66%. The researchers generated the crack configurations through identical boundary conditions, crack tip sizes, and full mesh models. As the separation distance increases, the stress concentration increases. Assuming plane strain, the single edge crack has a stress distribution of 731.57 MPa. It is observed that symmetrical stress distribution occurs on the upper and the lower sides of the crack while the horizontal stress and shear stress occur at the crack tip. The analysis established that Mode I stress intensity factor depend on the variation of the symmetrical stresses on the upper and lower side of the crack tip, which is higher in single edge cracks than in multiple edge cracks. The shear stress is responsible for the development of the Mode II fracture on the crack and the stress distribution.

Gi *et al*. [31] study on the energy release rate of hyper-elastic solids with a nano-crack, carried out a molecular statistic computation to investigate the atomistic nature of fracturing and applied the concept of J-integral and compared the obtained results to those of finite element method [32]. The work used an edge crack model to perform simulations under plane strain conditions with boundary conditions on the Z- axis. The study applied the embedded atom method [33] and the modified embedded atom method [34] to describe the interatomic forces. Displacements displayed as v and -v were applied at ago, both on the top and bottom regions of the model respectively [31, 35]. For any closed contour in a hypothetic region

containing no singularities, J = 0, since it is path-independent on the integration contour [36]. Using the boundary conditions of the edge crack, it was determined that the value of J-integral obtained is signified as the energy release rate of the hyper elastic solid [31]. To obtain the critical energy release rate, an observation was made to a point of sudden drop in the average nominal stress [37].

The energy release rate was equally calculated using the finite element analysis in-built function on ABAQUS and the results were compared to the energy release rate obtained from the J-integral method [38]. The resultant energy release rate from finite element method, G^{LEFM} was 3.26 J/m^2 while that from the J-integral method was 4.04 J/m^2. This showed a correlation of the J-integral obtained from the strain energy density and the results of the directly measured energy release rate. This study also examined the effect of cack length on the energy release rate. It was determined that there was little to negligible influence of crack length on energy release rate. A range of 5 mm $\leq$ c $\leq$ 25 mm was tested and showed a correlation of the energy release rate from the finite element and the results from the J-integral in the influence of crack length [39]. The study concluded that the energy release rate is influenced by the hyper-elastic nature of the solids and the effect of the non-linear zone of hyper-elastic solids can be changed by varying the crack length at the nanoscale [40].

Abilash *et al.* [39] in the study on experimental investigation to establish total energy release rate for unidirectional glass composite under mixed mode loading, focused on the use of compact tension shear [41] and four-point band [42] mixed mode fracture specimen. Plots of the load against displacement data were made to evaluate the peak loads for both compact tension shear and four-point band specimen at different loading angles and crack positions [9]. The data were also used to estimate the total energy release rate during the tests. The specimen

used was of dimensions 75 mm x 45 mm x 9 mm. A crack was introduced, which is transverse to the fibre orientation. A load of 100 kN and a displacement of 2 mm/min were applied with an initial crack length of 22.5 mm, a geometric factor of 0.5, load angle of 0 - 90^0 at 15^0 increments.

The translaminar toughness was measured in terms of total energy release rate [9]. The stress intensity factors were also calculated from the data obtained from the experiment. The total energy release rate is the sum of the energy release rates from Mode I and Mode II [41]. It was determined that the energy release rate in Mode I fracture is greater than that released in mode II during the compact tension shear boundary conditions. The research also indicated that components loaded in bending and shear loads fail earlier in pure bend load than in mixed mode loading [9].

The study concluded that the energy release rate for Mode I load in four-point band specimen is found to be almost twenty times higher as compared to energy release rate with compact tension shear specimen. The work further established that energy release rate depends on the loading angle on the specimen. The energy release rate required to initiate cracks in Mode II is greater than the amount of energy required in Mode I.

2.3 Linear Elastic Fracture Mechanics and its Applications

Linear Elastic Fracture Mechanics (LEFM) is a theoretical framework used to analyse the behaviour of materials containing cracks under stress. This approach assumes that the material behaves elastically, meaning it returns to its original shape after the removal of applied loads, and that the crack tip experiences singular stress fields. LEFM is particularly useful for predicting the conditions under, which cracks will propagate in brittle materials [47]. Linear

Elastic Fracture Mechanics has key components that aid in the calculation of the various fracture mechanics parameters.

The Stress Intensity Factor (K) measures the intensity of the stress field near a crack tip and depends on the applied load, crack length, and the component's geometry. Fracture Toughness (Kc) is a material property that reflects a material's resistance to fracture. The critical stress intensity factor (Kc) signifies the point at which crack propagation begins; if the stress intensity factor exceeds Kc, unstable crack growth occurs. The Energy Release Rate (G) quantifies the energy released from a system as a crack expands. For stable crack growth, the energy release rate must be less than or equal to the critical energy release rate Gc [48].

LEFM has widespread applications in engineering fields such as civil engineering, mechanical engineering, and materials science. It helps engineers design structures and components by predicting failure modes and ensuring safety through proper material selection and structural integrity assessments.

While LEFM provides valuable insights into fracture behaviour, it has limitations; it primarily applies to brittle materials and situations where plastic deformation at the crack tip can be neglected [49]. For ductile materials or cases involving significant plasticity, other approaches such as J-integral methods or elastic-plastic fracture mechanics may be more appropriate [47].

2.4 Finite Element Analysis as a technique of solving Fracture Mechanics

Finite Element Analysis enables numerical approximation of solutions to problems involving stress, strain, and deformation in materials with intricate geometries and loading

conditions [50]. This method is particularly valuable when dealing with cracks in materials, as it can provide detailed insights into stress distribution and potential failure mechanisms.

It's especially powerful to evaluate Stress Intensity Factors (SIFs), predicting fatigue life using S-N curves and Paris' Law, Modeling crack growth paths in 2D and 3D domains, Assessing damage tolerance in materials like aluminum alloys. The cracks are modeled using refined meshes near the tip. Quarter-point elements are used to capture singular stress fields while Extended FEM (XFEM) allows modeling discontinuities without remeshing. It uses contour integration to determine J-integral and interaction integrals for mixed-mode cracks.

FEA is applicable in several sectors of engineering including automotive to predict the fatigue life under radial and cornering loads. In Aerospace to assess crack growth under cyclic thermal and mechanical loads. In pressure vessels to evaluate crack stability under internal pressure and in Biomedical implants to simulate fracture under physiological loading.

The first step in Finite Element Analysis involves discretizing the continuum into smaller, simpler parts called finite elements. These elements can take various shapes (triangular, quadrilateral, tetrahedral) depending on the geometry of the structure being analysed. The entire domain is represented by a mesh of these elements [50]. Each finite element is governed by its own set of equations that describe its behaviour under applied loads. These equations typically arise from fundamental principles such as equilibrium, compatibility, and material constitutive laws. The relationships between nodal displacements and stresses are established through shape functions [51]. Once individual element equations are formulated, they are assembled into a global system of equations that represents the entire structure or component being analysed. This process involves combining contributions from all elements while considering boundary conditions and constraints [52].

Properly defining boundary conditions is crucial in Finite Element Analysis as they dictate how the model interacts with its environment. Boundary conditions can include fixed supports, applied loads, or symmetry constraints that influence how stresses are distributed throughout the model. The assembled system of equations is then solved using numerical methods to obtain unknown nodal displacements. Common techniques include direct solvers like Gaussian elimination or iterative methods such as the conjugate gradient methods [52].

After obtaining nodal displacements, post-processing techniques are employed to derive other quantities of interest such as stress intensity factors at crack tips, stress concentration around the crack tip and energy release rates associated with crack propagation. Visualization tools help interpret results through deformation animations.

FEA is an indispensable tool in fracture mechanics due to its ability to handle complex geometries and loading scenarios. It can be used to compute stress intensity factors at crack tips under various loading conditions by analysing localized stress fields around cracks. By simulating incremental crack growth within a material under load, Finite Element Analysis can predict critical points where unstable crack propagation may occur based on material properties and loading scenarios. It allows for analysis under mixed-mode loading conditions, which is essential for understanding real-world applications where multiple forces act on structures. Advanced Finite Element Analysis techniques can accommodate nonlinear material behaviour near cracks, making it suitable for ductile materials where traditional linear elastic approaches may fail.

While Finite Element Analysis offers significant advantages in solving fracture mechanics problems, it also has limitations. These are not limited to; the accuracy of results heavily depends on mesh quality, poorly defined meshes can lead to inaccurate predictions.

Complex models with fine meshes require substantial computational resources and time for analysis. Effective use of Finite Element Analysis requires a deep understanding of both the software tools available and the underlying physical principles governing fracture mechanics [50].

2.5 Boundary Element Techniques

The boundary element technique (BET) is a numerical method used in fracture mechanics to analyse problems involving cracks and other discontinuities in materials. This method is particularly advantageous for solving problems in two-dimensional and three-dimensional elasticity, and for modelling the behaviour of structures under various loading conditions [53]. Below is a comprehensive description of the boundary element technique as it applies to fracture mechanics.

The boundary element method is based on the principle of reducing the dimensionality of the problem. Instead of discretizing the entire volume of the material, as done in finite element methods, BET only requires discretization of the boundaries where the physical phenomena occur. This approach significantly reduces the number of equations that need to be solved, making it computationally efficient [53]. The foundation of BET lies in potential theory and integral equations. In fracture mechanics, one typically uses boundary integral equations derived from fundamental solutions to describe how stresses and displacements behave around cracks or discontinuities [52].

In BET, cracks are represented as singularities along the boundaries. The stress intensity factors (SIFs), which are critical parameters for predicting crack propagation, can be computed directly from these boundary conditions without the need to mesh the interior domain. The boundary is discretized into elements in which each element contributes to the overall solution

by defining how loads are distributed along the crack surfaces and surrounding areas. The formulation typically involves setting up a system of linear equations based on boundary conditions. These equations are then solved using numerical techniques, allowing for calculation of unknown values at discrete points along the boundary [54].

Boundary Element Technique has various advantages over other techniques for solving fracture mechanics. Since only boundaries are discretized, there are fewer degrees of freedom compared to volume-based methods. BET can effectively model problems involving infinite or semi-infinite domains without requiring complex meshing techniques [52]. It therefore provides high accuracy for problems with singularities such as cracks due to its ability to capture stress concentration effects precisely.

Boundary element techniques have been widely applied in various fields including civil engineering, mechanical engineering, and materials science for analysing crack propagation, stress distribution around flaws, and evaluating structural integrity under different loading scenarios. While BET has many advantages, it also has limitations such as difficulties in handling non-linear problems and challenges associated with dynamic analysis or time-dependent loading conditions [52].

The Boundary Element Technique (BET) can be used to solve partial differential equations (PDEs) that have been reformulated as boundary integral equations. Unlike the Finite Element Method (FEM), which discretizes the entire domain, BEM only requires discretization of the boundary making it highly efficient for problems involving infinite or semi-infinite domains, like crack propagation. Fracture mechanics often deal with stress concentration near cracks, which are localized phenomena. BET is ideal because it reduces the problem

dimensionality; It provides high accuracy near singularities, such as crack tips; It allows efficient modeling of infinite domains, which is common in fracture analysis.

The main concepts in BET include transformation of the governing PDEs into boundary integral equations using Green's functions. For linear elastic fracture mechanics (LEFM), this involves Somigliana's identity for displacements and tractions. Special techniques like dual boundary element method allow modeling both crack surfaces independently, improving accuracy in mixed-mode fracture.

Other advantages of BET include accurate SIF evaluation and crack tip modeling, efficient handling of anisotropic and layered structures, BET can be extended using Dual Reciprocity Method for time-dependent analysis, BET handles coupled thermal-mechanical fields with fewer elements.

As compared to FEM, BET has the following advantages; while FEM consider the entire discretized domain, the BET considers only the domain boundaries. FEM requires remeshing of the entire crack model while BET handles cracks as internal boundaries. FEM has higher computational costs for a larger domain while BET has lower costs for the same domain size. FEM requires accurate refinement near the crack tips while BET naturally captures singularities at the crack tips.

Other techniques used within BET to analyze fracture include Dual Boundary Element Method (DBEM) which uses displacement and traction equations on opposite crack faces for mixed-mode analysis. Subregion BET which divides the domain into subregions for composite or multi-material problems. Discontinuous quarter-point elements which enhance accuracy near crack tips by capturing singular displacement fields.

2.6 Fatigue and Fracture Toughness Testing

Fracture toughness testing is a critical technique in the field of fracture mechanics, which is the study of the propagation of cracks in materials. Fracture toughness (K_{IC}) is defined as a material's ability to resist crack propagation when subjected to stress. It is an essential property for materials used in structural applications, where failure due to crack growth can lead to catastrophic consequences [4].

Fracture toughness testing typically involves the use of standardized specimens subjected to controlled loading conditions. The most common test methods include the ASTM E399 standard for plane strain fracture toughness and ASTM E1820 for elastic-plastic fracture toughness [1]. These tests provide quantitative measures of a material's toughness under various loading conditions.

Specimens are usually made from homogeneous materials and are often shaped into specific geometries, such as compact tension (CT) or three-point bend (TPB) configurations [43]. The geometry is crucial as it influences stress distribution around the crack tip. A pre-existing crack is introduced into the specimen, which serves as a stress concentrator. This crack can be created through mechanical means or by using fatigue loading techniques, ensuring that it has a well-defined length and orientation. The specimen is then subjected to tensile until fracture occurs. The loading rate can also be varied to study dynamic versus static fracture behaviour [55].

During testing, data such as load versus displacement curves are recorded. The maximum load at which the specimen fractures provide critical information about its toughness. After fracture, the resulting surfaces are examined using fractography techniques such as

observation under optical microscope or under Scanning Electron Microscope [56] to understand the failure mechanisms involved, whether they were ductile or brittle in nature and how they relate to the material's microstructure. The results from these tests allow engineers and scientists to calculate the critical stress intensity factor (K_{IC}), which indicates whether a material will fail under given service conditions based on its inherent properties and existing flaws [2]. Fracture toughness testing plays an essential role in material selection for engineering applications, particularly in industries such as aerospace, automotive, and civil engineering where safety and reliability are important.

Fatigue testing is a critical technique employed in the field of fracture mechanics to evaluate the durability and reliability of materials under cyclic loading conditions. This method is essential for understanding how materials behave when subjected to repeated stress, which can lead to the initiation and propagation of cracks over time [4]. The fatigue test simulates real-world conditions where components experience fluctuating loads, thereby providing insights into their performance and lifespan. It involves subjecting a material or component to repeated cycles of stress and strain until failure occurs. The primary purpose is to determine the endurance limit, which indicates the maximum stress level that a material can withstand for an infinite number of cycles without failing.

There are several types of fatigue tests, including: Rotating Beam Tests which is used primarily for metals, where a specimen is rotated under bending loads until failure occur [57]; Axial Load Tests which involves applying axial loads on specimens to assess their response under tension-compression cycles [58]; Bending Tests, where specimens are subjected to bending stresses until failure occurs and Torsional Tests in which twisting forces are applied to evaluate torsional fatigue resistance.

Fracture mechanics provides a framework for understanding crack initiation and growth in materials. By integrating fatigue testing with fracture mechanics principles, engineers can predict how cracks will propagate under cyclic loading conditions. This integration helps in assessing the structural integrity of components and predicting failure modes. During the fracture mechanics tests, graphical interpretation of data is done for further understanding of the fatigue behaviour of a material. These graphs include:

S-N Curve: This is a plot relates cyclic stress (S) and the number of cycles to failure (N). It is fundamental in characterizing material behaviour under fatigue.

Fatigue Crack Growth Rate (da/dN): This parameter measures how quickly a crack grows per cycle of loading [49]. It is often plotted against the range of stress intensity factors (ΔK) [21].

Energy release rate curve: This graph shows the rate of energy release or absorption with time during the fracture mechanics tests, more so during the cyclic loading. It can also be plotted in terms of J-integral against time [31].

Fatigue testing is majorly used in industries, including aerospace, automotive, civil engineering, and manufacturing. It aids in designing safer structures by allowing engineers to predict potential failure points and enhance material selection processes. Post-failure analysis from fatigue tests often reveals characteristic finite element analysis issues such as beach marks or striations on fracture surfaces, which provide insights into the mechanisms leading up to failure. Fatigue testing serves as an indispensable technique within fracture mechanics by enabling researchers and engineers to understand material behaviour under cyclic loading

conditions effectively. This understanding is crucial for ensuring safety and reliability in engineering applications.

2.7 Summary

From the researchers' works on fracture mechanics and its parameters as discussed in this chapter, it is evident that there is an interrelation between the Equations used to obtain the specific parameters. These include equations of obtaining Stress intensity factors, energy release rates and stress concentration factors. As the researchers explored different parameters in the investigations, one point of note is that fracture mechanics in a material is dependent on the applied stresses, the radius or length of initial crack and the geometric factor associated with the thickness and material used during the test. It is therefore, important that further research on fracture mechanics should employ a methodology that will corroborate or compare with the results of the previous studies. It is also evident that fracture mechanics form part of daily challenges that engineers must deal with or must consider in design work, either to minimize its effect or to prolong the life estimation of the crack above the service life of the material used on a component.

CHAPTER THREE

3.1 Methodology

3.1.1 Introduction

Fracture mechanics as a field or science and materials engineering, deals with the initiation of cracks, stress distribution around the crack and the energy released as the crack grows. In this study, various techniques including Linear Elastic Fracture Mechanics (LEFM), Finite element Method (FEM), Boundary techniques (BET) [43], Fatigue and Fracture testing methods (Tensile Test), were used to study these fracture mechanics parameters. Software such as MatLab [44] and Ansys Mechanical [45] were used to analyse the results and to obtain simulated data respectively. These software have been identified due to their robustness and incorporation of most techniques used in the analysis of fracture mechanics problems [46]. After the experiments, the fractured samples were observed under a scanning electron microscope against an unfractured sample to determine whether the fracture undergone by the samples is brittle or ductile. This observation will also help in the determination of the physical effects of fracture on the areas around the crack tip.

The methodology of research is strongly anchored on the experiments from the tensile and fracture test machines and the simulation that will result into use of software to analyse the collected data as summarised in the Figure 3.1. For this research, Mode I fracture is the point of focus; it is determined that using MatLab for analysis and Ansys 2024R2 for simulation, best results for the parameters under study objectives would be arrived at. Therefore, this research narrows down to have the data analysed through MatLab software as it can generate the nodal and elemental behaviour of the meshed specimen and incorporate the finite element and

boundary layer techniques. MatLab also provides the interface for graphical presentation of the data and incorporation of mathematical formulae used in the analysis of the behaviour of the alloy under loading. On the other hand, Ansys enables the collection and simulation of the behaviour of the material through various set of boundary conditions and loading. For purposes of ease of presentation and analysis, the two software are a perfect fit for this research. To further study the effects of the loading on the material, an analysis through scanning electron microscope was conducted to determine whether the fracture is brittle or ductile, images of which are attached in the results discussion section.

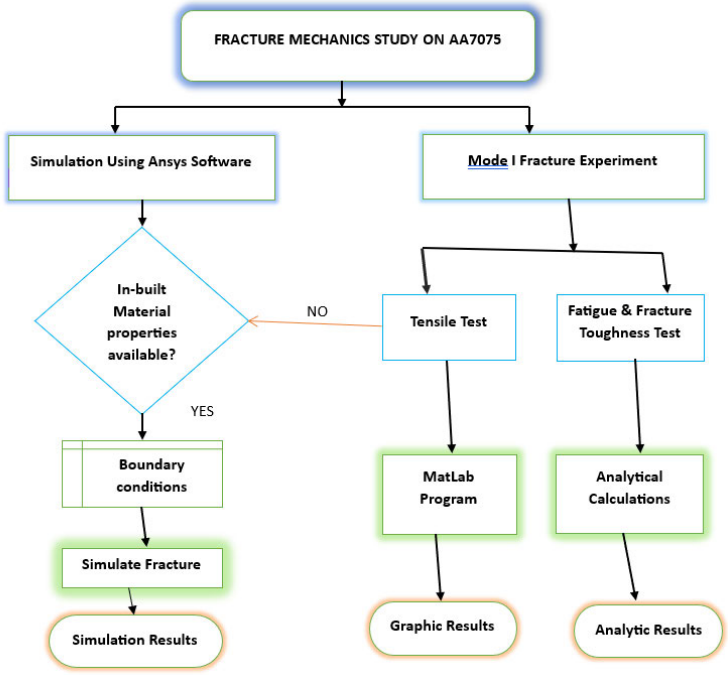

Figure 3.1: Summary Flowchart of the Research Methodology

3.2 Methodology of achieving the Objectives

3.2.1 Tensile and Fatigue Test

Introduction and Purpose

Fatigue testing on an edge-cracked specimen was performed to investigate the crack growth behaviour of materials under repeated cyclic loading. The main goal of the test was to determine how the crack propagates with respect to the applied stress intensity range and to extract key parameters such as the fatigue crack growth rate and the material constants used in fatigue life prediction models. This experimental procedure provides the foundation for understanding crack initiation, stable crack propagation, and the transition to final fracture within the framework of fracture mechanics.

Specimen Preparation

The test began with the fabrication of a standardized specimen for a single-edge notched tension (SENT) configuration. The material was machined to precise dimensions according to relevant testing standards such as ASTM E647. An artificial notch was introduced on one side of the specimen using a fine machining process to serve as a crack starter. To ensure a sharp crack tip and realistic stress concentration, the specimen was then fatigue pre-cracked by applying controlled cyclic loading at a low amplitude. This pre-cracking process eliminated the influence of machining marks and produced a natural crack tip with minimal plastic deformation.

Test Setup and Instrumentation

The prepared specimen was mounted on a servo-hydraulic fatigue testing machine equipped with load control and displacement measurement systems. The test fixture is aligned carefully to prevent misalignment that could affect the crack growth behavior. A crack-length measurement system was used to track crack propagation during the test. The load cell and sensors are calibrated to ensure accurate force and displacement readings throughout the experiment.

Loading Conditions and Fatigue Cycling

The fatigue test was carried out by applying cyclic tensile loading with a constant load ratio, defined as the ratio of minimum to maximum load in each cycle. The amplitude of the applied load was set such that the stress intensity range is sufficient to produce measurable crack growth but below the level that would cause immediate fracture. The test machine automatically cycled the load, and crack length data were recorded continuously at intervals as the test progressed.

Monitoring Crack Growth

Crack growth was monitored throughout the test to determine how the crack length evolves with the number of load cycles. The approach involved a compliance method, where changes in specimen flexibility indicate crack extension. Alternatively, direct observation can be done using a traveling microscope, digital camera, or crack-length gauge. At regular intervals, the machine was paused to measure or verify crack length accurately. This information was used to construct a crack growth history, showing the relationship between the crack extension and the number of applied cycles.

Data Acquisition and Analysis

During the test, the fatigue testing system continuously recorded applied load, displacement, and cycle count. The data collected were processed to compute the crack growth rate, defined as the rate of change of crack length per loading cycle. This rate was then correlated with the corresponding stress intensity range for each crack length interval. The resulting data were typically plotted on a logarithmic scale to obtain a fatigue crack growth curve, which was used to identify different crack growth regimes, such as the near-threshold region, stable crack growth region, and rapid fracture region.

Determination of Material Constants

From the fatigue crack growth curve, key material parameters are extracted to describe fatigue behaviour. These include the constants that define the slope and intercept of the crack growth law used for fatigue life prediction. The experimentally derived relationship allows engineers to predict how long a component can operate safely under cyclic loading before reaching a critical crack size. These constants were unique to the material and are influenced by factors such as microstructure, environment, and loading frequency.

Crack Propagation and Fracture Observation

Once the crack grows to a critical size, the specimen typically undergoes final fracture. The fractured surfaces were examined using scanning electron microscopy to study the crack path and to confirm that the fracture mode is predominantly fatigue controlled. Features such as beach marks or striations were observed, confirming incremental crack growth under cyclic

loading. The final fracture appearance also helped identify any transition from stable crack growth to unstable failure.

Post-Test Calculations and Validation

After the experiment, the measured data were validated by checking for consistency between different measurement methods and by comparing the results to reference standards or published data. The final analysis involved estimating the total fatigue life, evaluating the influence of loading ratio and frequency, and assessing any deviations from expected behavior. The reliability of the data was confirmed through repeat tests under varied load amplitudes to ensure repeatability and accuracy.

Reporting and Interpretation of Results

The final stage involved compiling all measured data, test conditions, and observations into a structured report. This report typically includes specimen geometry, material properties, loading conditions, pre-crack details, and the fatigue crack growth curve. Interpretations focused on how the material resists crack propagation, the rate of fatigue damage accumulation, and the implications for design or maintenance of structural components. The results serve as a basis for validating numerical models and for developing predictive maintenance strategies in engineering applications.

3.2.2 Linear Finite Element Method

Specimen geometry and measurements

Before conducting the fracture test, all specimen dimensions such as thickness, width, and crack length were measured accurately using calibrated instruments. These measurements

ensure that the geometry used in the stress intensity factor calculations truly represents the tested sample. Small errors in these dimensions would have led to significant deviations in the computed fracture parameters, so it was essential to record them carefully and verify that they fall within the standard's recommended limits for the chosen specimen type.

Pre-Crack preparation and sharpness

This was achieved by fatigue pre-cracking under cyclic loading to produce a natural, atomically sharp crack front. The pre-crack extends beyond any machining marks from the original notch so that the actual fracture got initiated from the fatigue crack rather than from residual damage or blunt edges. Ensuring a sharp pre-crack helped to minimize plastic blunting and allows the test to reflect true linear-elastic fracture behaviour.

Loading rate and data recording

The loading was applied slowly and under controlled conditions so that the material's response remained quasi-static and not influenced by strain rate effects. Rapid loading would have induced dynamic effects that invalidate the assumption of linear elasticity. During the test, the load and displacement data were sampled continuously and at a high enough frequency to capture the complete fracture event, including the point of crack initiation and propagation.

Measurement system calibration

Accurate displacement measurement was critical for evaluating the specimen's compliance and for determining the load at fracture. This was achieved by attaching a crack mouth opening displacement (CMOD) gauge or clip gauge at the notch mouth. Calibration of the gauges eliminated measurement errors and guaranteed that the load–displacement curve accurately represents the specimen behavior.

Verification of small-scale yielding

To ensure that the test remained within the linear elastic regime, the plastic zone around the crack tip was made small relative to the crack length and specimen dimensions. After the test, an estimate of the plastic zone size was made to confirm that plastic deformation did not dominate the response. This step validated that the assumptions of linear elasticity hold and that the stress intensity factor accurately represented the material's resistance to crack growth.

Plane-strain condition and specimen thickness

For the measured fracture toughness to be considered a true material property, the specimen was of considerable thickness to achieve plane-strain conditions at the crack tip. This condition ensured that out-of-plane deformations are restrained, producing the most conservative and reproducible measure of fracture toughness. If the thickness was too small, the stress state would become plane-stress dominated, and the result is only a conditional toughness value rather than a valid plane-strain value.

Reliability of the results

To confirm that the measured fracture toughness represented the material rather than a single specimen anomaly, three valid tests were performed under the same conditions. Consistent results across multiple specimens indicated that the test setup, material behavior, and data analysis were reliable. Repetition also helped identify outliers that might have arisen from specimen preparation errors, instrumentation problems, or material variability.

3.3 Finite Element and Boundary Element Methodology

3.3.1 Finite Element Methodology

Geometry definition and Material properties

This involved the creation of a geometric model of the specimen, including the crack length and orientation. The geometry accurately represented the test specimen, ensuring all features influencing stress concentration are included. Appropriate material properties such as Young's modulus, Poisson's ratio, and yield stress were assigned. To consider the plastic behavior of the material, the full stress–strain curve was defined. This step was aimed at establishing the foundation for a physically realistic simulation.

Meshing and Crack tip refinement

The model was then discretized into finite elements. Mesh refinement near the crack tip was critical, as this region experiences steep stress gradients. Special crack-tip elements, such as quarter-point were used to simulate the singularity in the stress field accurately. The rest of the model had a coarser mesh to reduce computational cost. The mesh was properly refined to ensure minimized numerical errors and that the stress intensity factor and energy release rate were extracted accurately.

Boundary conditions and Loading

Boundary conditions were applied to replicate the physical loading scenario, which was tensile load. The constraints prevented rigid body motion while not over-restraining the model. The applied loads represented realistic service conditions, and symmetry was used where applicable to simplify the model.

Stress field analysis

After setting up the mesh and boundary conditions, the finite element solver was run to compute displacements, strains, and stresses across the model. The results near the crack tip were carefully examined to ensure that the expected singular stress distribution appeared. The accuracy of the numerical results depended strongly on the mesh density, convergence criteria, and numerical precision of the solver.

Fracture parameters extraction

Once the analysis were complete, post-processing was carried out to determine key fracture parameters such as the stress intensity factor, energy release rate, and the J-integral. These were extracted using techniques of displacement correlation method, the virtual crack closure technique, and the domain integral method. The computed values were verified for path independence and convergence to ensure they represent true physical quantities rather than numerical artifacts.

Crack propagation Modelling

For simulations involving crack growth, the crack front was advanced incrementally based on the computed fracture criterion. This involved remeshing the region around the new crack tip and using extended finite element methods that allow crack propagation without remeshing. The crack growth direction was be determined using criteria of maximum energy release rate.

Validation and convergence checks

Finally, the results were validated to confirm their accuracy. This involves comparing the computed stress intensity factors or energy release rates with analytical solutions and experimental data for similar configurations. Mesh refinement studies were conducted to ensure convergence, meaning that further mesh refinement does not significantly change the results.

3.3.2 Boundary Element Technique Methodology.

Model definition and crack representation

In the boundary element approach, only the boundaries of the structure are discretized instead of the entire volume, reducing the computational effort. The geometry of the structure and crack was defined by its surface and edge boundaries. Material properties, such as elasticity constants, were also specified at this stage. For fracture problems, the crack surfaces were modeled explicitly, and their positions and orientations were carefully defined to capture the correct stress concentration behavior.

Discretization of Boundaries

The boundary of the model, including the crack faces, were divided into boundary elements. Finer discretization was applied around the crack tip, where stress gradients were highest. Elements in these regions were made smaller to accurately resolve the singular stress and displacement fields near the crack tip. The rest of the boundary were meshed more coarsely to reduce computational demand.

Application of Boundary Conditions

Boundary conditions were applied in terms of displacements on the model's surface. These conditions replicate the real-world loading and constraint scenarios. For cracks, the boundary conditions on the crack faces were typically traction-free, allowing them to open naturally under applied loads. The application of these conditions was critical, as inaccuracies here could lead to unrealistic stress results near the crack tip.

Solution of Boundary Integral Equations

The boundary integral equations, which relate stress and displacements at the boundaries, were then assembled and solved. Unlike FEM, where the entire volume is discretized, BEM requires solving only for boundary nodes. This step produced the displacement and traction distributions along the boundaries and around the crack surfaces. The accuracy of this solution strongly depended on the proper formulation of singular integrals near the crack tip and on numerical stability during matrix inversion.

Evaluation of Fracture Parameters

Once the boundary solution was obtained, the stress intensity factor and energy release rate were determined from the near-tip stresses and displacements. In BEM, this is typically done through specialized displacement extrapolation techniques that capture the singular field. The computed fracture parameters were then compared to critical material values to assess the likelihood of crack growth.

Crack growth Simulations

For crack propagation analysis, the crack front was advanced incrementally using the calculated fracture parameters. The direction and rate of crack growth were determined using fracture criteria, and the boundary mesh was updated accordingly. Because only the boundaries were discretized, updating the mesh in BEM is generally simpler and more efficient than in FEM. The process continued iteratively until the crack reached a critical length or the structure failed, like in sample 3.

Validation and Verification

As with FEM, the final step in BEM analysis was to validate the numerical results. This involved checking the consistency of the computed fracture parameters with theoretical or experimental data and ensuring that results were independent of mesh density or element type. Verification against analytical solutions for edge in simple geometries, helps confirm the accuracy and stability of the model before applying it to complex engineering problems.

3.4 Analytical Evaluation of Fracture Mechanics Parameters.

3.4.1 Stress intensity factor Evaluation.

Several researchers including [41, 42, 59] have done studies in fracture mechanics area to determine the relationship between load application in various modes of fracture and the stress intensity factors. The expressions obtained from these studies are used in this research to obtain the stress intensity factor of AA7075 under mode I fracture. The stress intensity factor is obtained from Equation 3.1 [41].

$$K_I = Y.\sigma_x\sqrt{\alpha.\pi} \qquad (3.1)$$

where σ_x is the applied stress, α is the crack length and *Y* is the geometry factor.

The geometry factor for the crack at the centre of the edge of a specimen in an infinite plate under uniform tension is given by Equation 3.2 [42].

$$Y = 1.12 - 0.231(a/B) + 10.55(a/B)^2 - 21.72(a/B)^3 + 30.39(a/B)^4 \quad (3.2)$$

where **B** is the width and **a** is the initial crack length of the material sample.

3.4.2 Fatigue crack growth and Crack life estimation of A7075

Cracks are mostly present on the surface and the jointed parts of equipment. It is important to determine the life estimation of the crack growth to ensure that the service life of the equipment is longer than the crack growth lifespan. This research borrows from the research done by [4, 21] to express the experimental value of this parameter. The crack life estimation can be obtained using the expressions in Equation 3.3 adopted from Paris' Law [3]

$$\frac{da}{dN} = c\Delta K^m; \quad (3.3)$$

where c and m are Paris' material constants.

The change in stress intensity factor is obtained from Equation 3.4 and 3.5 [3].

$$\Delta K = (1 - R)\, K_{max} \quad (3.4)$$

$$R = \frac{K_{min}}{K_{max}} \quad (3.5)$$

Replacing R into Equation 3.5, the change in stress intensity is obtained as;

$$\Delta K = (Kmax - K_{min}) \quad (3.6)$$

The values of c and m for AA7075 are 8.87E-8 and 3.14, respectively.

The total crack growth is obtained as the sum of the crack growth rate and the length of the original crack as shown in Equation 3.7 [13]

$$\frac{da}{dN} + a = a' \qquad (3.7)$$

where a' is the estimated crack length and a is the original crack notch length.

3.4.3 Stress distribution around the crack tip.

Upon loading, the crack tip and the areas around the crack propagation experiences stresses. These stresses vary with the proximity of the propagation areas to crack tip. As the crack displacement advances, the stress distribution can be obtained using the expressions in Equations 3.8 – 3.10 [49]

$$\sigma_x = \frac{1}{\sqrt{2\pi r}}\left(K_I \cos\left(\frac{\theta}{2}\right)\left[1 - \sin\frac{\theta}{2}\sin\frac{3\theta}{2}\right]\right) \qquad (3.8)$$

$$\sigma_y = \frac{1}{\sqrt{2\pi r}}\left(K_I \cos\left(\frac{\theta}{2}\right)\left[1 + \sin\frac{\theta}{2}\sin\frac{3\theta}{2}\right]\right) \qquad (3.9)$$

$$\tau_{xy} = \frac{-1}{\sqrt{2\pi r}}\left(K_I \cos\left(\frac{\theta}{2}\right)\sin\frac{\theta}{2}\sin\frac{3\theta}{2}\right) \qquad (3.10)$$

Since just before the fracture begins the angle of the crack is 0, the equations reduce to Equations 3.11 – 3.13 [49].

$$\sigma_x = \frac{1}{\sqrt{2\pi r}}\left(K_I \cos\left(\frac{\theta}{2}\right)\right) \qquad (3.11)$$

$$\sigma_y = \frac{-1}{\sqrt{2\pi r}}\left(K_I \cos\left(\frac{\theta}{2}\right)\right) \qquad (3.12)$$

$$\tau_{xy} = 0 \qquad (3.13)$$

3.4.4 Energy Release rate during fracture

To evaluate the energy released during the fracture, the stress intensity factor and dimension properties of the specimen including the thickness are importantly considered. The expression for the energy released during fracture is shown in Equations 3.14 [49].

$$G = \frac{B}{E} K_I{}^2 \qquad (3.14)$$

where B is the width of the specimen and E is the Young's modulus, K_I is the SIF.

3.5 Simulation of Fracture Mechanics.

In this research, it was important to choose a technique, which is user friendly, less tedious and has the capability to merge both the boundary technique, linear elastic fracture method parameters and the finite element method [43].

ANSYS is a powerful FEA platform that enables engineers to; Simulate crack initiation and propagation under various loading conditions, evaluate stress intensity factors (SIFs), J-integrals, and energy release rates, predict fatigue life using S-N curves and Paris' Law, model complex geometries and materials, including composites and anisotropic media.

It supports both Linear Elastic Fracture Mechanics (LEFM) and Elastic-Plastic Fracture Mechanics (EPFM), making it versatile for brittle and ductile failure analysis. ANSYS provides Crack objects for common shapes and defines the crack location using a local coordinate system. Crack faces are treated as internal boundaries with singular stress fields. Ansys uses Quarter-point elements to capture singularities at crack tips and refined mesh zones improve

accuracy of SIF and CTOD calculations. It also utilizes XFEM to allow modeling discontinuities without remeshing.

Ansys uses various methods to analyze specific parameters such as; displacement extrapolation and interaction integral to model stress intensity factors. Contour integration around crack tip to compute the J-integral, virtual crack closure technique to model the energy release rate. Ansys also uses direct measurement from nodal displacements to model crack tip opening displacement. ANSYS Workbench supports the analysis for fatigue life prediction using S-N curves and Miner's rule, crack growth modeling via SMART crack growth technology, and cyclic loading analysis to simulate real-world fatigue scenarios.

For the simulation, this study settled on the use of Ansys software as it has robust and variety of boundary conditions related to fracture mechanics and assignment of material properties, which made it more reliable. The software's interface is user friendly and easy to operate. Its official version is available both for industrial and free student version. This made it easier to acquire for the research.

The specimen's specifications on dimension were used to design a sample and the material (AA7075) was assigned to the designed sample. Specifications on load and boundary conditions were applied and data regarding the stress intensity, strain energy and stress distribution during the fracture simulation were collected for the analysis.

MATLAB is a high-level programming environment ideal for numerical simulations, data post-processing, algorithm development, visualization and automation. In fracture mechanics, it's used to solve PDEs related to crack propagation, analyze experimental data,

implement custom models like Paris' Law or cohesive zone models, perform parametric studies and sensitivity analysis.

It is applied in crack growth simulation, and to simulate fatigue life and crack length evolution over cycles, in calculations of stress intensity factor (SIF) analysis and in post-process ANSYS results to extract SIFs and fit them to analytical models. MATLAB uses interpolation and curve fitting to refine SIF vs. crack length relationships. In fracture pattern quantification and peri dynamic simulations. MATLAB codes like PeriFast or Dynamics solve dynamic fracture problems using fast convolution-based methods which are ideal for modeling crack branching and coalescence in brittle materials.

MATLAB has certain advantages over ANSYS for specific tasks including having High-quality plots, animations, 3D rendering, utilizes statistical analysis such as regression, ANOVA, Monte Carlo simulations, uses machine-learning methods such as crack classification and damage prediction, uses optimizations methods such as genetic algorithms and gradient descent. Using MATLAB also enables easy implementation of Paris, Forman and NASGRO equations of fracture mechanics.

The experimental data were analysed using MatLab software. This choice was due to the existence of finite element, linear elastic fracture, and boundary conditions as in-built programs within the software. This made it possible to analyse the data without having a lot of errors. Through the software, outputs in form of graphical and mathematical expressions were obtained, which made it easy to interpret the results immediately.

A Scanning Electron Microscope (SEM) was incorporated to evaluate the variations of the surface roughness and the appearance of the areas affected by the fracture during the test.

This was done to determine whether the fracture was ductile or brittle. The choice of the SEM over an optical microscope was due to its high resolution of up to x100,000 and up to 15 kV of focus which is not possible with an optical microscope [56]. The SEM provided a more physical interpretation of the effect of stress concentration around the crack tip as it propagates, results of which are attached and discussed in Chapter 4.

CHAPTER FOUR

4.1 Introduction

This study focused on the experimental data collection, analysis, and simulation of the behaviour of aluminium alloy AA7075-T6. This alloy contains alloying elements such as Zinc, Magnesium, Copper, Chromium, Silicon among other elements, which contribute to a smaller percentage, to achieve certain desirable properties like corrosion resistance, weldability, and good fatigue resistance making it suitable for applications subjected to cyclic loading [60]. The compositions of the individual elements in the AA7075-T6 are as shown in Table 4.1. The properties of the alloy include high strength-to-weight ratio due to the combined presence of Zn, Mg, and Cu. The alloy responds well to heat treatment, especially aging processes which further enhance strength. Corrosion Considerations, which stands out since proper protective coatings are recommended in harsh environments. Good fatigue resistance which is ideal for components subjected to cyclic loading.

Table 4.1: Chemical composition of AA7075 by wt% of each element

Alloy	Element Chemical composition									
	Zn	Mg	Cu	Mn	Cr	Si	Fe	Zr	Ti	Al
AA7075	5.1	1.8	1.24	1.65	0.25	0.61	0.18	<0.1	<0.1	Balance

The alloy sheet used here was of dimension 100 mm length, 20 mm width and 3 mm thickness. The material specimen preparation involved cutting a pre-notch of 3 mm at the centre of the length along the width of the material as shown in Figure 4.1.

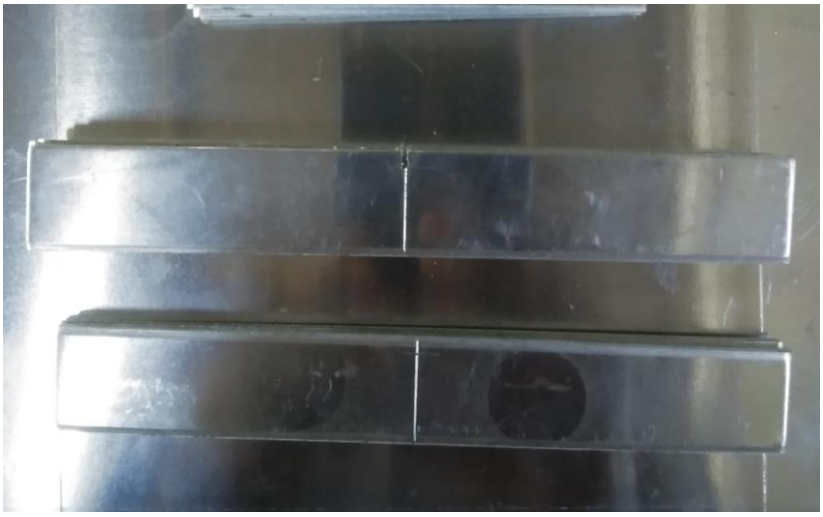

Figure 4.1: Specimens with a 3mm pre-notch.

A tensile testing machine was used to evaluate the fracture properties of the material by applying a tensile load of up to 10 kN on the specimen. Data of time duration of the tests, crack length, crack extension, and corresponding loads were collected to be used in the experimental analysis. These are shown on the Appendix A.

The simulation data was collected from the use of Ansys 2024 R2 software. Most of the parameters including stress concentration and distribution, force applied, energy released, crack extension and strains were obtained from inbuilt functions. These data are as shown in Appendix B. The study also involved a simulation of the fracture mechanics behaviour of the same alloy, with similar dimensions to the experimental test one. The boundary conditions were applied and the alloy properties such as the Young's modulus and the Poison's ratio were inserted during the simulation to help in the analysis.

4.2 Results of the Fatigue test experiment.

The results of the experiments were in line with the objectives of the study. Laws and formulae of fracture mechanics were used to interpret the collected data and calculate the

required parameters for this study. These laws include William's criteria, Paris's Law, and Griffith's law. The values of test durations, applied stresses, stroke, and crack growth and propagation rates were used within equations and laws such as Paris' law, William's criterion, and Griffith's criterion to obtain parameters, which include energy release rates, stress concentration factors and fatigues life estimation of the crack. To ensure accuracy and reliability of the resulting data, three sets of experiment were conducted, and the samples are as illustrated in Figure 4.2. Sample I and Sample III were loaded to a point just before snaping while Sample II was used as the control experiment, thus it was loaded until it snapped into two pieces.

These data enabled the generation of graphical interpretation of the data during analysis through MatLab software, which align with the objectives of the research. The simplified results obtained from the experiment are as shown in Tables 4.2 and 4.3. However, the detailed results are as shown in Appendix A.

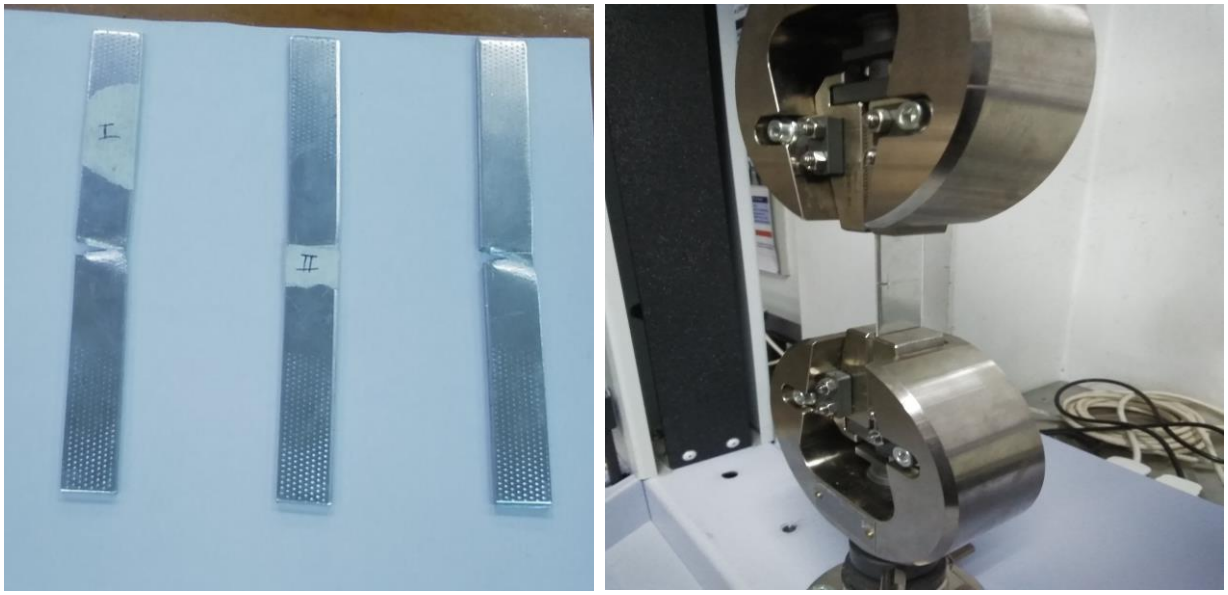

Figure 4.2: Samples used for the tensile test and the loaded sample.

Table 4.2: Experimental data collected during the Fracture test.

Name	Max_Disp.	Max_Strain	Max_Time	Max_Disp_Force
Parameters	Calc. at Entire Areas	Calc. at Entire Areas	Calc. at Entire Areas	
Unit	mm	%	sec	N
Sample 1	2.54100	5.08200	30.4900	1539.43
Sample 2	2.54013	5.08027	30.4800	2214.11
Sample 3	2.52093	5.04187	30.2500	1505.04

Table 4.3: Experimental data calculated during fracture test.

Name	Force	Stress	Stroke	Strain
Parameters	At Entire Areas	At Entire Areas	At Entire Areas	At Entire Areas
Unit	N	N/mm^2	mm	%
Sample 1	5691.13	94.8521	2.54100	5.08200
Sample 2	5794.62	96.5770	2.54013	5.08027
Sample 3	5634.85	93.9142	2.52093	5.04187

The Force against Stroke graph for the data collected is as shown in Figure 4.3.

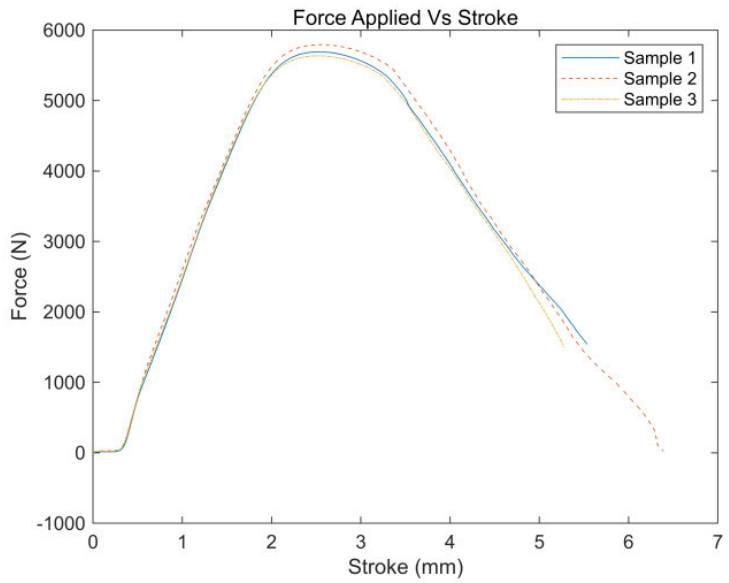

Figure 4.3: Force applied against the corresponding stroke.

The results obtained from the experimental data were analysed using the MatLab software with the focus being on the study objectives, the research hypothesis, the study aims and to answer the research questions on the behaviour of the aluminium alloy AA7075. The data were used to process parameters such as:

4.2.1 Evaluation of Stress Intensity Factor (SIF)

The Ansys simulation automatically generates the stress intensity factor, K. However, the calculation of the stress intensity factor for the Mode I fracture was obtained by substituting the values of the experimental data into Equation 3.1 and 3.2, respectively.

$$Y = 1.12 - 0 \cdot 231\left(\frac{3}{20}\right) + 10 \cdot 55\left(\frac{3}{20}\right)^2 - 21.72\left(\frac{3}{20}\right)^3 + 30.39\left(\frac{3}{20}\right)^4$$

Y = 1.2648

$$K_I = 1.2648\ x\ 94.85\sqrt{3\ x\ \pi}$$

K_I = 368.30 MPa√mm

This indicates that the stress concentration factor at the onset of the test was 0.368 MPa√m.

The stress intensity factors values obtained were used in the calculation of the change in stress intensity factors to obtain the life estimation and crack growth of the material. Applying the average values obtained from the experiment data, the stress intensity factor can be obtained at each point of the experiment duration. Figure 4.4 shows the graph of stress intensity factor against time for the experiment. From the graph, it can be observed that for the three samples under investigation, there are slight variations in the stress intensity factors over time.

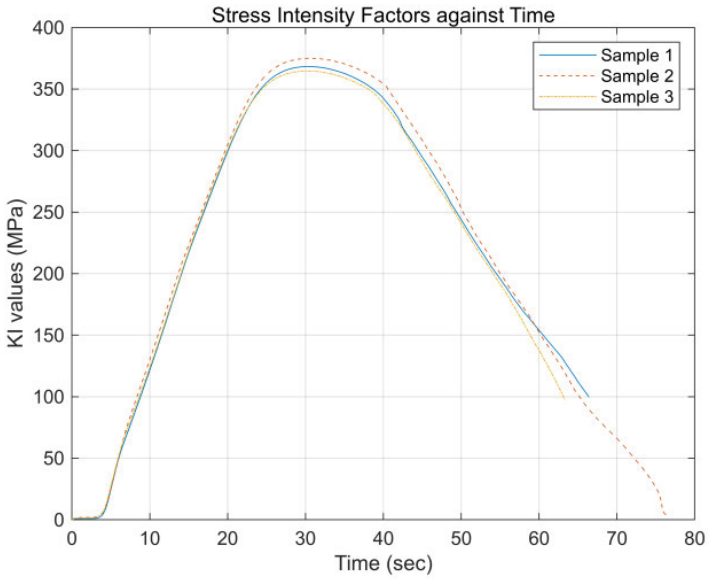

Figure 4.4: Stress intensity against time graph.

4.2.2 Evaluation of Fatigue Crack growth and Life Estimation

Using the data collected and the Paris' law, the crack growth and life estimation can be determined. The initial notch acted as a crack. Its growth happened in three phases: Crack initiation, linear elastic fracture propagation and rapid failure due to fracture. From the experiment, the initial notch was 3 mm in depth. For each loading cycle, it is assumed that the crack growth underwent a linear growth [10], therefore crack length propagated at equal lengths of 3 mm.

Figure 4.5 shows the graph of crack length against the number of loading cycles. It is observable that as the loading cycles increase, the crack length widens in a proportional manner until the critical crack length, which equals the width of the material specimen is achieved. At this point, the material under loading snaps.

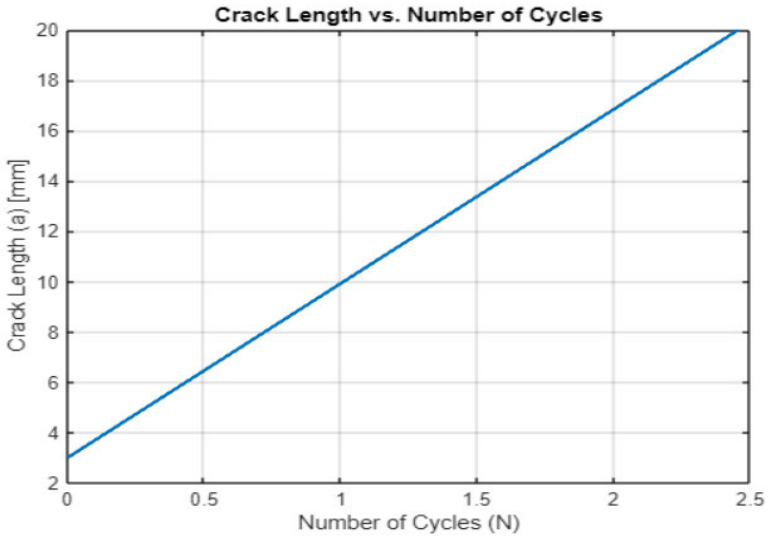

Figure 4.5: Change in crack length with increase in loading cycles.

Taking the case of sample 1 and inserting the data obtained, the rate of crack growth and the life estimation of the crack are obtained using Equations 3.3 – 3.6.

$\frac{da}{dN} = 8.87e - 8\Delta K^{3.14}$;

ΔK = (368.31 – 0.0025)

ΔK = 368.3075

$\frac{da}{dN} = 8.87e - 8\ x\ 368.3075^{3.14}$;

$\frac{da}{dN}$ = 10.135

From Equation 3.7,

a’ = 3.0 + 10.135

a’ = 13.135 mm

Therefore, this shows that after the first cycle of loading, the crack extended by 10.135mm and the crack length grew to 13.135mm.

From the MatLab analysis, a graph of crack growth rate against the change in stress intensity factor was generated as shown in Figure 4.6. The graphs take a similar shape as the creep of the material. The initial stages of the experiment show the material’s resistance to fracture due to electrostatic bonds within its crystallographic points. This represents the fatigue threshold region. The change in stress intensity factor is too low to propagate the crack. As the force applied increased over time, the fracture began, and it was linear along the crack. A stable crack was observed as a result. This is referred to as the steady state. At the advanced stages, the fracture becomes rapid. Any slight change in stress intensity results in a larger crack growth rate. The graph develops a non-linear shape, and this stage is referred to as non-steady state. This indicates that as ΔK increases, so does da/dN, suggesting that higher stress intensity ranges

lead to faster crack propagation rates. This makes the fracture non-linear and unstable. This phenomenon is described as the resistance curve, **r-curve**. The r-curve is used to interpret the J-integral of the material during fracture [61]. This is the rate of strain energy release over time. It is observable that the energy release rate, as discussed in the forthcoming sections, is directly proportional to the rate of crack growth and the stress intensity factor of the loaded material under mode I fracture.

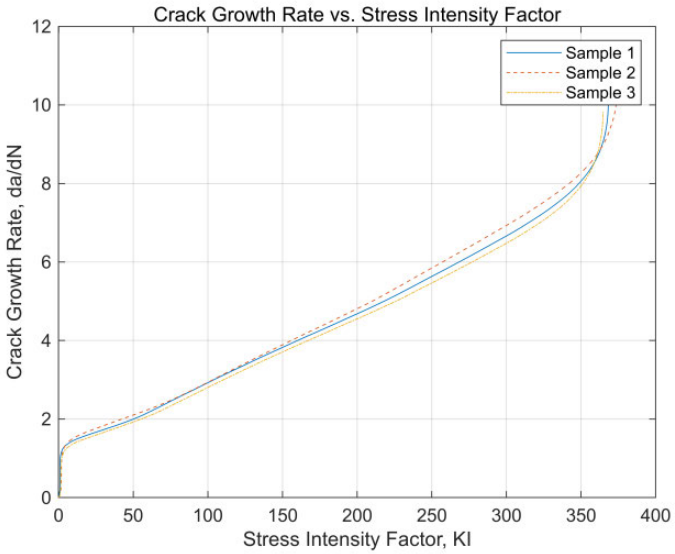

Figure 4.6: Crack growth rate against change in stress intensity factor(r-Curve)

4.2.3 Evaluation of Energy Release Rate

The energy release rate due to fracture of the AA7075 during the experiment was obtained by using the Griffith's law. Griffith postulated that a crack grows when the energy release rate exceeds the critical energy release rate associated with the material's toughness, $G > G_C$. The energy release rate is also dependent on the stress intensity factor of the material.

Using the data from the experiment and substituting for the value of K_I into Equation 3.14, the energy release rate is obtained as;

$$G = \frac{0.003}{70\ x\ 10\text{^}9} x\ 368.31^2$$

$G = 5.81 \times 10^{-9}$ J/m^2

If the thickness of the plate did not affect the stress distribution around the crack tip, the energy release rate would be expressed as:

$$G = \frac{1}{70\ x\ 10\text{^}9} x\ 368.31^2$$

$G = 1.937 \times 10^{-6}$ J/m^2

Figure 4.7 shows the data and graphical presentation of the energy release rate against time as obtained from the experiment. Since energy release rate is dependent on the stress intensity factor, the graph depicts the same profile as that of the crack growth and life estimation curve. It is therefore observed that to initiate fracture, the energy required is greater than the energy released during propagation. This proved the hypothesis that the energy release rate for crack initiation is greater than the energy release during crack growth.

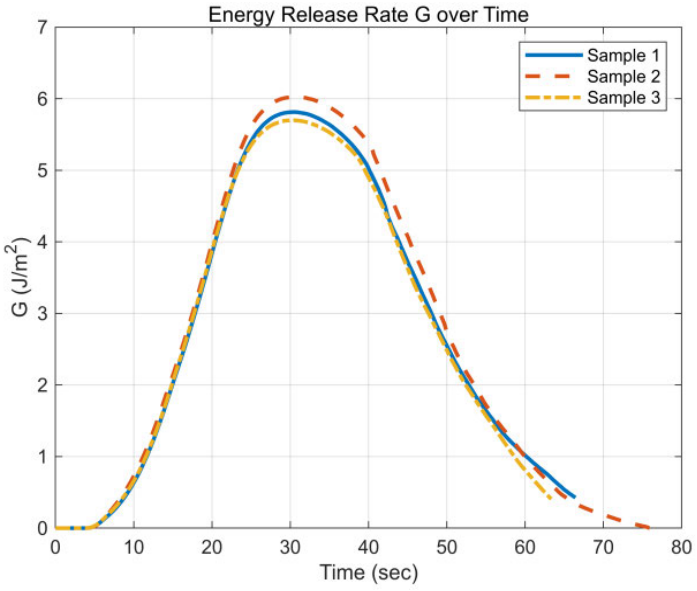

Figure 4.7: Energy release rate against time graph.

4.2.4 Evaluation of Stress Distribution at the Crack tip

The initial notch on the AA7075 was made with a crack angle of 45^0. As the crack grows during fracture, each loading cycle creates a different crack angle at the crack tip. The William's solution is applied in this case in the determination of the stress concentration around the crack tip. Williams' solution provides essential insights into fracture mechanics by characterizing stress fields around cracks. For this study, the stress distribution around the crack tip and propagation areas was obtained by substituting the experiment data into Equations 3.8 – 3.13.

Since the crack angle varies from 0 to 2π, at a crack angle of 45^0 the resulting stresses are obtained by substituting the values of the SIF and Crack angle into Equations 3.8 – 3.10.

$$\sigma_x = \frac{1}{\sqrt{2\ x\ \pi\ x\ 0.003}} (368.31\ cos(45/2)\ x\ 0.6464)$$

$\sigma_x = 1.602$ MPa

For the stress concentration in the y-direction, σ_y.

$$\sigma_y = \frac{1}{\sqrt{2\ x\ \pi\ x\ 0.003}}(368.31\ cos(45/2)\ x\ 0.5)$$

σ_y = 3.355 MPa

The shear stresses experienced due to hydrodynamic stresses within the material during tensional loading is resultant as;

$$\tau_{xy} = \frac{-1}{\sqrt{2\pi\ x\ 0.003}}(368.31\ x\ 0.32664)$$

τ_{xy} = -0.876 MPa

In most instances, these hydrodynamic stresses, which result into shear stresses are assumed to be negligible and therefore does not add to the overall fracture of the material under loading.

At the onset of the fracture, the stress distribution at the crack tip with crack angle of zero, the stress distribution factor was obtained from Equations 3.11 – 3.12:

$$\sigma_x = \frac{1}{\sqrt{2\ x\ \pi\ x\ 0.0015}}(368.31\ cos(0))$$

σ_x = 2.682 MPa

For the stress concentration in the y-direction, σ_y.

$$\sigma_y = \frac{1}{\sqrt{2\ x\ \pi\ x\ 0.0015}}(368.31\ cos(0))$$

σ_y = 2.682 MPa

It is observable that as the crack growth increases, the stress concentration around the crack tip also increases until the critical crack length is attained. At this point, the fracture

becomes rapid and the stress concentration around the crack tip declines with advancement of the crack length.

The detailed data from the tensile testing machine were loaded into the MatLab software and the graphical representations shown in Figure 4.8 and Figure 4.9 were generated.

The red pigment represents the stress developed at the crack tip; the green pigment shows the stress variation around the crack tip while the blue zones are the stress concentration around the crack propagation zone. It is observable that as the crack propagates, the crack angle increases, this in turn leads to the decrease in stress concentration around the crack tip while the stress around the crack propagation region increases, as shown in Figure 4.8 where the green and blue pigments become more pronounced with increase in the value of crack tip angle, theta. This confirms the hypothesis that the stress concentration at the crack tip is greater during the crack initiation stage than at the crack propagation zones. It is also evident that rapid fracture happens immediately at the end of the linear fracture phase. At this point, the angle widens further compared to the initial stages. Considering the linear section of the fracture, it is observable that the stress concentration lies in a divergent form from the crack tip. Stress concentration is high at the crack tip than the areas surrounding the crack and its propagation. This is shown in Figure 4.9.

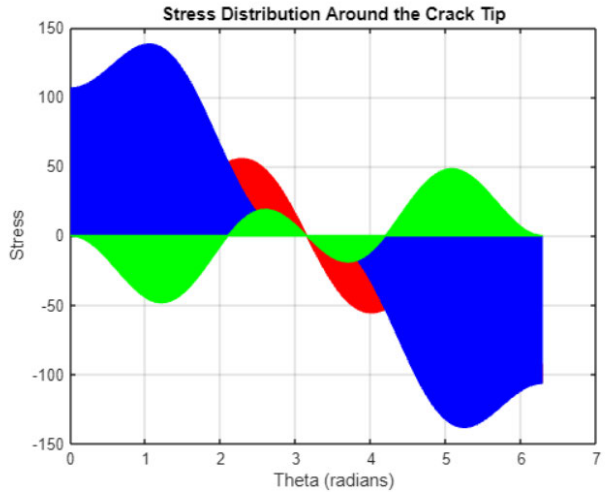

Figure 4.8: Linear Stress distribution simulation around crack tip and propagation areas.

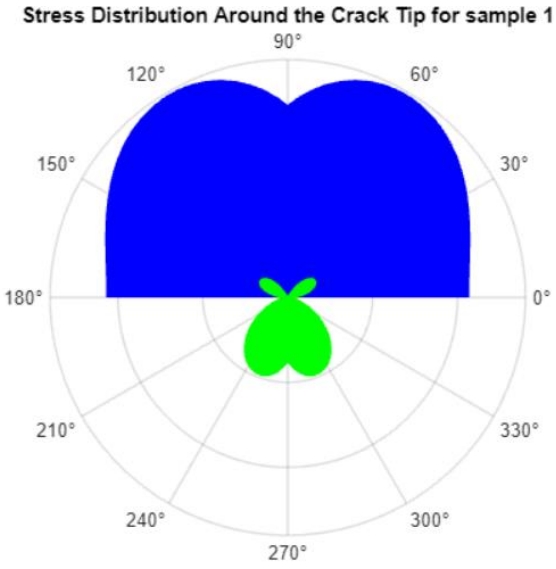

Figure 4.9: Polar Stress Distribution simulation around the crack tip and propagation areas.

4.3 Results from the simulation

In this study, apart from the experiments, a simulation using Ansys 2024 R2 Software to help in the determination of the behaviour of the aluminium AA7075 was done. Data regarding the parameters of fracture mechanics simulation shown in Figures 4.10 – 4.13, which

are Deformation of the material to evaluate its life estimation, strain energy and stress distribution.

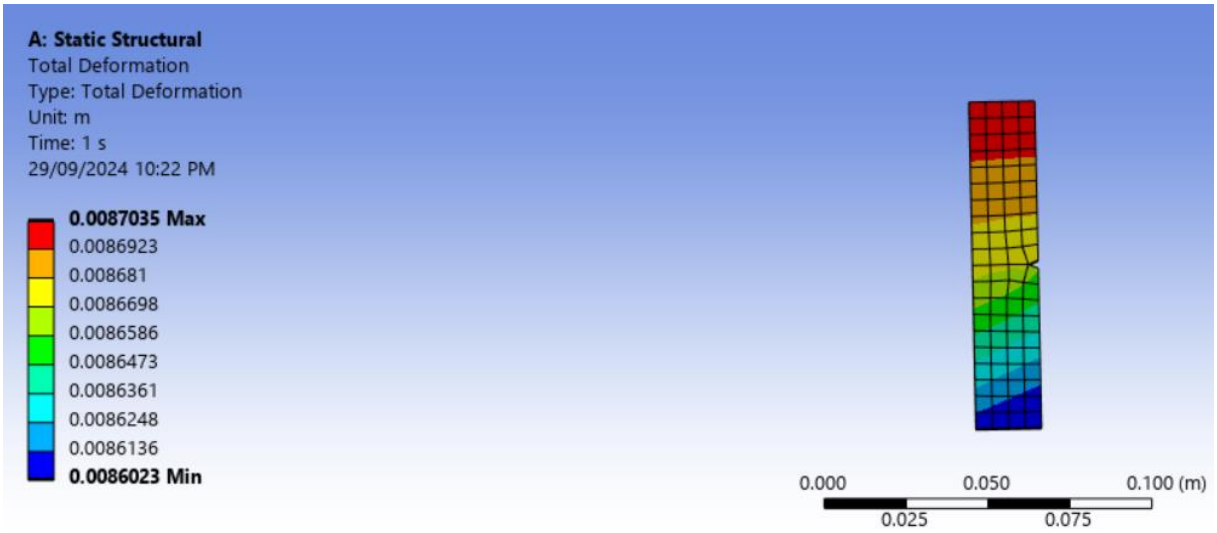

Figure 4.10: Simulated deformation under loading.

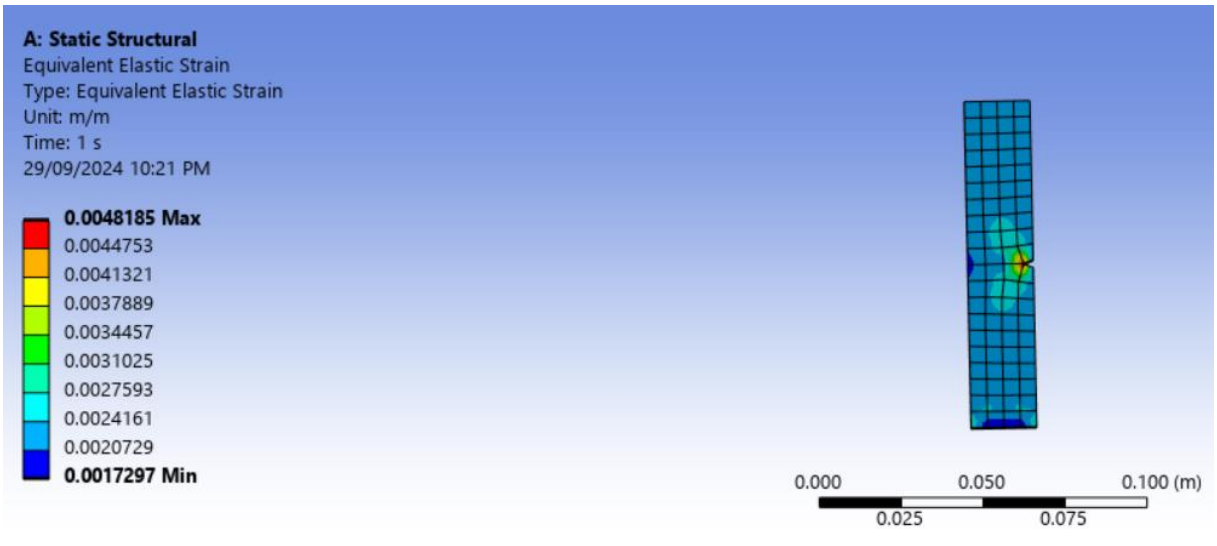

Figure 4.11: Equivalent simulated elastic strain.

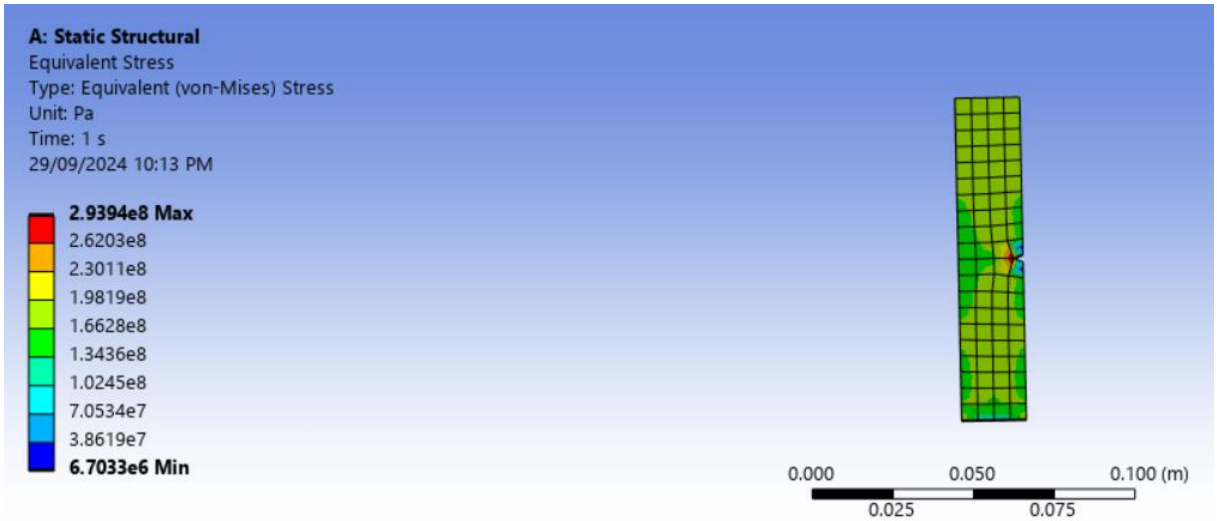

Figure 4.12: Simulated stress distribution around crack tip and propagation area.

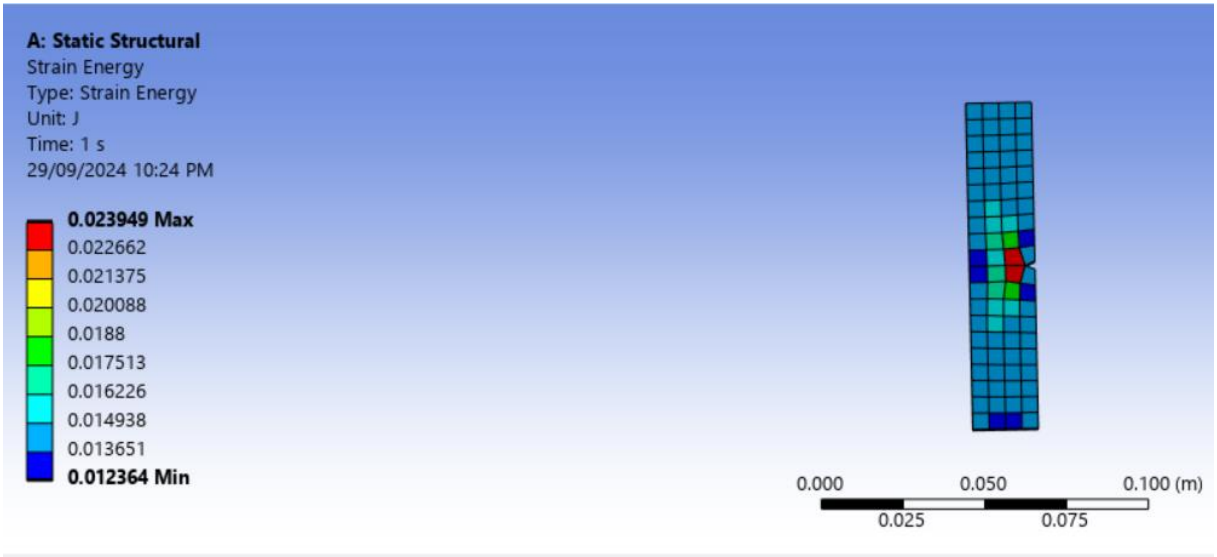

Figure 4.13: Simulated Strain Energy distribution.

4.4 Comparison of Experimental and Simulated Data

From the experiment and the simulation, it was observed that the behaviour of the AA7075 was comparatively the same. A margin error of 8% – 15% was observed in the computation of various parameters between the experiment and simulation. The parameters

under observation and comparison included stress concentration at the crack tip, strain energy released, elastic strain and deformation or extension under loading. These have been tabled as shown in Table 4.4.

Table 4.4: Comparison of Experimental and Simulation results

Parameter	Max Stress (Pa)	Max Strain	Max Energy released (J)	Max Extension (m)
Experiment	2.5114×10^8	0.005082	0.024932	0.006392
Simulation	2.9394×10^8	0.004819	0.023949	0.008704
% Error	14.56	5.175	3.940	4.654

The main purpose for this comparison is the fact that experiments were conducted in the laboratories. The study environment does not depict the environmental condition under which the material will be in use; for example, on an airplane's body where various environmental factors would lead to fatigue, crack initiation and therefore fracture. Having simulated data helps in eliminating some other factors like hysteresis within the machine, errors in calibration of the machine or other errors that may occur due to human errors during loading, data collection and computation of the specific parameters under study and specimen preparation.

The simulation is a sure way of having precise dimensions, loading and accurate data collection without errors arising from physical factors and machine incapacities. However, the simulated data might not depict 100% behaviour of the material in an ideal use; it gives much more accurate data compared to the experiment due to its less limitations as compared to experimentation and analysis limitations.

Through this comparison, a choice can be made to determine which of the two methods is most applicable at various times and conditions of the research. For instance, it is quite relevant to use experiment route if studies are to be done on an already corroded material than to use a simulation since the inbuilt functions in the Ansys do not have an option for simulation using used materials. The general assumption in the simulation is that the material is brand new and free of defects. This is not the case in real-world situation.

4.5 Scanning Electron Microscope observation of the specimen

The samples developed fractures during the experiment, and it was observable that the deformation influenced the material properties in the areas of stress distribution. To establish the magnitude of the defects and the nature of fracture that the samples underwent, a Scanning Electron Microscope was used. The fractured samples surface and fracture region properties were compared against those of the unused sample, in this research referred to as the control experiment sample. These are shown in Figure 4.14. From the SEM images on Figure 4.14, it is observable that there are striations on the control experiment sample. These contribute to the irregularity of the material's surface roughness. The irregularity in surface roughness influences the crack initiation and growth that can lead to fracture. On closer and higher magnification on a section of the control sample, it was observed that there were already developed cracks on the surface. These surface irregularities may result from the inhomogeneity of the alloy elements on the material from which they were cut or due to surface roughness of the material that may result during specimen preparation or alloy rolling.

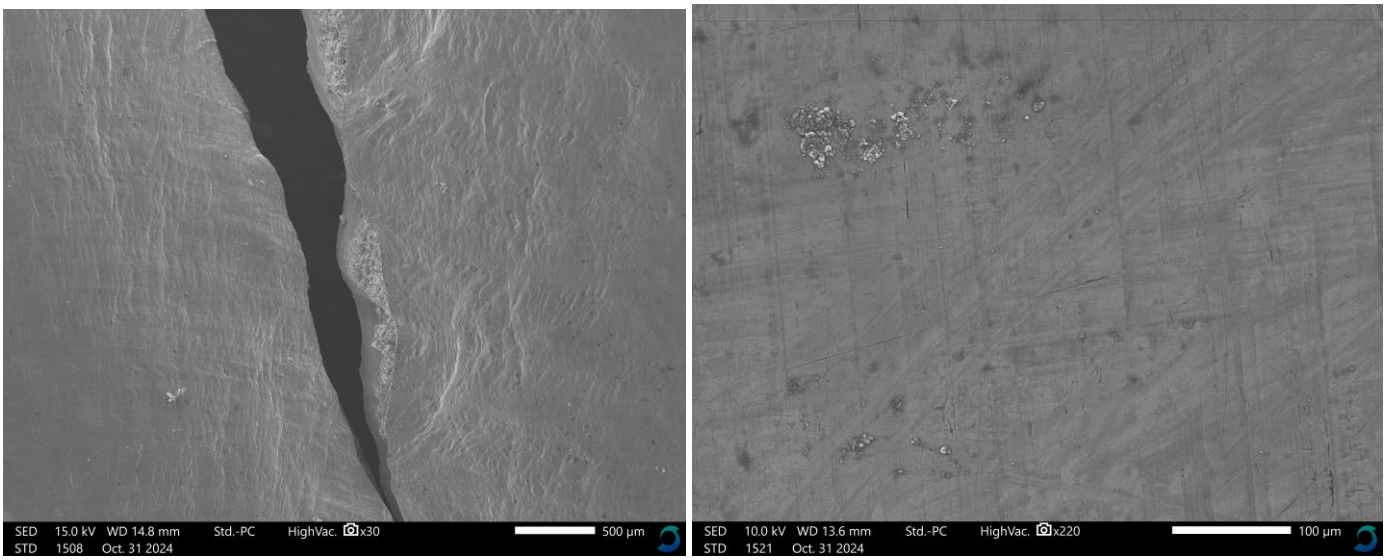

Figure 4.14: Cracked surface of AA7075 sample as observed at x2300 magnification on SEM.

In the process of the experiment, the material underwent brittle fracture. This is evidenced by the shiny appearance of the fractured surface and the rapid fracture that was observed during the experiment. The roughness of the fractured surface and the rippled areas around the crack were evidence of a brittle fracture. These are evidenced in Figure 4.15 and 4.16.

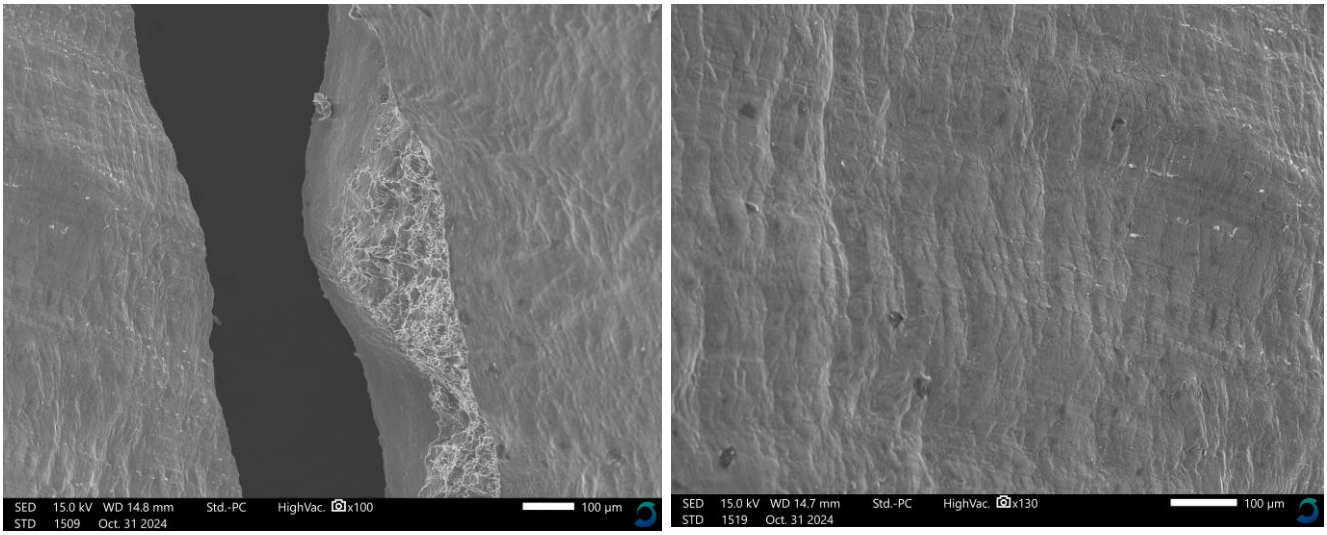

Figure 4.15: Surface appearance of crack and area around crack after fracture tests.

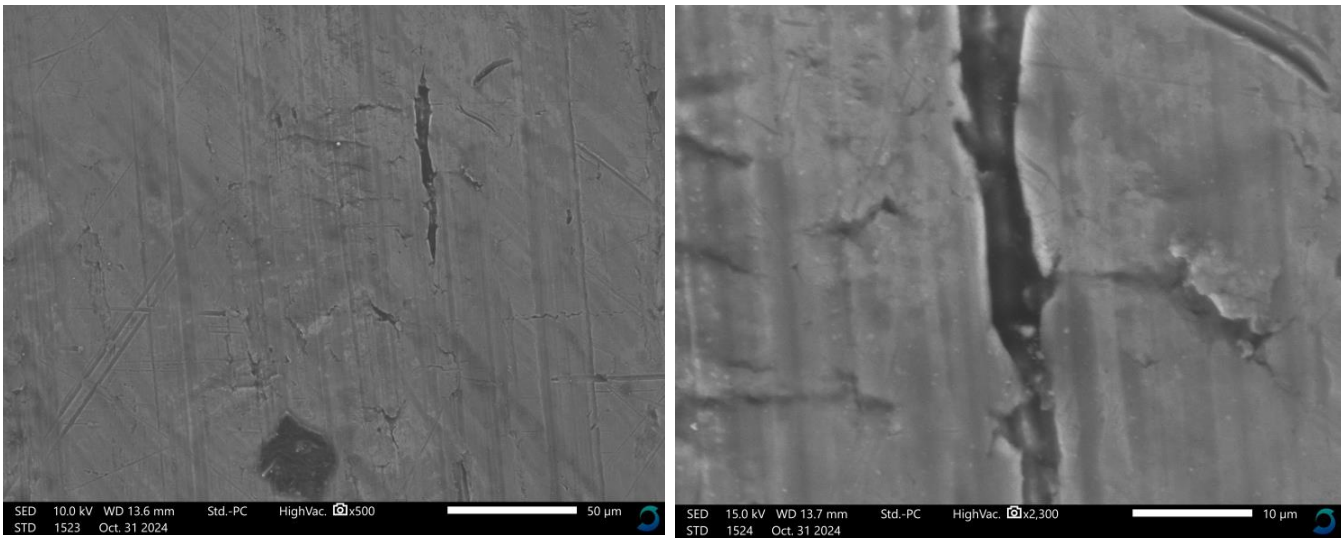

Figure 4.16: Surface appearance of crack and area around crack before fracture tests

The surface roughness and the inhomogeneity in the material lattice structure are a cause of the error in the stress distribution, stress intensity factor and the energy release values observed in the calculations. Another possible cause of this occurrence may be due to uneven loading application resulting from inaccuracies in the machine and machine calibration inefficiencies [59]. The rapid fracture after the critical stress intensity factor was observed and it resulted from brittle fracture of the material due to existence of inclusions and voids in the alloy structure as observed in Figure 4.14. Further supportive fractography images are attached in Appendix B.

An observation and analysis of the SEM image's surface defects indicated that the pre-existing notches and cracks were of significant areas and lengths, which could have contributed to the rapid crack growth during loading. The sample specimen's image was analysed under ImageJ software and the findings indicate a crack of almost 0.1mm and a notch of 0.001mm^2 as illustrated in Figure 4.17 and Table 4.5.

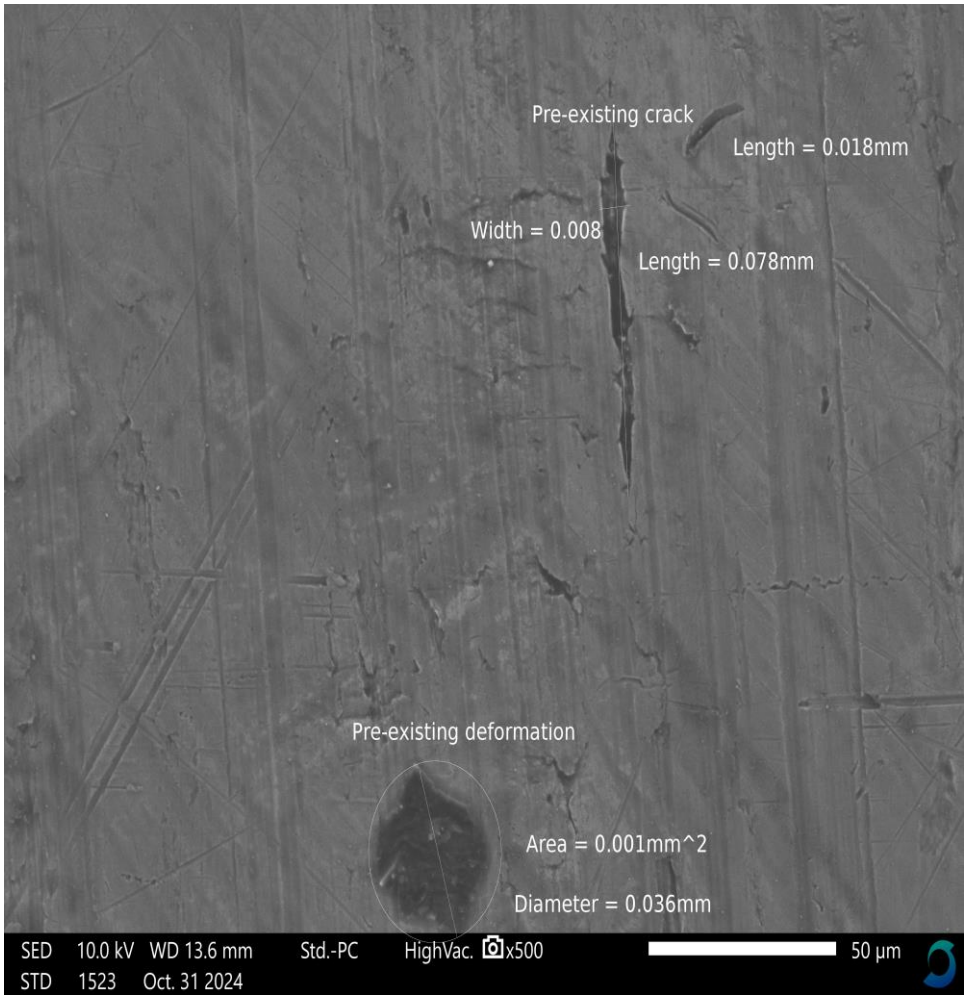

Figure 4.17: ImageJ analysis of the control sample specimen for existing deformities before fracture tests.

Table 4.5: ImageJ results of dimensions of pre-existing deformation and pre-crack sizes on the control sample specimen

	Area	**Mean**	**Min**	**Max**	**Angle**	**Length**
Length_1	3.87E-06	76.671	55.617	142.899	-87.079	**0.078**
Length_2	8.98E-07	97.372	60.684	142.091	33.341	**0.018**
Width_1	3.99E-07	96.121	68.265	180.429	5.711	**0.008**
Diameter_3	1.76E-06	72.106	0	127.583	-73.791	**0.036**
Area_3	**0.001**	81.115	0	255	0	0

4.6 Correlations of the results to the Objectives.

Mode I Fracture Experiments on Crack Initiation and Life Estimation

Mode I fracture, characterized by the opening mode, is critical for analyzing crack initiation in structural materials like aluminium 7075. Compact tension specimens machined from AA7075 with pre-cracked regions were subjected to tensile loading. At various load levels, crack initiation was recorded using digital image correlation (DIC) sensors within the mechatronic tensile machine. Surface micrographs indicated cleavage and dimple rupture mechanisms as captured by SEM. The crack growth rate was analyzed using Paris' Law, and subsequently crack propagation rates were determined. The Fatigue life prediction under cyclic loading conditions revealed that AA7075 experienced a reduction in fatigue resistance due to microstructural heterogeneity, particularly grain boundary precipitates. The derived fatigue crack growth models will help estimate component lifetime in aerospace automotive applications, where cyclic stresses are dominant.

Energy Release Rate and Crack Formation Energy

Energy release rate represents the energy dissipated per unit crack extension and is central to fracture toughness evaluation. The load-displacement curves show the estimation of

the energy release rate of the allow under tensile loading. ANSYS and MATLAB-based fracture modules modeled crack extension on the basis of Finite Element and Boundary layer techniques. Energy release zones around crack tips were visualized using strain energy density functions. The simulations closely matched experimental ERR values within ±5%, validating model accuracy.

The SEM imaging revealed that microvoid coalescence required significant localized energy. Crack formation energy exceeded theoretical cleavage energy due to plastic deformation. A portion of the external work was absorbed in elastic deformation, while the rest contributed to surface creation and plastic dissipation.

Stress Analysis for Linear and Polar Fracture

Linear and polar fracture geometries present different stress intensity profiles, crucial for understanding load path dependency. For center-cracked plate geometries, stress intensity factor was calculated and the stress maps indicated peak intensities at crack tips. The stress distributions in polar coordinates were modeled. At high angles near crack tips, stress singularity increased sharply. Color-coded stress contours and ERR maps showed that Mode I loading induced symmetric stress fields around crack tips in linear geometry but produced asymmetric fields in polar cracks.

In conclusion, AA7075 exhibits complex fracture behavior influenced by microstructural features, geometry, and environmental conditions. Mode I fracture testing paired with simulation provides robust models for life prediction and design optimization. Energy-based metrics like ERR and formation energy offer quantitative insight into material

toughness. Graphical stress analyses aid in intuitive understanding and communication of fracture mechanics phenomena.

CHAPTER FIVE

5.1 Conclusion and Recommendations from the Study

The alloy behaviour during the experiment was as expected even though some errors might have occurred, as indicated in Chapter 4, that lead to the disparity with the simulated results. This study however brings out the strength of the use of simulation and analytical software in the study of fracture, more so for high strength alloys such as the AA7075. Through the study, the research objectives were met, and various deductions were made as a result.

5.1.1 Conclusion from the Study

1. It is observed that the stress concentration at the crack tip is greater that the stress experienced on the whole material and the areas around the crack propagation. The stress distribution around the crack tip was highly dependent on the stress intensity factors at every point of the crack growth.
2. It is also observed that the stress intensity factor during the fracture varies as the fracture propagates from the crack initiation stage, the linear fracture stage to the rapid non-linear stage of fracture. The stress intensity is dependent on the stress applied, the crack length and the geometry of the sample which majorly influenced the value of the geometric factor Y.
3. It is concluded that the energy release rate during the crack initiation is greater than the energy absorbed or released as the fracture propagates. The energy release rate depended on the value of the stress intensity factor and the modulus of elasticity of the material.

4. The crack tip angle during propagation highly influenced the amount of energy released during the fracture. It also determined the stress concentration at the crack tip as the crack advanced into the sample past the critical stress intensity.
5. It is observable that the boundary conditions applied during the simulation were workable and the results are comparatively close to those obtained from the experimental analysis of the collected data, with below 12% disparity. The Ansys 2024R2 and the MatLab software are highly effective in the study of the behaviour of the alloy and the analysis of the experimental data while also displaying the simulated data for comparison.

5.1.2 Recommendations

From the results discussed in Chapter 4 and the above discussed limitations, it is most likely that there is disparity between the experiment on fracture mechanics behaviours and the real-world behaviour of the same alloy due to fractural failure. Further studies involving exposure of the specimen to the real-world loading scenario would lead to collection of accurate data. The limitations can be overcome through advancement of the test machines and the environmental conditions in the laboratories while sophisticating the loading modes to resemble the ways in which a component may fail on an equipment. It is also noted that incorporation of the sophisticated loading techniques in the simulation software will lead to even more practical results that requires limited comparison to assess results. Since this research only focused on a rectangular sheet of 3mm thickness, it would be prudent of future researchers to conduct their studies on other geometries (triangular, circular, and trapezoidal) and of bigger thickness. These also form part of components and parts used in structures. Through the studies, further fatalities or economic losses can be reduced at design stage or component joinery stages.

Summarily, Aluminium 7075 exhibits distinct fracture initiation behavior under Mode I loading due to its microstructural features such as grain boundary precipitates and inclusions. Fatigue life prediction models, like Paris' Law, effectively estimate crack propagation rates when calibrated against experimental data.

The energy release rate (ERR) derived both experimentally and through finite element simulation reliably characterizes the fracture toughness of AA7075. Crack formation requires energy beyond theoretical cleavage predictions due to plastic deformation. The simulations closely mirrored experimental ERR values, validating computational tools like ANSYS for modeling fractures in aerospace-grade aluminium.

Stress analysis reveals that crack tip stress intensities are highly geometry dependent. Linear cracks showed symmetric stress fields, while polar cracks exhibited asymmetric stress intensity profiles. Graphical outputs demonstrated the dynamic nature of stress intensity factors and energy release zones, aiding visualization of fracture progression and failure zones.

Future Research Recommendations

I. Explore fracture under mixed-mode loading to understand interaction effects between shear and tensile stresses.
II. Investigate microstructural enhancements (e.g., nano-precipitates) to improve fracture resistance.
III. Extend the study to include temperature-dependent fracture behavior, especially for environments with thermal cycling.

REFERENCES

[1] S. Maksimović, "Fatigue life analysis of aircraft structural components," *a a,* vol. 3, no. 1, p. 1, 2005.

[2] K. Maksimović, "Strength analysis of structural components with respect to damage tolerance damages under dynamic loads," Master Thesis, Faculty of Mechanical Engineering, University of Kragujevac …, 2003.

[3] M. Specification, "MIL-A-83444—Airplane Damage Tolerance Requirements," *USAF,* 1974.

[4] D. Stamenković, K. Maksimović, V. Nikolić-Stanojević, S. Maksimović, S. Stupar, and I. Vasović, "Fatigue life estimation of notched structural components," *Strojniški vestnik-Journal of Mechanical Engineering,* vol. 56, no. 12, pp. 846-852, 2010.

[5] G. C. Sih, *Mechanics of fracture initiation and propagation: surface and volume energy density applied as failure criterion*. Springer Science & Business Media, 2012.

[6] R. S. Barsoum, "Triangular quarter-point elements as elastic and perfectly-plastic crack tip elements," *International Journal for numerical Methods in engineering,* vol. 11, no. 1, pp. 85-98, 1977.

[7] I. Vasovic, M. Maksimovic, and K. Maksimovic, "Residual fatigue life estimation of structural components under mode-I and mixed mode crack problems," in *International Conference of Experimental and Numerical Investigations and New Technologies*, 2018: Springer, pp. 3-21.

[8] K. Maksimović, "Estimation of residual strength for aircraft structural elements," *J. Technical Diagnostics,* no. 3, pp. 54-57, 2002.

[9] V. Butala, M. Milinović, and P. Škraba, "Strojniški vestnik–Journal of Mechanical Engineering (SV-JME)," *Journal of Mechanical Engineering,* vol. 58, no. 6, pp. 416-421, 2012.

[10] E. E. Gdoutos, *Fracture mechanics criteria and applications*. Springer Science & Business Media, 2012.

[11] K. Walker, "The effect of stress ratio during crack propagation and fatigue for 2024-T3 and 7075-T6 aluminum," *Effects of environment and complex load history on fatigue life,* pp. 1-14, 1970.

[12] S. Boljanović and S. Maksimović, "Fatigue damage analysis of wing-fuselage attachment lug," *Procedia Structural Integrity,* vol. 5, pp. 801-808, 2017.

[13] R. Ghfiri, A. Amrouche, A. Imad*, and G. Mesmacque, "Fatigue life estimation after crack repair in 6005 A-T6 aluminium alloy using the cold expansion hole technique,"

Fatigue & Fracture of Engineering Materials & Structures, vol. 23, no. 11, pp. 911-916, 2000.

[14] K. Tanaka, Y. Nakai, and R. Kawashima, "Fracture mechanics approach to fatigue crack initiation from deep notches," *Engineering Fracture Mechanics,* vol. 18, no. 5, pp. 1011-1023, 1983.

[15] C. Shin, C. Wang, and P. Song, "Fatigue damage repair: a comparison of some possible methods," *International Journal of fatigue,* vol. 18, no. 8, pp. 535-546, 1996.

[16] Ž. Domazet, "Comparison of fatigue crack retardation methods," *Engineering Failure Analysis,* vol. 3, no. 2, pp. 137-147, 1996.

[17] M. Goto, H. Miyagawa, and H. Nisitani, "Crack growth arresting property of a hole and Brinell-type dimple," *Fatigue & Fracture of Engineering Materials & Structures,* vol. 19, no. 1, pp. 39-49, 1996.

[18] A. Standard, "Standard test method for measurement of fatigue crack growth rates," *(No Title),* vol. 3, 2002.

[19] S. Maksimović, I. Vasović, M. Maksimović, and M. Đurić, "Residual life estimation of damaged structural components using low-cycle fatigue properties," in *Third Serbian Congress Theoretical and Applied Mechanics, Vlasina Lake*, 2011, pp. 605-617.

[20] D. Broek, "The practical use of fracture mechanics kluwer academic publishers," ed: Dordrecht, 1989.

[21] S. Maksimovic, M. Đuric, M. Maksimovic, and I. Vasovic, "Fatigue life estimation of aircraft structural components with surface cracks under load spectrum," *Acta Technica Corviniensis-Bulletin of Engineering,* vol. 9, no. 2, p. 41, 2016.

[22] B. Sredanović, Đ. Čiča, S. Borojević, S. Tešić, and D. Kramar, "DEMI 2021," *PROCEEDINGS DEMI 2021,* p. 71.

[23] S. Maksimovic and K. Maksimovic, "Improved computation method in residual life estimation of structural components," *Theoretical and Applied Mechanics,* vol. 40, no. 2, pp. 247-261, 2013.

[24] M. Blažić, K. Maksimović, and Y. Assoul, "Determination of stress intensity factors of structural elements by surface cracks," in *Third Serbian Congress Theoretical and Applied Mechanics, Vlasina Lake*, 2011, pp. 374-383.

[25] M. Chargin and O. Gartmeier, "A finite element procedure for calculating fluid-structure interaction using MSC/NASTRAN," 1990.

[26] W. Fujimoto, "Determination of crack growth and fracture toughness parameters for surface flaws emanating from fastener holes," in *17th Structures, Structural Dynamics, and Materials Conference*, 1976, p. 1552.

[27] J. R. Rice, "Matrix computations and mathematical software," 1981.

[28] N. Bisht, P. Gope, and K. Panwar, "Influence of crack offset distance on the interaction of multiple cracks on the same side in a rectangular plate," *Frattura ed Integrità Strutturale,* vol. 9, no. 32, pp. 1-12, 2015.

[29] S. Boljanović and S. Maksimović, "Analysis of the crack growth propagation process under mixed-mode loading," *Engineering fracture mechanics,* vol. 78, no. 8, pp. 1565-1576, 2011.

[30] P. Kumar, *Elements of fracture mechanics*. McGraw-Hill Education LLC., 2009.

[31] G. H. Lee, C. Y. Cui, and H. G. Beom, "Energy release rate of hyperelastic solids with a nanocrack," *Philosophical Magazine Letters,* vol. 100, no. 9, pp. 425-434, 2020.

[32] B. Jelinek *et al.*, "Modified embedded atom method potential for Al, Si, Mg, Cu, and Fe alloys," *Physical Review B—Condensed Matter and Materials Physics,* vol. 85, no. 24, p. 245102, 2012.

[33] S. Plimpton, "Fast parallel algorithms for short-range molecular dynamics," *Journal of computational physics,* vol. 117, no. 1, pp. 1-19, 1995.

[34] J. R. Rice, "A path independent integral and the approximate analysis of strain concentration by notches and cracks," 1968.

[35] G. H. Lee, Y. J. Chung, S. M. Na, and H. G. Beom, "Atomistic investigation of the T-stress effect on fracture toughness of copper and aluminum single crystals," *Journal of Mechanical Science and Technology,* vol. 32, pp. 3765-3774, 2018.

[36] H. Richard and K. Benitz, "A loading device for the creation of mixed mode in fracture mechanics," *international Journal of Fracture,* vol. 22, pp. R55-R58, 1983.

[37] A. Shahani and S. Tabatabaei, "Effect of T-stress on the fracture of a four point bend specimen," *Materials & Design,* vol. 30, no. 7, pp. 2630-2635, 2009.

[38] A. Desai, C. Sharanaprabhu, and S. Kudari, "Experimental investigation on the effects of fiber orientation on translaminar fracture toughness for glass-epoxy composite under mixed Mode I/II load," in *AIP Conference Proceedings*, 2019, vol. 2057, no. 1: AIP Publishing.

[39] A. Desai, C. Sharanaprabhu, and S. Kudari, "Experimental investigation to evaluate total energy release rate for unidirectional glass/epoxy composite under Mixed mode-I/II load," *Sādhanā,* vol. 45, no. 1, p. 251, 2020.

[40] H. Richard, "Some theoretical and experimental aspects of mixed mode fractures," in *Fracture 84*: Elsevier, 1984, pp. 3337-3344.

[41] S. Lin, Z. Feng, and R. Rowlands, "Thermoelastic determination of stress intensity factors in orthotropic composites using the J-integral," *Engineering Fracture Mechanics,* vol. 56, no. 4, pp. 579-592, 1997.

[42] E. Triki, B. Zouari, and F. Dammak, "Dependence of the interlaminar fracture toughness of E-Glass/Polyester woven fabric composites laminates on ply orientation," *Engineering Fracture Mechanics,* vol. 159, pp. 63-78, 2016.

[43] B. Latham, "WorldWidescience. org," *Reference Reviews,* vol. 23, no. 4, 2009.

[44] D. J. Higham and N. J. Higham, *MATLAB guide*. SIAM, 2016.

[45] M. K. Thompson and J. M. Thompson, *ANSYS mechanical APDL for finite element analysis*. Butterworth-Heinemann, 2017.

[46] S. Jamian, K. A. Kamarudin, M. K. M. Nor, M. N. Ibrahim, and M. A. Choiron, "An overview of fracture mechanics with ANSYS," *International Journal of Integrated Engineering,* vol. 10, no. 5, 2018.

[47] N. Perez, *Linear elastic fracture mechanics*. Springer, 2004.

[48] B. Atzori, A. Campagnolo, M. Ricotta, and G. Meneghetti, "Analysis and comparison of some LEFM parameters," *Procedia Structural Integrity,* vol. 18, pp. 413-421, 2019.

[49] B. Farahmand, "Fundamentals of Composites and Their Methods of Fabrications."

[50] M. Kuna, "Finite elements in fracture mechanics," *Solid Mech. Its Appl,* vol. 201, pp. 153-192, 2013.

[51] N. Sukumar, J. Dolbow, and N. Moës, "Extended finite element method in computational fracture mechanics: a retrospective examination," *International Journal of Fracture,* vol. 196, pp. 189-206, 2015.

[52] H.-G. Maschke and M. Kuna, "A review of boundary and finite element methods in fracture mechanics," *Theoretical and applied fracture mechanics,* vol. 4, no. 3, pp. 181-189, 1985.

[53] M. Aliabadi, "Boundary element formulations in fracture mechanics," 1997.

[54] T. A. Cruse, *Boundary element analysis in computational fracture mechanics*. Springer Science & Business Media, 2012.

[55] J. P. M. Ferreira, "Pre-strain effects on fatigue crack propagation behaviour of a pressure vessels steel," 2017.

[56] A. Mohammed and A. Abdullah, "Scanning electron microscopy (SEM): A review," in *Proceedings of the 2018 International Conference on Hydraulics and Pneumatics—HERVEX, Băile Govora, Romania*, 2018, vol. 2018, pp. 7-9.

[57] M. Isakov, O. Rantalainen, T. Saarinen, and A. Lehtovaara, "Large-Scale Fatigue Testing Based on the Rotating Beam Method," *Experimental Techniques,* vol. 47, no. 3, pp. 553-563, 2023.

[58] H.-J. Hwang, T.-S. Eom, H.-G. Park, and S.-H. Lee, "Axial load and cyclic lateral load tests for composite columns with steel angles," *Journal of Structural Engineering,* vol. 142, no. 5, p. 04016001, 2016.

[59] S. Kudari and C. Sharanaprabhu, "On the relationship between stress intensity factor (K) and minimum plastic zone radius (MPZR) for four point bend specimen under mixed mode loading," *International Journal of Engineering, Science and Technology,* vol. 2, no. 5, pp. 13-22, 2010.

[60] W. D. Callister Jr and D. G. Rethwisch, *Materials science and engineering: an introduction*. John wiley & sons, 2020.

[61] D. Stamenkovic and B. M. Eng, "Determination of fracture mechanics parameters using FEM and J-integral approach," in *Finite element simulation of the high risk constructions, Special Session, within 2nd WSEAS International Conference on Applied and Theoretical Mechanics (MECHANICS'06), Eds Mijuca, D and Maksimovic, S., Venice*, 2006.

APPENDIX

Simulation Data and Analysis Results

Model of the AA7075 strip with A 3mm notch

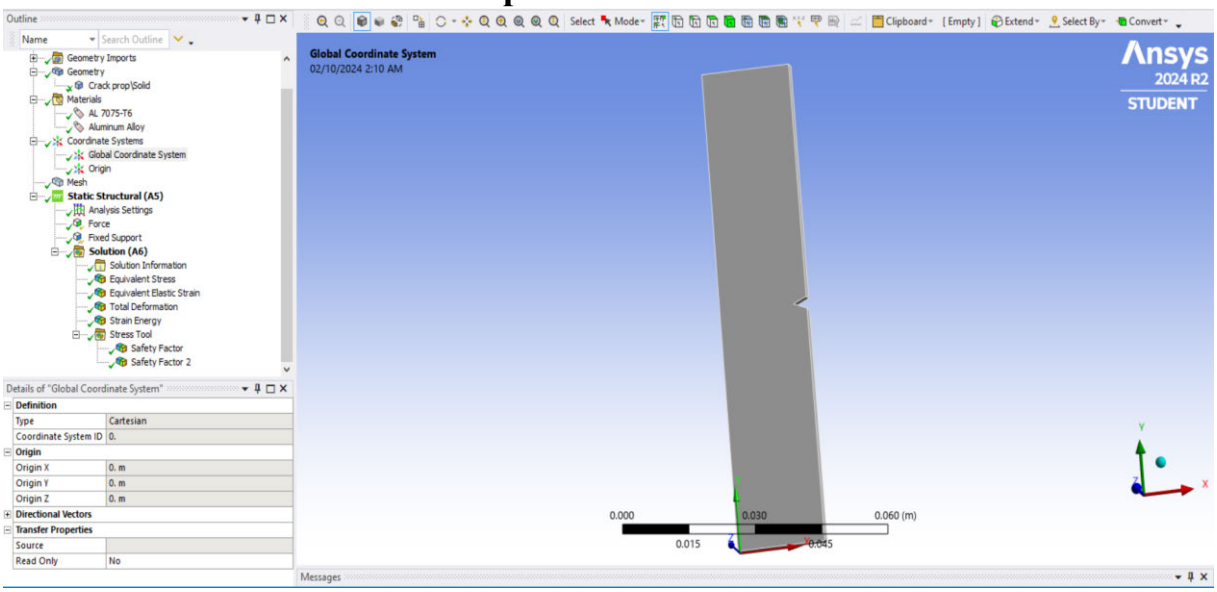

Properties of Aluminium Alloy 7075-T6

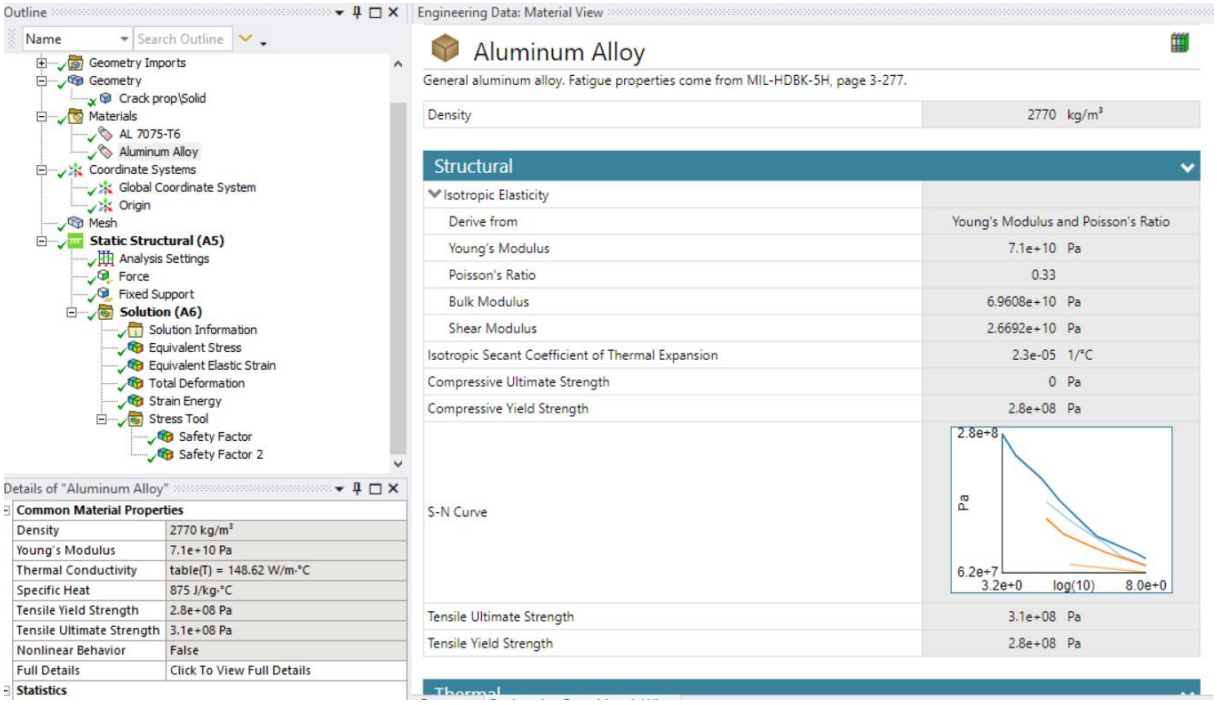

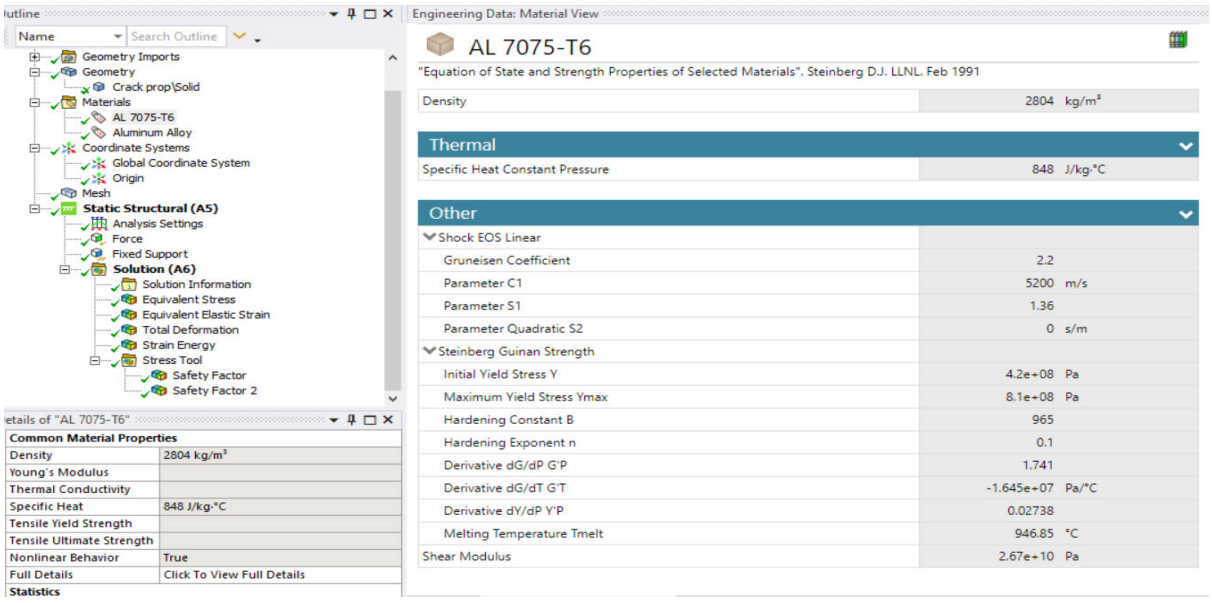

Stress distribution at the crack tip.

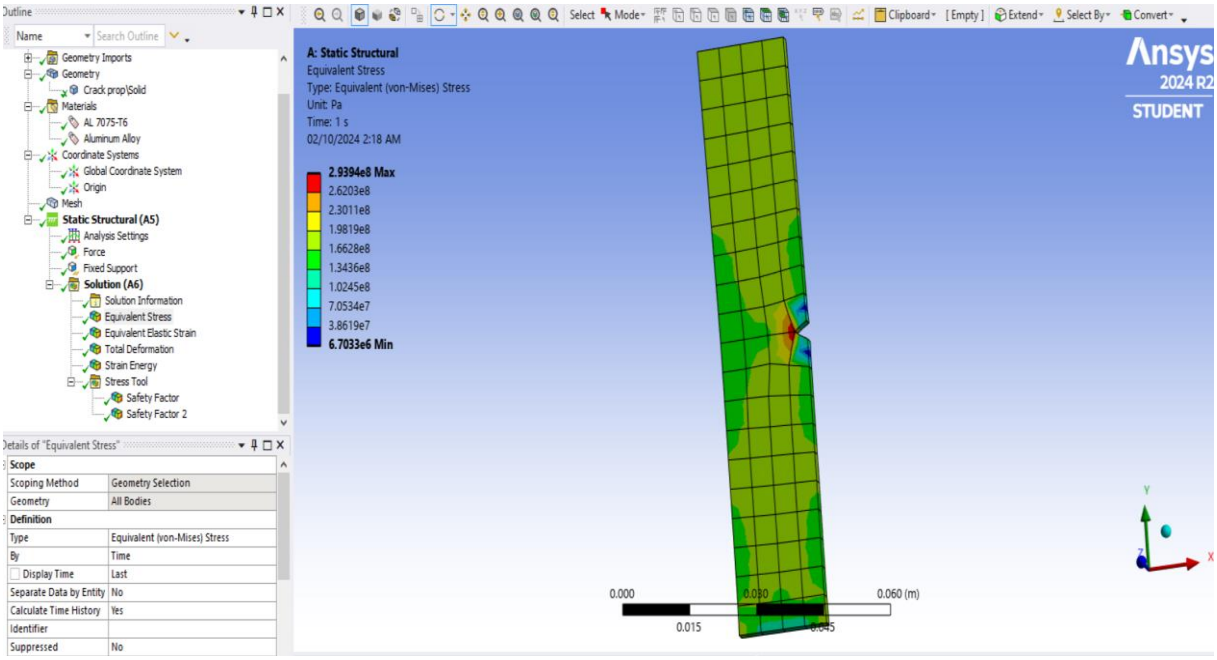

Simulated Elastic Strain

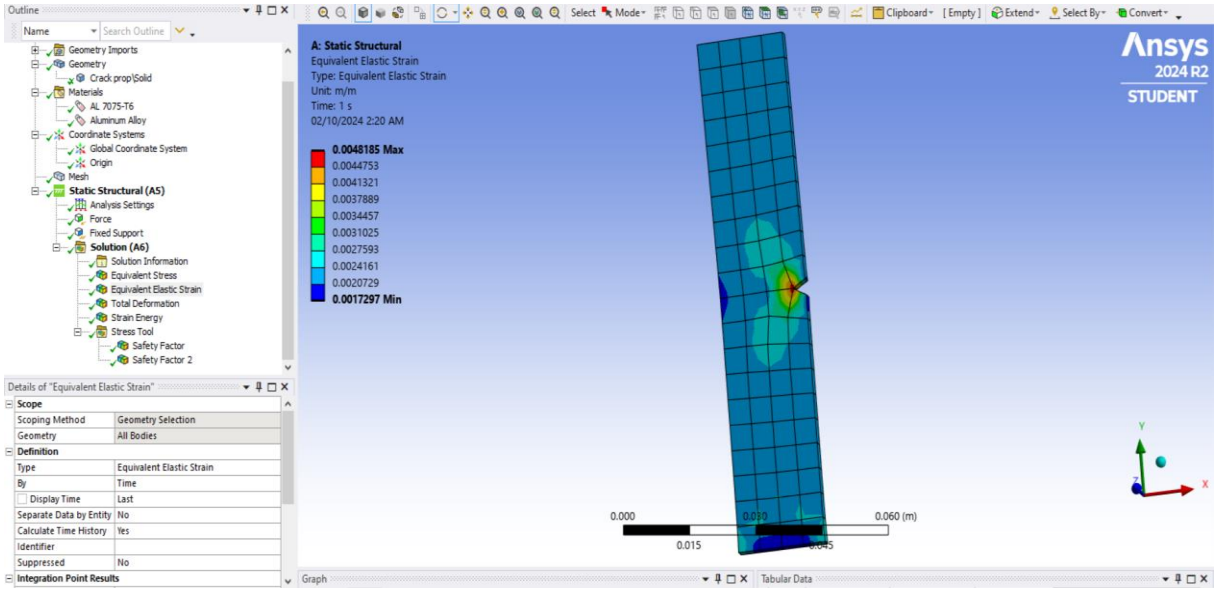

Deformation and Life Cycle Estimation

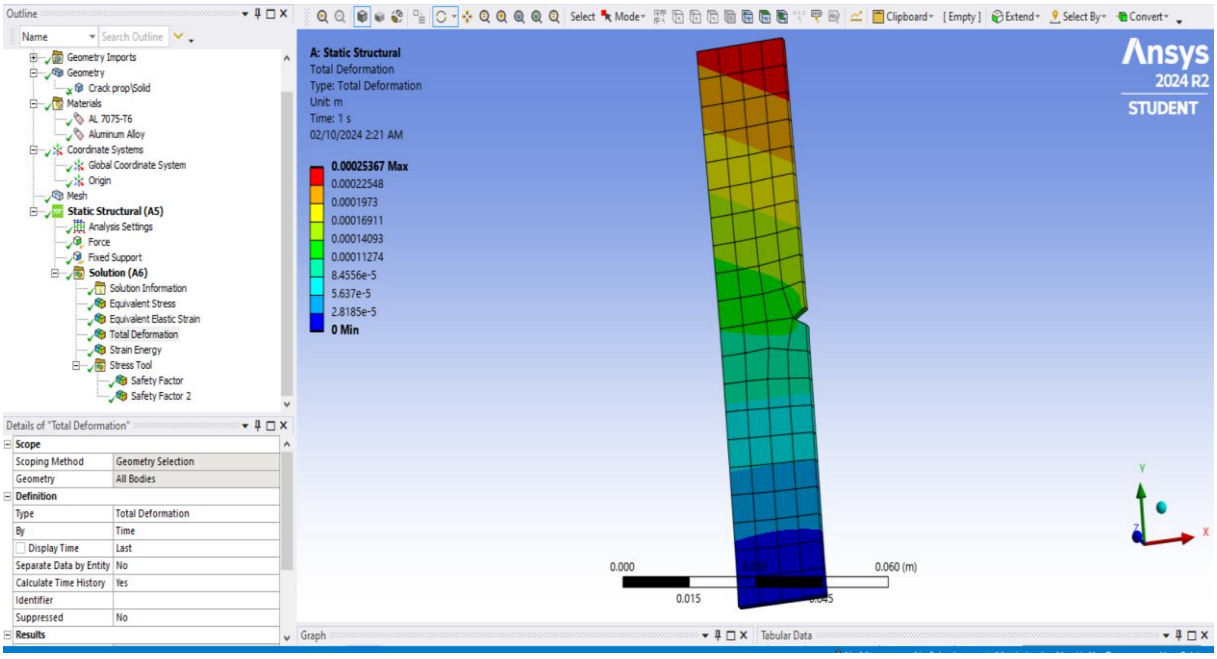

Simulated Strain Energy Release Rate

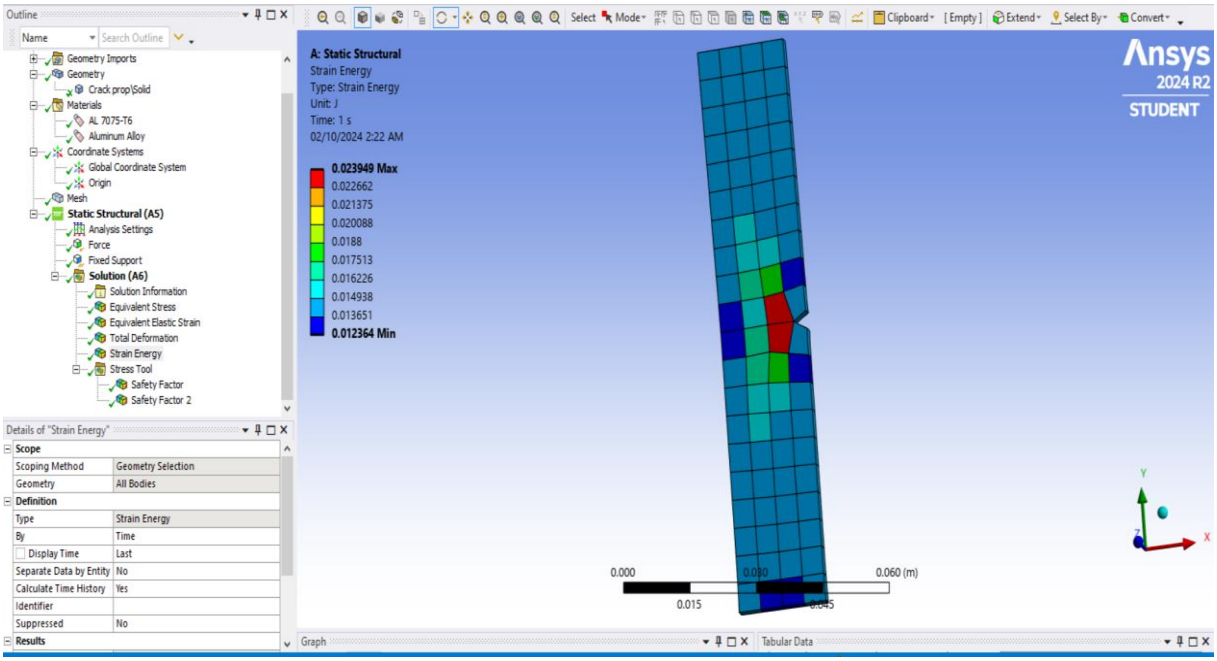

Scanning Electron Microscope Results

Surface roughness and Striations on an unfractured test sample

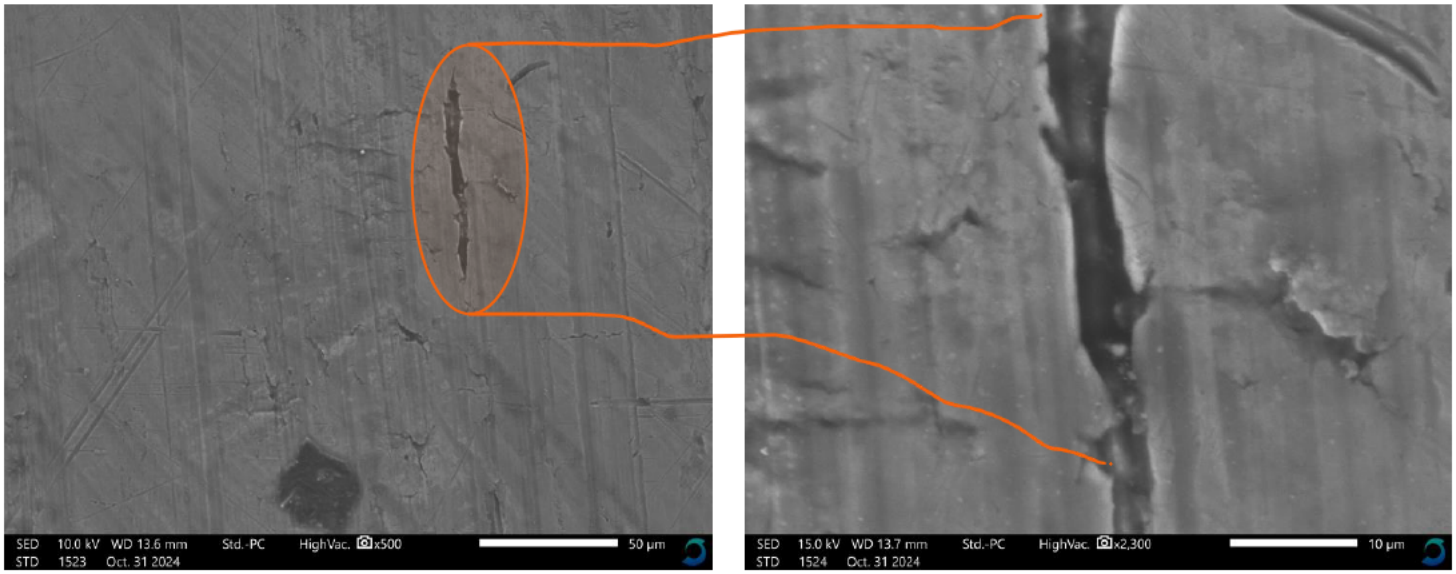

Bright and Shiny appearance of the fractured surface

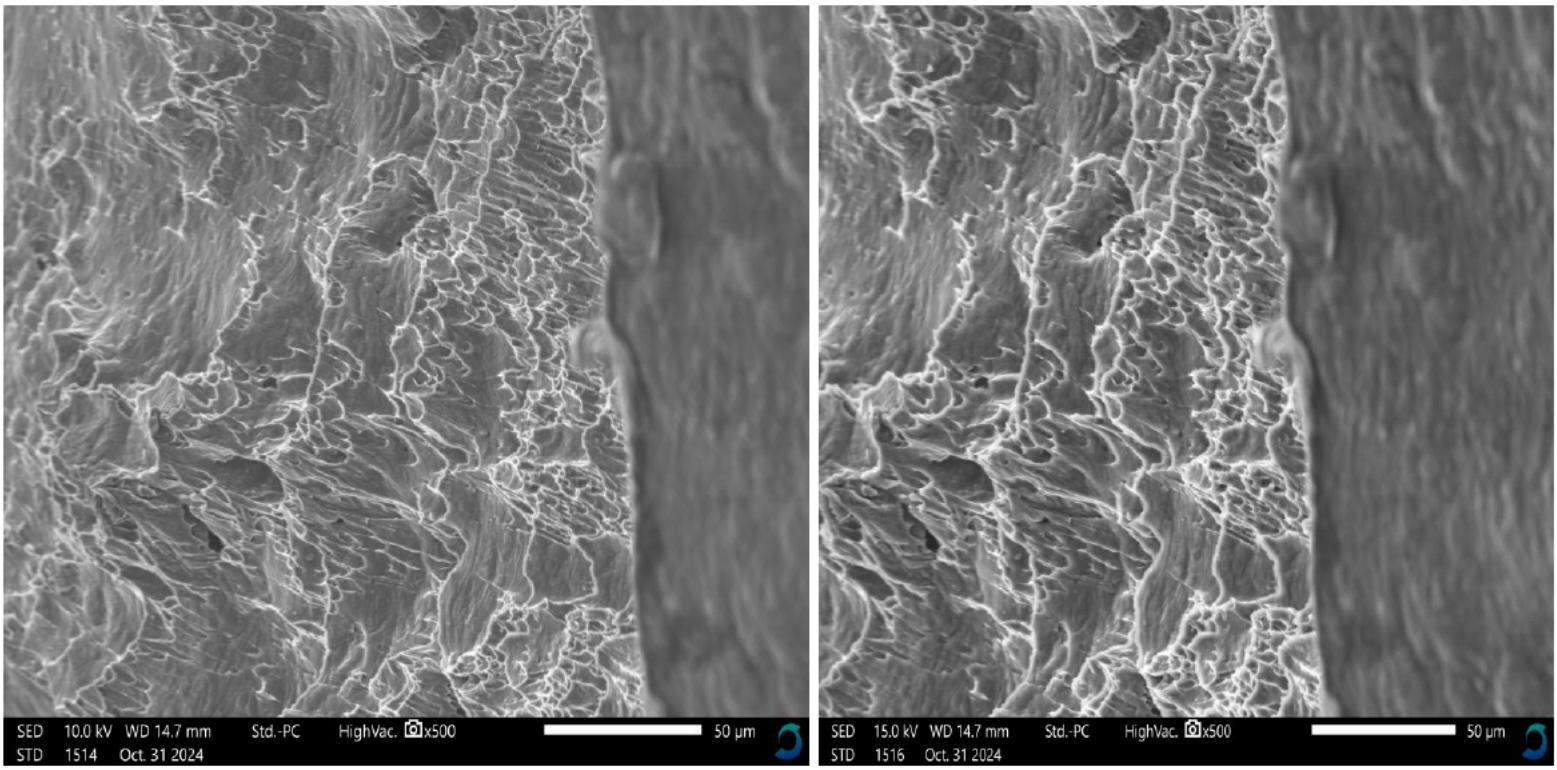

STEP 1: LOAD THE DATA INTO MATLAB INITIALISE MATERIAL PROPERTIES

```
% Constants and material properties
W = 20;  % width of the specimen in mm
t = 3;   % thickness of the specimen in mm
a_0 = 3; % initial crack length in mm
Y = 1.12; % geometry factor

 % Define the file name
filename = 'Sample 3.csv';

% Read the data from the CSV file and preserve the original column headers
opts = detectImportOptions(filename);
opts.VariableNamingRule = 'preserve';
data = readtable(filename, opts);

% disp(data);

% Access the columns for the first set (1_1)
time_1_1 = data.('1 _ 1');
force_1_1 = data.('Var2');
stroke_1_1 = data.('Var3');

% Access the columns for the second set (1_2)
time_1_2 = data.('1 _ 2');
force_1_2 = data.('Var5');
stroke_1_2 = data.('Var6');

% Access the columns for the third set (1_3)
time_1_3 = data.('1 _ 3');
force_1_3 = data.('Var8');
stroke_1_3 = data.('Var9');

figure;
plot(stroke_1_1,force_1_1);
hold on;
plot(stroke_1_2, force_1_2);
plot(stroke_1_3, force_1_3);
ylabel('Force (N)');
xlabel("Stroke (mm)")
title("Force Applied Vs Stroke")
hold off;
legend('Sample 1', 'Sample 2', 'Sample 3');
```

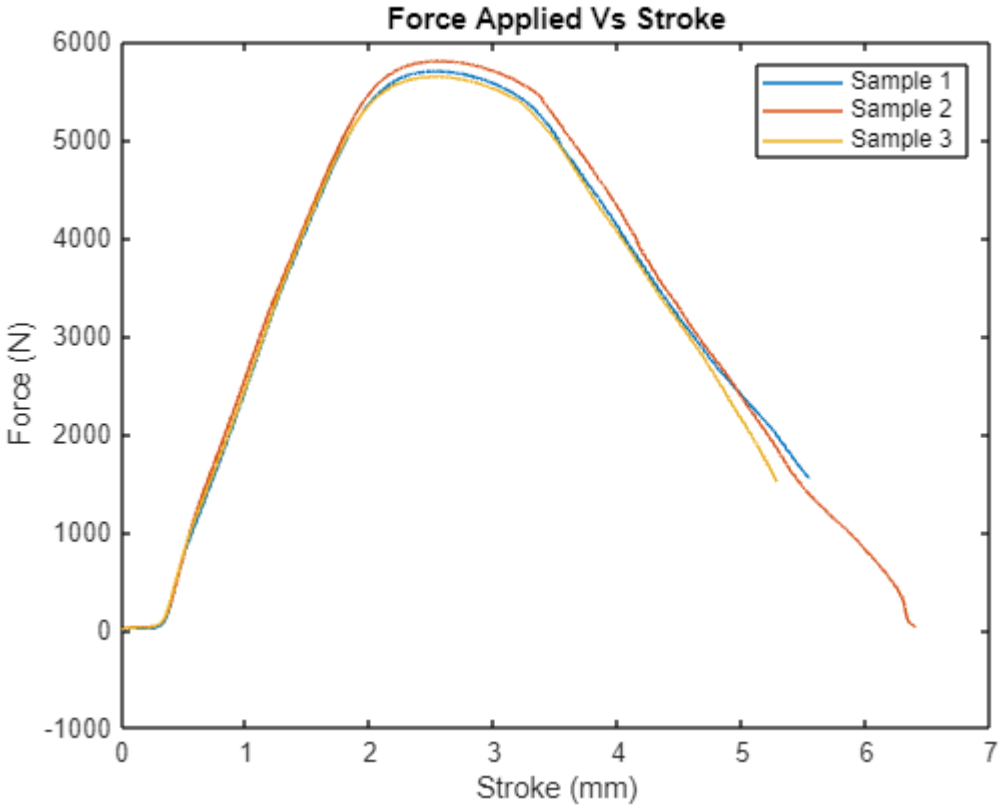

CALCULATION OF STRESS INTENSITY FACTORS

```
% Initialize arrays to store calculated values
n = length(force_1_1);


crack_length = a_0;  % Start with the initial crack length

% Calculate stress (sigma) in MPa
stress_1_1 = force_1_1 ./ (W * t); % MPa = N / m
stress_1_2 = force_1_2 ./ (W * t); % MPa = N / m
stress_1_3 = force_1_3 ./ (W * t); % MPa = N / m


% Calculate the stress intensity factor (K_I) in MPa·m^1/2
KI_1_1 = stress_1_1 .* sqrt(pi * crack_length) * Y; % MPa·m^1/2
KI_1_2 = stress_1_2 .* sqrt(pi * crack_length) * Y; % MPa·m^1/2
KI_1_3 = stress_1_3 .* sqrt(pi * crack_length) * Y; % MPa·m^1/2


figure;
```

```
plot(time_1_1,KI_1_1);
hold on
plot(time_1_2,KI_1_2);
plot(time_1_3,KI_1_3);
xlabel('Time (sec)');
ylabel("KI values (MPa)")
title("Stress Intensity Factors against Time")
grid on;
legend('Sample 1', 'Sample 2', 'Sample 3');
hold off
```

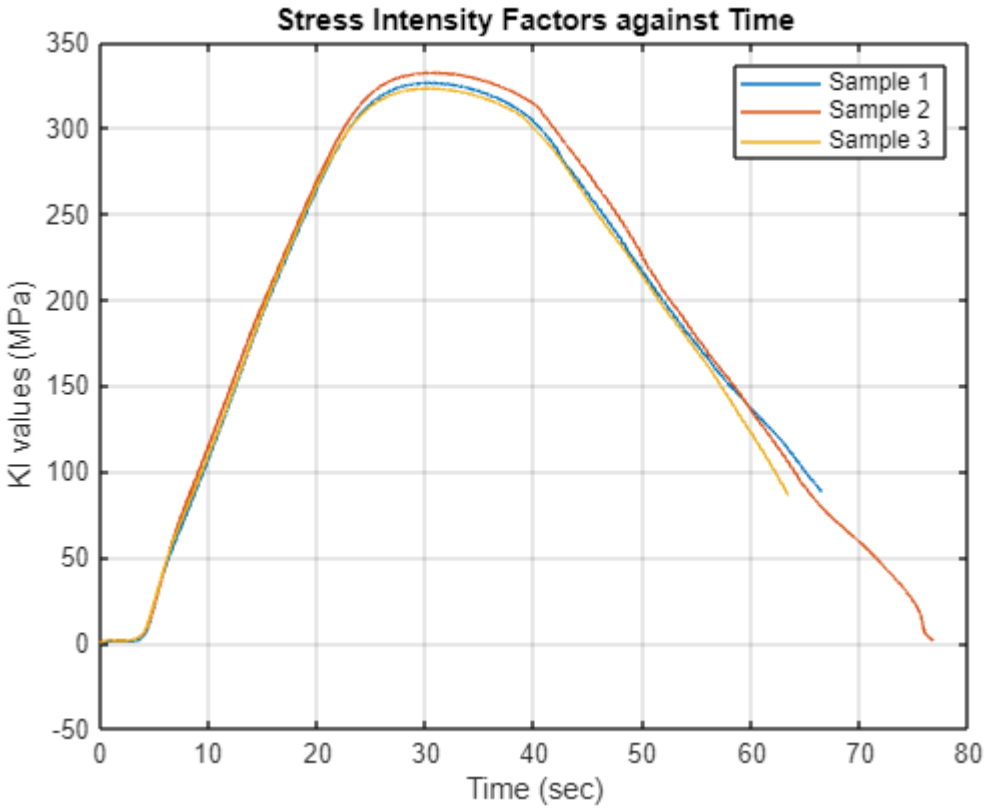


```
% EXPORTING RELEVANT VARIABLES TO AN EXCEL FILE
%

% Combine arrays into a matrix
matrix = [time_1_3,
force_1_1,stress_1_1,KI_1_1,force_1_2,stress_1_2,KI_1_2,force_1_3,stress_1_3,KI_1_3]
;

% Create cell array with headers
headers = {'Time', 'Force1', 'Stress1','KI_1','Force2', 'Stress2','KI_2','Force3',
'Stress3','KI_3'};
data = [headers; num2cell(matrix)]; % Combine headers and matrix data

% Specify the filename
filename = 'Results.xlsx';
```

```
% Write the cell array to the Excel file
writecell(data, filename);

% Read the data from the Excel file
filename = 'Results.xlsx';
data1 = readcell(filename);

% Extract the headers and the data matrix separately
headers = data1(1, :);
matrixData = cell2mat(data(2:6010, :));

% Define the indices of interest

indices= 0:600:6000;

% Convert the indices to row numbers
rowNumbers = indices + 1; % Adding 1 to convert to 1-based indexing

% Extract Time, KI_1, KI_2, and KI_3 at the specified indices
Time = matrixData(rowNumbers, strcmp(headers, 'Time'));
KI_1 = matrixData(rowNumbers, strcmp(headers, 'KI_1'));
KI_2 = matrixData(rowNumbers, strcmp(headers, 'KI_2'));
KI_3 = matrixData(rowNumbers, strcmp(headers, 'KI_3'));

% Create a table with the extracted values
KI_table = table(Time, KI_1, KI_2, KI_3, ...
    'VariableNames', {'Time', 'KI_1', 'KI_2', 'KI_3'});

% Display the table
disp(KI_table);
```

Time	KI_1	KI_2	KI_3
0	0.0024593	-0.0024593	-0.026688
6	44.029	44.814	45.697
12	141.12	148.62	142.6
18	236.78	241.47	238.45
24	308.15	313.83	307.22
30	326.08	331.93	322.87
36	318.76	326.07	315.79
42	288.07	298.13	285.18
48	234.69	245.87	231.24
54	181.02	186.56	178.03
60	136.34	135.02	121.91

CALCULATE THE STRESS DISTRIBUTION

SAMPLE 1

```
% Calculate Stress Distribution around the crack tip (polar coordinates)
```

```
initial_crack_length=3;
r= initial_crack_length /2; % Distance from crack tip

theta = linspace(0, 2*pi, 100); % Angle range from 0 to 2π
sigma_x = (1/sqrt(2*pi*r)) * KI_1_1 .* cos(theta/2) .* (1 - sin(theta/2) .*
sin(3*theta/2));
sigma_y = (1/sqrt(2*pi*r)) * KI_1_1 .* cos(theta/2) .* (1 + sin(theta/2) .*
sin(3*theta/2));
tau_xy = (-1/sqrt(2*pi*r)) * KI_1_1 .* cos(theta/2) .* sin(theta/2) .*
sin(3*theta/2);


% Plot Stress Distribution around Crack Tip
    figure;
    polarplot(theta, sigma_x, '-r');
    hold on;
    polarplot(theta, sigma_y, '-b');
    polarplot(theta, tau_xy, '-g');
    title('Stress Distribution Around the Crack Tip for sample 1');
    hold off;
```

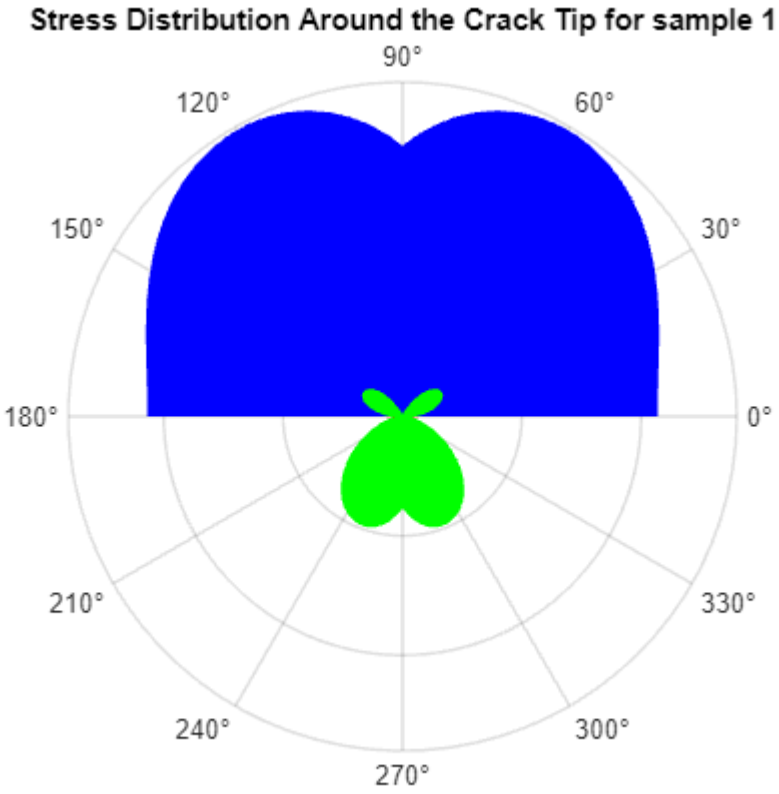


```
% Parameters
initial_crack_length = 3;
r = initial_crack_length / 2; % Distance from crack tip

theta = linspace(0, 2*pi, 100); % Angle range from 0 to 2π
```

```
% Stress components in polar coordinates
sigma_x = (1/sqrt(2*pi*r)) * KI_1_1 .* cos(theta/2) .* (1 - sin(theta/2) .*
sin(3*theta/2));
sigma_y = (1/sqrt(2*pi*r)) * KI_1_1 .* cos(theta/2) .* (1 + sin(theta/2) .*
sin(3*theta/2));
tau_xy = (-1/sqrt(2*pi*r)) * KI_1_1 .* cos(theta/2) .* sin(theta/2) .*
sin(3*theta/2);

% Convert polar to Cartesian coordinates
x = r * cos(theta);
y = r * sin(theta);

% Plot Stress Distribution in Cartesian coordinates
figure;
plot(x, sigma_x);
hold on;
plot(x, sigma_y);
plot(x, tau_xy);
title('Stress Distribution Around the Crack Tip for Sample 1');
xlabel('x');
ylabel('Stress (MPa)');

grid on;
hold off;
```

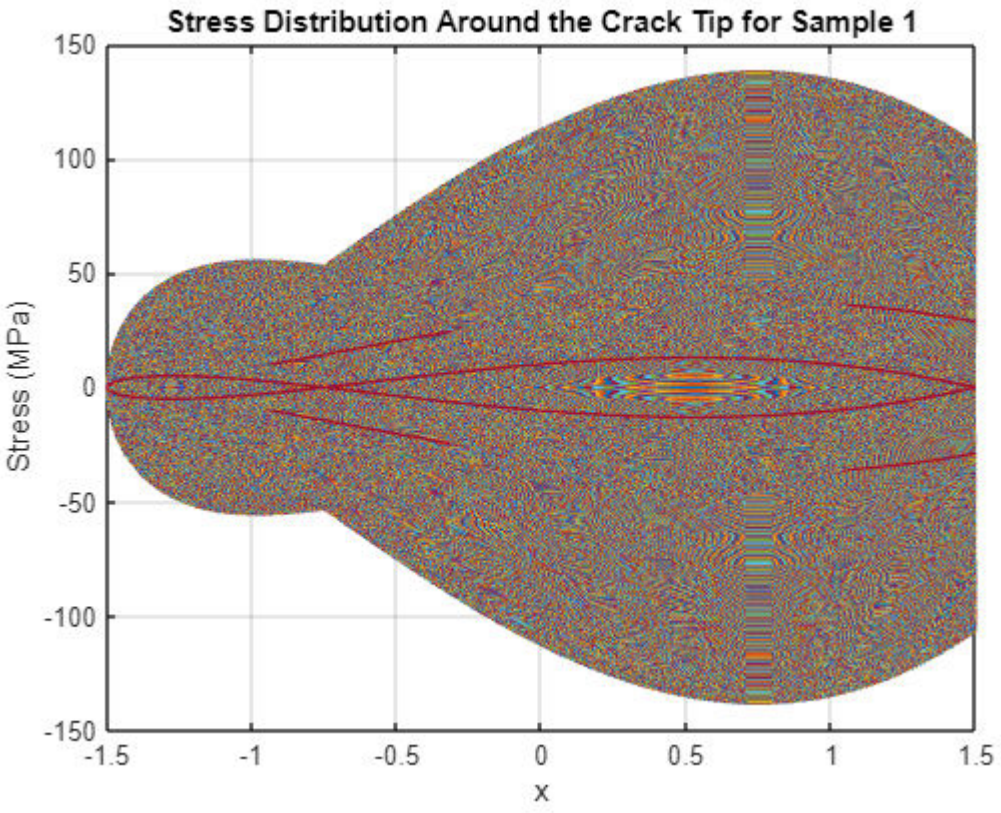

```
figure;
plot(theta, sigma_x, '-r');
hold on;
plot(theta, sigma_y, '-b');
plot(theta, tau_xy, '-g');
xlabel('Theta (radians)');
ylabel('Stress');
title('Stress Distribution Around the Crack Tip');

grid on;
hold off;
```

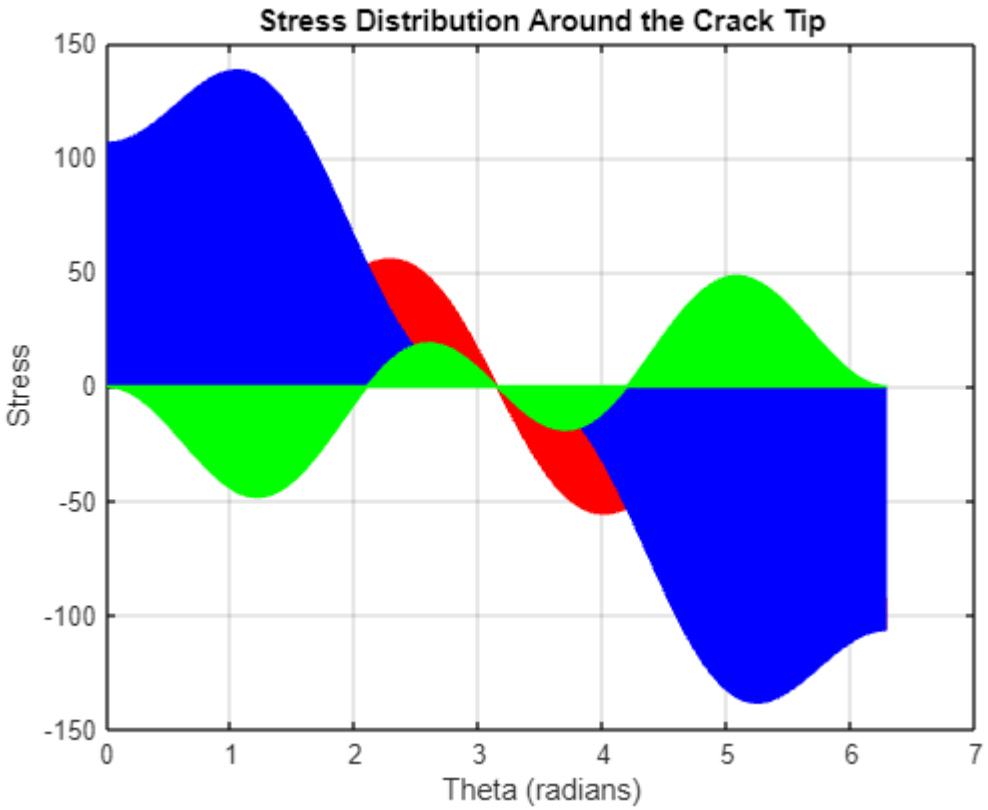

Warning: Graphics timeout occurred. To share details of this issue with MathWorks technical support, please include that this is an unresponsive graphics client with your service request.

STRESS DISTRIBUTION FOR SAMPLE 2

```
% Calculate Stress Distribution around the crack tip (polar coordinates)
r= initial_crack_length /2; % Distance from crack tip

theta = linspace(0, 2*pi, 100); % Angle range from 0 to 2π
```

```
sigma_x2 = (1/sqrt(2*pi*r)) * KI_1_2 .* cos(theta/2) .* (1 - sin(theta/2) .*
sin(3*theta/2));
sigma_y2 = (1/sqrt(2*pi*r)) * KI_1_2 .* cos(theta/2) .* (1 + sin(theta/2) .*
sin(3*theta/2));
tau_xy2 = (-1/sqrt(2*pi*r)) * KI_1_2 .* cos(theta/2) .* sin(theta/2) .*
sin(3*theta/2);


% Plot Stress Distribution around Crack Tip
    figure;
    polarplot(theta, sigma_x2, '-r');
    hold on;
    polarplot(theta, sigma_y2, '-b');
    polarplot(theta, tau_xy2, '-g');
    title('Stress Distribution Around the Crack Tip for sample 2');
    hold off;
```

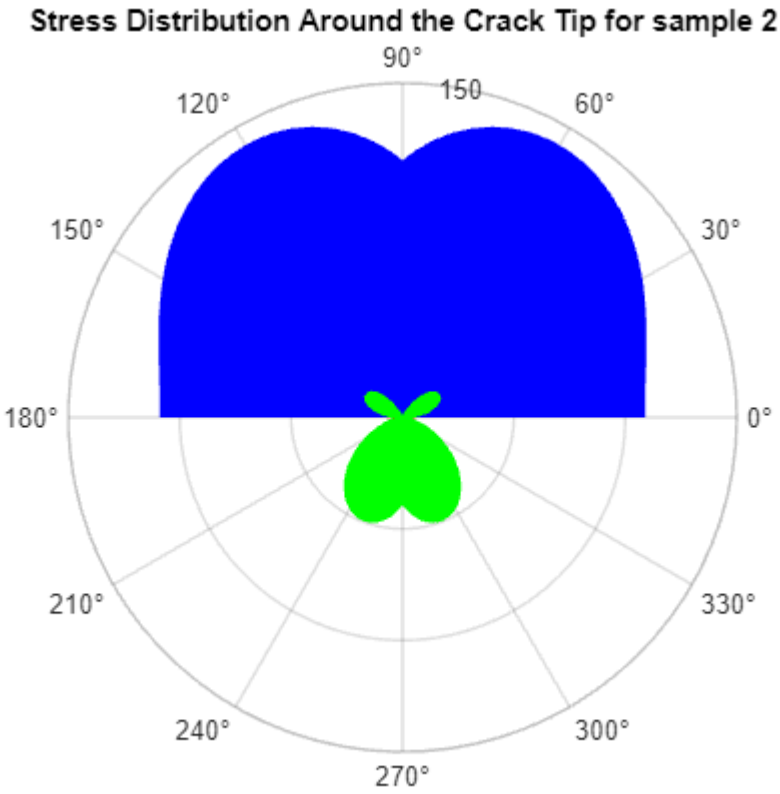

STRESS DISTRIBUTION FOR SAMPLE 3

```
 % Calculate Stress Distribution around the crack tip (polar coordinates)
r= initial_crack_length /2; % Distance from crack tip

theta = linspace(0, 2*pi, 100); % Angle range from 0 to 2π
sigma_x3 = (1/sqrt(2*pi*r)) * KI_1_3 .* cos(theta/2) .* (1 - sin(theta/2) .*
sin(3*theta/2));
```

```
sigma_y3 = (1/sqrt(2*pi*r)) * KI_1_3 .* cos(theta/2) .* (1 + sin(theta/2) .*
sin(3*theta/2));
tau_xy3 = (-1/sqrt(2*pi*r)) * KI_1_3 .* cos(theta/2) .* sin(theta/2) .*
sin(3*theta/2);


% Plot Stress Distribution around Crack Tip
    figure;
    polarplot(theta, sigma_x3, '-r');
    hold on;
    polarplot(theta, sigma_y3, '-b');
    polarplot(theta, tau_xy3, '-g');
    title('Stress Distribution Around the Crack Tip for sample 3');
    hold off;
```

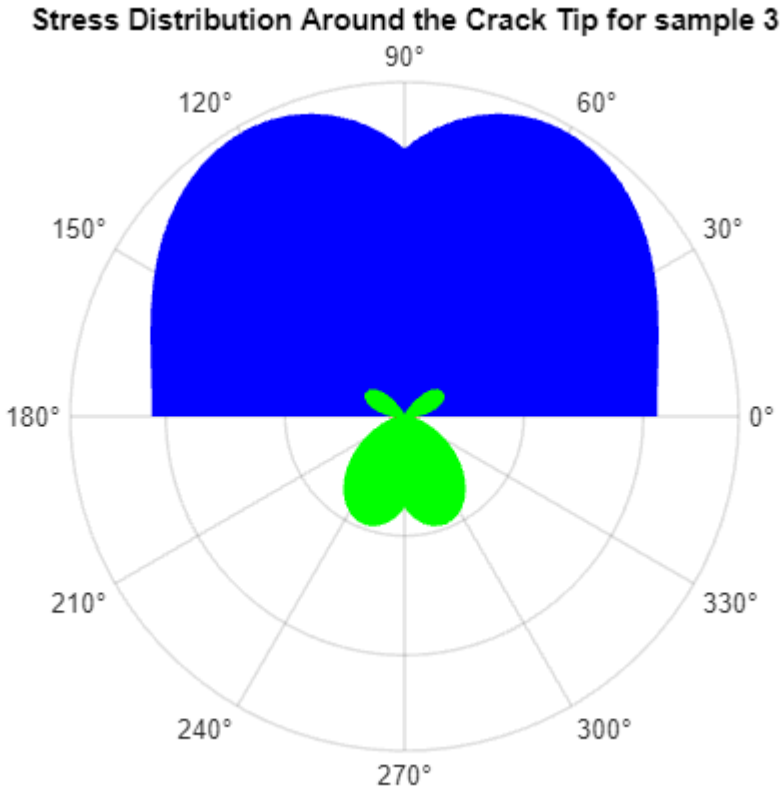


```
% Paris Law constants
C = 8.87e-8;  % Paris law constant C
M = 3.14;     % Paris law constant M
% Initial crack length


% Initial crack length
initial_crack_length = 3;  % mm
critical_crack_length = 20;  % mm
```

```
%%%%%%%%%%% SAMPLE 1 %%%%%%%%%%%%%

% Variables to store the life estimate
crack_length = initial_crack_length;  % Start with the initial crack length
num_cycles = 0;  % Initialize cycle count
% Find K_max and K_min for this cycle (from your provided K_I data)
    K_max = max(KI_1_1);  % Maximum KI in this cycle
    K_min = min(KI_1_1);  % Minimum KI in this cycle

    % Calculate Delta K
    delta_K = K_max - K_min;

while crack_length < critical_crack_length


    % Apply Paris Law to calculate crack growth per cycle
    da_dN1 = C * (delta_K^M);

    % Update crack length
    crack_length = crack_length + da_dN1;

    % Increment the number of cycles
    num_cycles = num_cycles + 1;
end

% Display the estimated number of cycles to failure
disp(['Estimated life of the crack in sample 1 (in cycles): ',
num2str(num_cycles)]);
```

```
Estimated life of the crack in sample 1 (in cycles): 3
```

```
%%%%%%%%%%% SAMPLE 2 %%%%%%%%%%%%%


% Find K_max and K_min for this cycle (from your provided K_I data)
    K_max = max(KI_1_2);  % Maximum KI in this cycle
    K_min = min(KI_1_2);  % Minimum KI in this cycle

    % Calculate Delta K
    delta_K = K_max - K_min;

    % Apply Paris Law to calculate crack growth per cycle
    da_dN2 = C * (delta_K^M);

while crack_length < critical_crack_length

    % Update crack length
    crack_length = crack_length + da_dN2;
```

```
    % Increment the number of cycles
    num_cycles = num_cycles + 1;
end

% Display the estimated number of cycles to failure
disp(['Estimated life of the crack in sample 2 (in cycles): ',
num2str(num_cycles)]);
```

```
Estimated life of the crack in sample 2 (in cycles): 3
```

```
%%%%%%%%%%% SAMPLE 3 %%%%%%%%%%%%%%

% Initialize arrays to store crack lengths and cycles
crack_lengths = [];   % Array to store crack lengths
cycles = [];          % Array to store the number of cycles
% Find K_max and K_min for this cycle (from your provided K_I data)
    K_max = max(KI_1_3);  % Maximum KI in this cycle
    K_min = min(KI_1_3);  % Minimum KI in this cycle

    % Calculate Delta K
    delta_K = K_max - K_min;

     % Apply Paris Law to calculate crack growth per cycle
    da_dN3 = C * (delta_K^M);
    disp (da_dN3);
```

```
    6.7075
```

```
while crack_length < critical_crack_length




    % Update crack length
    crack_length = crack_length + da_dN3;

    % Store the current crack length and number of cycles
    crack_lengths(end+1) = crack_length;
    cycles(end+1) = num_cycles;

    % Increment the number of cycles
    num_cycles = num_cycles + 1;
end

% Display the estimated number of cycles to failure
```

```
disp(['Estimated life of the crack in sample 3 (in cycles): ',
num2str(num_cycles)]);
```

```
Estimated life of the crack in sample 3 (in cycles): 3
```

```

% Paris' Law Crack Growth Estimation and Plotting
% Variables
C = 8.87e-8;  % Paris law constant C
M = 3.14;     % Paris law constant M % Material exponent
DeltaK1 =max(KI_1_1)-min(KI_1_1); % Stress intensity factor range
DeltaK2 =max(KI_1_2)-min(KI_1_2);
DeltaK3 =max(KI_1_3)-min(KI_1_3);
a0 = 3;  % Initial crack length in mm
af = 20;  % Final (critical) crack length in mm
da = 1e-3;   % Small increment for crack growth integration

% Initialize variables for storing crack lengths and cycle numbers
a_values = a0:da:af;  % Array of crack lengths from a0 to af
a_values2 = a0:da:af;
a_values3 = a0:da:af;

N_values1 = zeros(size(a_values));  % Array to store the number of cycles
N_values2 = zeros(size(a_values));
N_values3 = zeros(size(a_values));

% Perform the integration in a loop to calculate the number of cycles at each crack
length
N_total1 = 0; % Initialize the total number of cycles
N_total2 = 0;
N_total3 = 0;
for i = 2:length(a_values)
    % Calculate delta N for the current crack length using Paris' Law
    deltaN1 = da / (C * (DeltaK1^M));
    deltaN2 = da / (C * (DeltaK2^M));
    deltaN3 = da / (C * (DeltaK3^M));

    % Accumulate the total number of cycles
    N_total1 = N_total1 + deltaN1;
    N_total2 = N_total2 + deltaN2;
    N_total3 = N_total3 + deltaN3;

    % Store the number of cycles corresponding to the current crack length
    N_values1(i) = N_total1;
    N_values2(i) = N_total2;
    N_values3(i) = N_total3;
end
```

```
% Print the total life estimation of the crack (in terms of number of cycles)
fprintf('Total life estimation of the crack (from %.3f mm to %.3f mm) is
approximately %.0f cycles.\n', a0, af, N_total1);
```

```
Total life estimation of the crack (from 3.000 mm to 20.000 mm) is approximately 2 cycles.
```

```
% Plot crack length vs. number of cycles
figure;
plot(N_values1, a_values, 'LineWidth', 2);
xlabel('Number of Cycles (N)');
ylabel('Crack Length (a) [mm]');
title('Crack Length vs. Number of Cycles');
grid on;
```

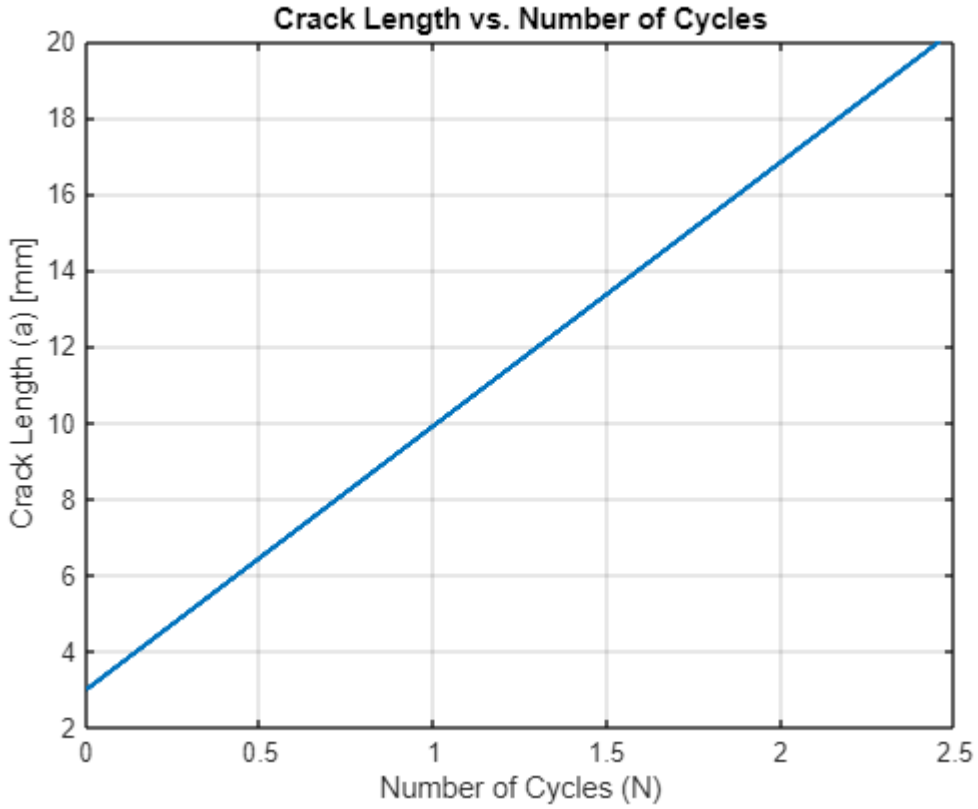


```
% Define the target value you want to extract up to
targetValue1 = max(KI_1_1);
targetValue2 = max(KI_1_2);
targetValue3 = max(KI_1_3);

% Find the index of the target value
index1 = find( KI_1_1== targetValue1, 1);  % '1' ensures it finds the first
occurrence
```

```
index2 = find( KI_1_2== targetValue2, 1);
index3 = find( KI_1_3== targetValue3, 1);

% Extract values from the beginning up to the target value
if ~isempty(index1)
    KI_filtered1 = KI_1_1(1:index1);

end
if ~isempty(index2)

    KI_filtered2 = KI_1_2(1:index2);

end

if ~isempty(index3)

    KI_filtered3 = KI_1_3(1:index3);

end


da_dN_values1 = linspace(0,da_dN1,length(KI_filtered1));
da_dN_values2 = linspace(0,da_dN2,length(KI_filtered2));
da_dN_values3 = linspace(0,da_dN3,length(KI_filtered3));

% Plot da/dN against KI
figure;
plot(KI_filtered1, da_dN_values1, 'LineWidth', 2);
hold on;
plot(KI_filtered2, da_dN_values2, 'LineWidth', 2);
plot(KI_filtered3, da_dN_values3, 'LineWidth', 2);
xlabel('Stress Intensity Factor, KI');
ylabel('Crack Growth Rate, da/dN');
title('Crack Growth Rate vs. Stress Intensity Factor');
grid on;
legend('Sample 1', 'Sample 2', 'Sample 3');
hold off;
```

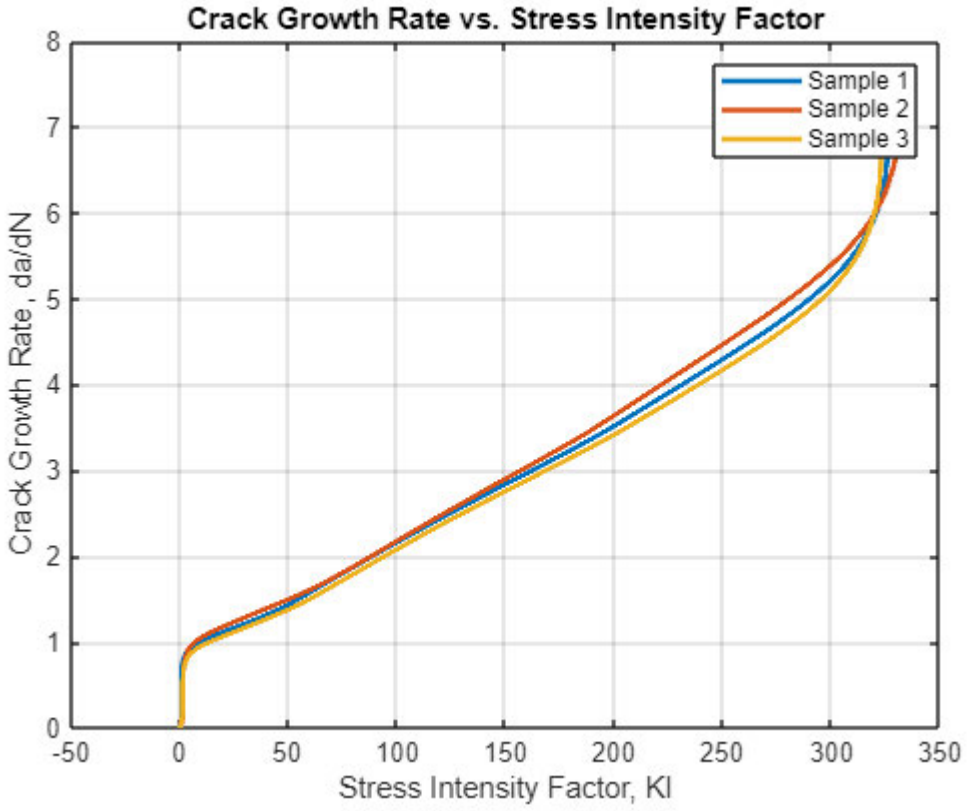


```
table1=[KI_filtered1,(da_dN_values1)'];
% KI_filtered2, da_dN_values2,KI_filtered3,da_dN_values3];
% disp (table1);
indices = 0:300:3000;


% Adjust indices for MATLAB's 1-based indexing.
adjustedIndices = (indices)' + 1;
table2= table1(adjustedIndices,:);

% Create a table with headers
table3 = array2table(table2, 'VariableNames', {'KI_values', 'Crack Length'});

% Display the table
disp('da_dN against KI values for Sample1');
```

```
da_dN against KI values for Sample1
```

```
disp(table3);
```

```
    KI_values    Crack Length
    _________    ____________

    0.0024593           0
      0.97671       0.6807
       44.029       1.3614
```

```
  91.6       2.0421
141.12       2.7228
192.28       3.4035
236.78       4.0842
   278       4.7649
308.15       5.4456
322.33       6.1263
326.08        6.807
```

```
table1=[KI_filtered2,(da_dN_values2)'];

% disp (table1);
indices = 0:300:3000;


% Adjust indices for MATLAB's 1-based indexing.
adjustedIndices = (indices)' + 1;
table2= table1(adjustedIndices,:);

% Create a table with headers
table3 = array2table(table2, 'VariableNames', {'KI_values', 'Crack Length'});

% Display the table
disp('da_dN against KI values for Sample2');
```

```
da_dN against KI values for Sample2
```

```
disp(table3);
```

```
    KI_values     Crack Length
    _________     ____________

    -0.0024593           0
         1.988       0.7206
        44.814       1.4412
        98.977       2.1618
        148.62       2.8824
        197.77        3.603
        241.47       4.3236
        282.99       5.0442
        313.83       5.7648
        328.03       6.4854
        331.93        7.206
```

```
table1=[KI_filtered3,(da_dN_values3)'];
% KI_filtered2, da_dN_values2,KI_filtered3,da_dN_values3];
% disp (table1);
indices = 0:300:3000;


% Adjust indices for MATLAB's 1-based indexing.
adjustedIndices = (indices)' + 1;
table2= table1(adjustedIndices,:);
```

```
% Create a table with headers
table3 = array2table(table2, 'VariableNames', {'KI_values', 'Crack Length'});

% Display the table
disp('da_dN against KI values for Sample3');
```

```
da_dN against KI values for Sample3
```

```
disp(table3);
```

```
    KI_values    Crack Length
    _________    ____________

    -0.026688           0
       1.7028     0.66521
       45.697      1.3304
       94.046      1.9956
        142.6      2.6608
        193.5      3.3261
       238.45      3.9913
       279.02      4.6565
       307.22      5.3217
       319.71      5.9869
       322.87      6.6521
```

ENERGY RELEASE RATE

We use the formula

$$G = \frac{B}{E} K_I^2$$

```
% Define material properties
E = 70e9;          % Young's modulus (Pa) for the material
nu = 0.33;         % Poisson's ratio for the material
B = 3e-3;          % Thickness of the plate (mm)

% Calculate Energy Release Rate G
G_1_1 = (B * KI_1_1.^2) / E;
G_1_2 = (B * KI_1_2.^2) / E;
G_1_3 = (B * KI_1_3.^2) / E;


% Plot Energy Release Rate G over time
 figure;
 plot(time_1_1, G_1_1, 'LineWidth', 2);
 hold on
 plot(time_1_2, G_1_2, 'LineWidth', 2);
 plot(time_1_3, G_1_3, 'LineWidth', 2);
 title('Energy Release Rate G over Time');
 xlabel('Time (sec)');
 ylabel('G (J/m^2)');
 grid on;
```

```
legend('Sample 1', 'Sample 2', 'Sample 3');
hold off;
```

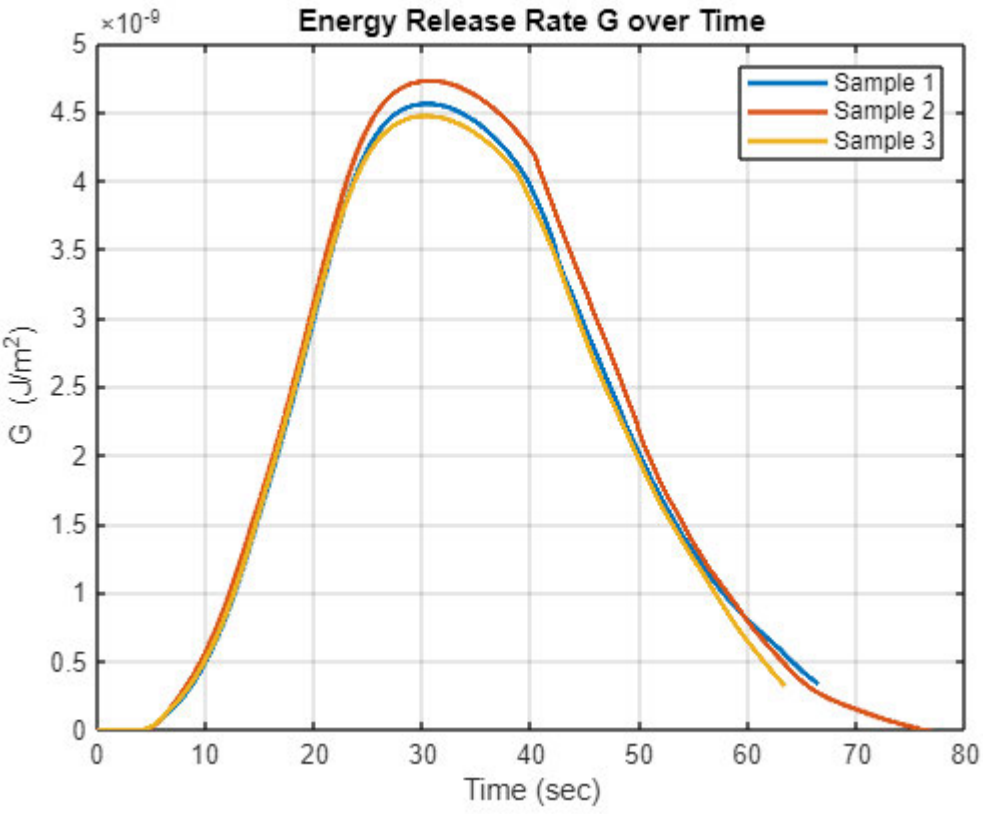


```
% EXPORTING RELEVANT VARIABLES TO AN EXCEL FILE (ENERGY RELEASE RATE)

% Combine arrays into a matrix
matrix1 = [time_1_1, G_1_1, G_1_2, G_1_3];

% Create cell array with headers
headers1 = {'Time', 'Sample 1', 'Sample 2','Sample 3'};
data1 = [headers1; num2cell(matrix1)]; % Combine headers and matrix data

% Specify the filename
filename = 'Energy Release Results.xlsx';

% Write the cell array to the Excel file
writecell(data1, filename);
```

```
% Read the data from the Excel file
filename = 'Energy Release Results.xlsx';
data1 = readcell(filename);

% Extract the headers and the data matrix separately
headers = data1(1, :);
matrixData = cell2mat(data1(2:6010, :));

% Define the indices of interest

indices= 0:600:6000;

% Convert the indices to row numbers
rowNumbers = indices + 1; % Adding 1 to convert to 1-based indexing

% Extract Time, KI_1, KI_2, and KI_3 at the specified indices
Time = matrixData(rowNumbers, strcmp(headers, 'Time'));
 G_1_1= matrixData(rowNumbers, strcmp(headers, 'Sample 1'));
G_1_2 = matrixData(rowNumbers, strcmp(headers, 'Sample 2'));
G_1_3 = matrixData(rowNumbers, strcmp(headers, 'Sample 3'));

% Create a table with the extracted values
Energy_table = table(Time, G_1_1, G_1_2, G_1_3, ...
    'VariableNames', {'Time', 'Sample 1', 'Sample 2', 'Sample 3'});

% Display the table
disp(Energy_table);
```

Time	Sample 1	Sample 2	Sample 3
0	2.5921e-19	2.5921e-19	3.0525e-17
6	8.308e-11	8.6071e-11	8.9496e-11
12	8.535e-10	9.4665e-10	8.7149e-10
18	2.4027e-09	2.4988e-09	2.4369e-09
24	4.0695e-09	4.2211e-09	4.0449e-09
30	4.5568e-09	4.7219e-09	4.4676e-09
36	4.3546e-09	4.5566e-09	4.274e-09
42	3.5565e-09	3.8091e-09	3.4855e-09
48	2.3605e-09	2.5908e-09	2.2917e-09
54	1.4044e-09	1.4917e-09	1.3583e-09
60	7.9661e-10	7.8133e-10	6.3698e-10

Fracture of AA7075

Key Word	Fracture	**Product Name**	AA7075
Test File Name	Mr. Oloo's Test	**Method File Name**	Al Tensile Test.xmak
Report Date	9/23/2024	**Test Date**	9/23/2024
Test Mode	Single	**Test Type**	Tensile
Speed	5mm/min	**Shape**	Plate
No of Batches:	1	**Qty/Batch:**	3

Name	Thickness	Elastic	YP(%FS)_Force	YP(%FS)_Stress
Parameters		Force 10 – 20 N	0.1 %	0.1 %
Unit	mm	N/mm2	N	N/mm2
Sample 1	3.0000	14.3860	-.-	-.-
Sample 2	3.0000	364.459	-.-	-.-
Sample 3	3.0000	171.382	-.-	-.-
Average	3.0000	183.409	-.-	-.-
Standard Deviation	0.00000	175.346	-.-	-.-
Range	0.00000	350.073	-.-	-.-

Name	YP(%FS)_Time	YS1_Force	YS1_Stress	YS1_Stroke
Parameters	0.1 %	0.2 %	0.2 %	0.2 %
Unit	sec	N	N/mm2	mm
Sample 1	-.-	-.-	-.-	-.-
Sample 2	-.-	28.6341	0.47723	0.15097
Sample 3	-.-	22.1666	0.36944	0.15927
Average	-.-	25.4004	0.42334	0.15512
Standard Deviation	-.-	4.57321	0.07622	0.00587
Range	-.-	6.46750	0.10779	0.00830

Name	YS1_Stroke_Strain	YS1_Disp.	YS1_Strain	YS1_Time
Parameters	0.2 %	0.2 %	0.2 %	0.2 %
Unit	%	mm	%	sec
Sample 1	-.-	-.-	-.-	-.-
Sample 2	0.30193	0.15097	0.30193	1.81000
Sample 3	0.31853	0.15927	0.31853	1.91000
Average	0.31023	0.15512	0.31023	1.86000
Standard Deviation	0.01174	0.00587	0.01174	0.07071
Range	0.01660	0.00830	0.01660	0.10000

Name	Max_Force	Max_Stress	Max_Stroke	Max_Stroke_Strain
Parameters	Calc. at Entire Areas	Calc. at Entire Areas	Calc. at Entire Areas	Calc. at Entire Areas
Unit	N	N/mm2	mm	%
Sample 1	5691.13	94.8521	2.54100	5.08200
Sample 2	5794.62	96.5770	2.54013	5.08027
Sample 3	5634.85	93.9142	2.52093	5.04187
Average	5706.87	95.1144	2.53402	5.06805
Standard Deviation	81.0392	1.35065	0.01134	0.02269

Range	159.770	2.66280	0.02007	0.04013

Name	Max_Disp.	Max_Strain	Max_Time	Max_Disp_Force
Parameters	Calc. at Entire Areas	Calc. at Entire Areas	Calc. at Entire Areas	
Unit	mm	%	sec	N
Sample 1	2.54100	5.08200	30.4900	1539.43
Sample 2	2.54013	5.08027	30.4800	22.1411
Sample 3	2.52093	5.04187	30.2500	1505.04
Average	2.53402	5.06805	30.4067	1022.20
Standard Deviation	0.01134	0.02269	0.13577	866.250
Range	0.02007	0.04013	0.24000	1517.29

Name	Max_Disp_Stress	Max_Disp_Stroke	Max_Disp_Stroke_Strain	Max_Disp_Disp.
Parameters				
Unit	N/mm2	mm	%	mm
Sample 1	25.6571	5.53370	11.0674	5.53370
Sample 2	0.36902	6.39160	12.7832	6.39160
Sample 3	25.0841	5.27640	10.5528	5.27640
Average	17.0367	5.73390	11.4678	5.73390
Standard Deviation	14.4375	0.58393	1.16787	0.58393
Range	25.2881	1.11520	2.23040	1.11520

Name	Max_Disp_Strain	Max_Disp_Time	Break_Force	Break_Stress
Parameters			Sensitivity: 10	Sensitivity: 10
Unit	%	sec	N	N/mm2
Sample 1	11.0674	66.4200	-.-	-.-
Sample 2	12.7832	76.7100	-.-	-.-
Sample 3	10.5528	63.3300	-.-	-.-
Average	11.4678	68.8200	-.-	-.-
Standard Deviation	1.16787	7.00543	-.-	-.-
Range	2.23040	13.3800	-.-	-.-

Comment
Normal behavior of the material.
Force is within the limits
Fracture is linear and rapid towards the end